Analytical Modeling of Fire Smoke Spread in High-rise Buildings

Dahai Qi

A Thesis Proposal

In the Department

of

Building, Civil and Environmental Engineering

Presented in Partial Fulfillment of the Requirements

for the Degree of Doctor of Philosophy at

Concordia University

Montreal, Quebec, Canada

September 2016

CONCORDIA UNIVERSITY

School of Graduate Studies

This is to certify that the thesis prepared

By: Dahai Qi

Entitled: Analytical Modeling of Fire Smoke Spread in High-rise Buildings

and submitted in partial fulfillment of the requirements for the degree of

Doctor of Philosophy (Building Engineering)

complies with the regulations of the University and meets the accepted standards with respect to originality and quality.

Signed by the final Examining Committee:

_____ Chair
Dr. Nematollaah Shiri

_____ External Examiner
Dr. Jie Ji

_____ External to Program
Dr. Marius Paraschivoiu

_____ Examiner
Dr. Samuel Li

_____ Examiner
Dr. Hua Ge

_____ Thesis Supervisor
Dr. Liangzhu (Leon) Wang & Dr. Radu Zmeureanu

Approved by

_____
Chair of Department or Graduate Program Director

_____
Dean of Faculty

Abstract

Analytical Modeling of Fire Smoke Spread in High-rise Buildings

Dahai Qi, Ph.D.

Concordia University, 2016

Canada has a large number of high-rise buildings; according to the National Fire Protection Association (NFPA) 101 Life Safety Code, a high-rise building is defined as a building with the height of more than 23 meters or that is roughly 7 stories tall. Fires in high-rise buildings are often disastrous and cause huge losses if the buildings are not well protected against fires. Historically, a high-rise fire is more likely to happen in the lower floors according to the statistics. Driven by stack effect, the resulting smoke from fires may spread to the higher levels more easily via the vertical shafts, e.g. stairs, elevators, light wells, ventilation ducts, than through leakage openings in the building structure. It was reported that smoke spread through shafts counts for about 95% or more of the upward movement of smoke in typical high-rise buildings. Therefore, much attention has been paid to the study of the smoke movement in vertical shafts.

Analytical models, numerical simulations and experimental studies are the commonly used methods to study the smoke movement through building shafts. For simplification, most of the previous studies on the analytical models and numerical simulations assumed adiabatic shaft walls and did not take heat transfer between smoke and shaft boundaries into consideration. In fact, the smoke temperature strongly depends on the heat exchange with the shaft walls and may vary significantly depending on the height. An accurate estimation of the temperature profile in a shaft

is crucial for the prediction of smoke movement during a fire, because the amount of smoke spreading through a shaft is closely coupled with the heat transfer during a fire. Numerical approaches normally include CFD model, zone model and mutizone network model, in which the mutizone network model is often used to study smoke movement during fires in high-rise buildings but temperature in each zone has to be specified by users due to the lack of energy model, which may results in errors in stimulation. In addition, full size experiments are often costly and unpractical to conduct, especially for high-rise buildings. Sub-scale experiment is the often used one but it lacks sound scaling law to maintain the similarity of scaled and full-size high-rise models.

The main objective of this research is to develop an analytical model and a numerical modeling approach of coupled heat and mass transfer of fire smoke movement through vertical shafts of high-rise buildings. Based on the analytical model, simple calculation method and empirical equation of neutral plane level were developed and validated by experimental data from the literature. It was found that the empirical equation is more accurate than the existing equation of neutral plane level. Studies on the dimensionless analytical solutions and similarity study were also conducted using the analytical model, which provide a new scaling method to sub-scale smoke spreads in high-rise shafts. The new scaling method was verified by experiments on different size and material shafts. The results indicated that compared to the common used scaling method, Froude modeling method, the new scaling method could achieve closer results between sub-scaled models and the full-size model. The numerical approach is based on a multizone program with an added energy equation, CONTAM97R, which can calculate the coupled heat and mass transfer inside the high-rise shafts. Different from floor zoning strategy (FZS) that is frequently used, a new zoning strategy called adaptive zoning strategy (AZS) was suggested by adapting the temperature gradient inside the shaft. Using this zoning strategy, a modeling method of smoke

movement in shafts during high-rise fires by the mutilizone and energy network program was proposed. It was concluded that AZS could achieve similar accuracy results as FZS but with fewer zones.

Acknowledgements

I would like to express my special acknowledgements to my co-supervisor, Dr. Liangzhu (Leon) Wang, for offering his encouragement and profound knowledge on heat and mass transfer in buildings. The same acknowledgements to my co-supervisor, Dr. Radu Zmeureanu, whose support and inspiring suggestions have been precious for the PhD study. Without their guidance and persistent assistance, this thesis would not have been possible.

I would like to thank the members of examining committee, Dr. Jie Ji, Dr. Marius Paraschivoiu, Dr. Samuel Li and Dr. Hua Ge, for their precious comments on my thesis work, especially Dr. Jie Ji for the experimental data from his papers. Without the data, I could not complete the thesis.

Besides, I would also thank my friend and colleague, Guanchao Zhao, who dedicated a lot to the experiments. He helped me to design, set up and conduct the whole experiments. In addition, I would like to extend my regards to the rest of my friends and colleagues, Dr. Cheng-Chun Lin, Weigang Li, Sui Jiang Si Tu, Jun Cheng, Sherif Goubran and Jiaqing He, for their friendship and knowledge.

Finally, my deepest gratitude goes to my mother, Wenqin Fang, my father, Guangqi Qi, for their unconditional love and respect for my choices; to my wife, Hui Chen, for her support in realizing my dreams and our child, Jason, who brings much happiness into my life.

Table of Contents

List of Figures

List of Tables

Nomenclature

a	absorption coefficient; thermal diffusivity
a_i	emissivity weighting factor for the i^{th} fictitious gray gas in the weighted sum of gray gases model
A	cross section area of the shaft (m^2)
A^*	effective area of opening (m^2)
A_h	cross-section area (m^2)
C	pressure correction coefficient; coefficient in the empirical equations
C_d	discharge coefficient
C_w	coefficient for natural convection
C_p	specific heat capacity of the smoke (J/(kg·K))
D	characteristic length (m)
E	heat source (kW); heat release rate (kW)
H	height of the shaft (m)
H_f	height of the fire floor (m)
H_f'	height of opening (m)
D_h	hydraulic diameter (m)
f	dimensionless friction factor
Fr	Froude mumber
h	heat transfer coefficient (W/(m^2·K)); head loss caused by friction (m) ; height (m)
k	conduction heat transfer coefficient of air (W/(m·K))
k_i	absorption efficient of the i^{th} gray gas in the weighted sum of gray gases model
l	characteristic length (m)

L	mean beam length (m)
$\dot{m}$	mass flow rate (kg/s)
N	coefficient in the empirical equations
NPL	neutral plane level
$NRMSE$	normalized root mean square error
p	pressure (Pa)
P	perimeter of the shaft (m); predicted/measured data
Pr	Prandtl number
$\dot{q}_x$	heat flux (W/m^2)
q''	convective heat flux from the shaft wall (W/m^2)
$\overline{\dot{q}_x}$	average heat flux (W/m^2)
Q	volumetric flow rate (m^3/s)
R	specific gas constant (J/(kg·K))
Re	Reynolds number
R_t	thermal resistance between two sides of the shaft ((m^2·K)/W)
t	time (s)
T	temperature (K)
$\overline{T}$	average temperature (K)
v	velocity (m/s)
W	thickness of the shaft wall (m)
W'	width of opening (m)
x	height of interests (m)

y	y axis

Greek symbols

α	temperature attenuation coefficient
a^*	a constant of fitting smoke temperatures (J. Ji et al. 2013)
β	a constant of fitting smoke temperatures (J. Ji et al. 2013)
τ	characteristic time
γ	relative smoke temperature at the top of the shaft
Δ	difference
ε	roughness (mm); emissivity
η	normalized temperature rise in the fire floor
θ	normalized temperature
λ	thermal conductivity (W/(m·K))
μ	dynamic viscosity (kg/(m·s))
ν	kinematic viscosity (m^2/s)
ρ	density (kg/m^3)
$\bar{\rho}$	Average density (kg/m^3)
$\boldsymbol{\rho}_f'$	average density of gas in the fire room (kg/m^3)
ϕ	ratio of bottom opening area and top opening area
σ	Stefan-Boltzmann constant ($W/(m^2 \cdot K^4)$)
φ	relative height
ω	geometry and thermal factor

Subscripts

0	ground level, the height of $x = 0$
1	expelling gas
a	atmospheric
b	bottom
c	convective
CO_2	carbon dioxide
couple	coupled equation
dy	dynamic
e	emittance
el	elevation in the shaft
ek	predicted results of empirical equation or Klote's equation
f	fire floor; full size
fr	friction
g	gas
H	height of the shaft
i	interior wall of the shaft; index of points of interests in the shaft; zone *i*; sub-section *i*; inside of the shaft
in	entry the shaft
j	zone *j*
k	wall *k*
l	lower
m	sub-scaled model scale

n	zone number
nf	non-fire floor
np	neutral pressure
o	exterior wall of the shaft
out	leave the shaft
r	radiant
sh	shaft
shl	lower section of shaft below neutral plane level
shu	upper section of shaft above neutral plane level
t	top
u	upper
w	wall

Preface

This is a manuscript-based thesis, a collection of three published journal papers and two manuscripts ready to be submitted. The five papers compose Chapter 3 ~ Chapter 7, and each manuscript is an independent chapter.

For the purpose of easy reading, these five manuscripts are modified from the original ones. The numbering of equations, tables, and figures includes the numbers of the chapters they belong to. References of different chapters are combined at the end of the thesis.

Chapter 1 Introduction

According to the National Fire Protection Association (NFPA) 101 Life Safety Code (2012), a high-rise building is defined as a building with the height of more than 23 m (roughly 7 stories). Canada has a large number of high-rise buildings. According to a statistic published on Wikipedia 2014, a list of top 120 cities with the most high-rise building in the world includes 9 Canadian cities; Toronto is among the top 9 cities with more than 2,500 high-rise buildings (see Table 1-1). Meanwhile, the number of high-rise buildings in Canada is increasing rapidly, e.g. 130 high-rise projects were under construction in the first quarter of 2014 in Toronto, Canada (CBC news 2014). It is however to be noted that, fires in high-rise buildings are often disastrous and cause huge amount of losses, when the buildings are not well protected against fires. The following section of this chapter will explain the problems in the design and research of high-rise fire protection, and then, highlights the objectives of the research presented in the thesis.

Table 1-1 List of cities with the most high-rise buildings

Rank	City	Country	Buildings	Population
1	Hong Kong	China	7,896	7,061,200
2	New York City	United States	6,504	8,310,212
3	São Paulo	Brazil	6,467	11,316,149
4	Singapore	Singapore	4,764	4,839,400
5	Caracas	Venezuela	3,864	5,962,259
6	Moscow	Russia	3,754	10,452,000

7	Seoul	South Korea	2,955	10,421,782
8	Rio de Janeiro	Brazil	2,947	6,161,047
9	Toronto	Canada	2,873	5,583,064
10	Tokyo	Japan	2,779	13,001,279
11	Istanbul	Turkey	2,439	11,372,613
12	Mumbai	India	2,299	20,748,395
13	Buenos Aires	Argentina	1,870	2,891,082
14	Delhi	India	1,805	21,753,486
15	St. Petersburg	Russia	1,770	4,568,000
16	Kiev	Ukraine	1,531	2,819,566
17	London	United Kingdom	1,478	8,174,000
18	Osaka	Japan	1,463	2,643,805
19	Mexico City	Mexico	1,364	8,836,045
20	Madrid	Spain	1,127	3,213,271
38	Vancouver	Canada	631	578,041
51	Montreal	Canada	475	1,620,693
60	Ottawa	Canada	351	883,391

78	Calgary	Canada	260	988,193
79	Edmonton	Canada	244	812,201
105	Burnaby	Canada	132	193,954
106	Winnipeg	Canada	132	519,544
113	London	Canada	116	470,000

1.1. Statement of the problem

Fires in high-rise buildings could lead to disastrous and enormous losses, if the buildings are not well protected against fires. It is more likely to have a high-rise fire start in the lower floors. Driven by stack effect, the resultant smoke may spread to the higher levels more easily via the vertical shafts, e.g. stairs, elevators, light wells, ventilation ducts, than through leakage openings in the building structure. It was reported that smoke spread through shafts counts for about 95% or more of the upward movement of smoke in typical high-rise buildings (Tamura 1994). Therefore, much attention has been paid to the study of the smoke movement in vertical shafts. The following paragraphs in this section highlight the problems in the analytical models, scaling method and numerical simulations, which are the commonly used approaches to study the smoke movement through buildings.

For simplification, the analytical models were often developed from the assumption of uniform temperature distribution and adiabatic walls in the shaft or rooms, so it could be applied as hand calculation methods in the fire protection design regulations or handbooks. e.g. Klote's model of neutral plane level . However, many researchers found that these assumptions can result in

inaccurate results. In fact, the smoke temperature strongly depends on the heat exchange with the shaft walls and may vary significantly depending on the height (Black 2009; Black 2010; Sun et al. 2011). Yang et al. (2012) calculated the temperature and pressure distributions, and mass flow rates in a shaft for different conditions, which consist of: uniform temperature inside the shaft, constant heat flux between the shaft wall and ambient air, and constant shaft wall temperature. The calculation results were compared with FDS (Fire Dynamics Simulator) (McGrattan et al. 2013), demonstrating that it is important to consider heat transfer from shaft wall, because it has a strong impact on the air temperature and thereby the location of neutral plane and mass flow rate through the shaft. Wang et al. (2013) also found that an accurate estimation of the temperature profile in a shaft is crucial for the prediction of smoke movement during a fire, because the amount of smoke spreading through a shaft is closely coupled to the heat transfer during a fire. Therefore it is necessary to study the analytical model of fire smoke transporting in the shaft with heat transfer from the shaft wall, and derive analytical solutions that could be used in a hand calculation way.

Sub-scaled experiments play an incredibly important role in the study of smoke movement in high-rise buildings. Experiments are done in the physical world and are thus more realistic (Klote et al. 2012); so the results are more reliable and computer simulation needs to be verified by experiments. Most of the experimental researches on smoke movement in high-rise shafts are conducted on sub-scaled physical models rather than full-size experiments, which are costly and often unpractical. Froude modeling is probably the most common approach to scale modeling of smoke movement in buildings, and is widely used for design analysis, verification of CFD simulation and fire reconstruction in a corridor and atrium fires. However, the Froude modeling is not always successful due to the neglect of heat transfer between smoke and the boundaries and interior structure resistance. Carey compared temperatures at different locations between a full and a 1/8

scaled compartments. It was found that the accuracy of the model does vary based on the distance from the fire. Due to heat transfer between the gas and the boundary, the temperatures measured near the boundaries are not as accurate as the temperatures measured closer to the fire. For the measuring a location of 5.1 cm below the ceiling and 5.76 m away from the fire of 250 kW gas burner, temperature rise of a full size model is 40°C but the difference between full model and 1/8 scaled model is up to 20°C (Carey 2010). Chow carried out experiments of natural smoke filling process on both full-scale atrium and a 1/26.5 scale atrium. The experiments were designed according to Froude modeling. However, it was observed that there are quite large deviations between the temperatures measured in the scale model and the full-size atrium. Therefore, it was suggested that the scaling law for temperature requires further examination (Chow and Lo 2008).

According to the purpose of building smoke analyses, different computer simulation analyses tools were developed. Currently, three types of models are usually employed to study smoke movement in buildings individually: zone models, computational fluid dynamics (CFD) models and multizone network models. However CFD simulation demands much computing time, and is unpractical for the calculation of smoke movement in high-rise buildings with a large number of compartments concerning the computational time currently, and zone models have limitations on the number of compartments that could be calculated by zone models. Multizone network models are qualified for the researches that focus on the average characteristics of pressure distribution, infiltration airflows, and lower computational costs. These models adapt many assumptions so that fast computing speed is achieved. CONTAM is one of the most popular multizone models for building fire smoke analysis as suggested by the Handbook of Smoke Control Engineering (ASHRAE), which was developed by the National Institute of Standards and Technology (NIST) (Walton and Dols 2013). However, CONTAM does not solve the energy conservation equation,

so the temperature in each zone has to be provided as an input from users, because it was originally developed without the intent for temperature predictions. With applications of CONTAM to more building types and various design problems, the lack of the energy equation has started to reveal its limitations, especially for buoyancy-driven flows in buildings, e.g. designs of natural ventilations or smoke control systems in high-rise buildings.

1.2. Objectives of this thesis

To solve the problem mentioned above, this thesis aims to develop analytical model of coupled heat and mass transfer of fire smoke through the vertical shafts of high-rise buildings. Based on the analytical model, a new scaling method was established by dimensional analysis. Similarity studies and empirical equations of the neutral plane level that presents pressure distribution were also derived. Considering that the analytical model mainly focuses on the high-rise shafts, rather than the whole building which is too complex to be modeled analytically, a mutlizone network program with energy equations was employed to model smoke spread in high-rise buildings.

The detailed work includes:

(1) Analytical model

The analytical model can be solved by simple hand-calculation. Values of mass flow rate, pressure and temperatures of the air/smoke in the shaft and non-fire floors can be obtained quickly, which are vital for the fire smoke protection design. On the basis of the analytical model, empirical equations of the neutral plane level that presents pressure distribution were derived. A new scaling method for smoke movement inside high-rise shafts was also developed by means of dimensionless analysis based on the analytical models or differential governing equations.

(2) Dimensionless analytical solutions and similarity study

Studies on dimensionless analytical solutions and similarity were conducted based on the analytical model, which provide a new scaling method to sub-scale smoke spreads in high-rise shafts. The new scaling method was verified by experiments on different size and material shafts.

(3) Numerical modeling

A multizone network program with energy equations was employed to model the smoke movement in high-rise buildings, including verification of energy equation in the multizone network model, the application in high-rise buildings with and without infiltrations. Using a dimensionless number that represents the temperature profile of smoke inside the shaft, the zoning method was optimized for the numerical modeling.

1.3. Summary and thesis work introduction

This chapter introduces the research gaps in the study of high-rise fire protection and objectives of this thesis. It was pointed out the vertical shafts in the high-rise buildings are the primary paths for the fire smoke spread from lower part of the building to the higher part, and therefore is the study subject in this thesis. Considering venting smoke is a sound alternative approach to protect smoke spread to non-fire area, this research focused on the venting shaft, including natural venting and mechanical venting. Problems in the previous researches were highlighted in Table 1-2.

To solve the problem of no heat transfer consideration in the analytical model, chapter 3 develops an analytical model of the coupled heat and mass transfer of fire smoke through high-rise shafts. Hand calculation method based on the analytical model is provided. Since the smoke movement in shafts is a thermal couple problem, including mechanical energy equation, energy equation and mass balance equation, iteration is needed in the hand calculation method. Because there is no discretion in the three equations, it is easier to obtain convergent results by the hand calculation

than the method with discretion like CFD approach. Iteration numbers with different convergence thresholds is also counted in the demo cases with different conditions to show this advantage.

Chapters 4 reports the development of dimensionless analytical solutions of smoke transport in non-adiabatic high-rise shafts during fires, which could provide a fundamental understanding of smoke transport physics.

Chapter 5 provides a method to develop an empirical equation to estimate the neutral plane level, which distinguishes from previous study of neutral plane level with the consideration of temperature variation with the height. The temperature variation is caused by heat exchange between smoke and shaft walls, and therefore the smoke temperature inside the shaft is non-uniform.

Chapters 6 presents studies on the similarity to identify groups of dimensionless numbers, and a new scaling method to sub-scale high-rise shafts with the consideration of heat exchange between smoke and shaft walls, and interior structure resistance.

Chapter 7 presents the approach to model smoke movement in high-rise buildings by a multizone airflow and energy network program, CONTAM97R. Chapters 3 ~ 6 mainly focus on the vertical shafts, which are the main paths for fire smoke spread in high-rise buildings. To expend the calculation of the heat and mass transfer to the whole building, the multizone program and its modeling method is presented in chapter 7.

Table 1-2 List of research gaps in previous studies and the corresponding solutions in the thesis

	Research gaps in previous studies	Solutions in this thesis
1	Lack of appropriate heat exchange consideration in analytical model	Chapter 3

2	Lack of appropriate heat exchange and structure resistance consideration in dimensionless analytical solutions and scaling law to design sub-scaled model	Chapters 4 &6
3	Lack of heat exchange consideration in modeling of neutral plane level	Chapter 5
4	Lack of modeling method of smoke spread in high-rise buildings by multizone network program with energy model	Chapter 7

This study contributes to an improved analytical model in terms of dimensionless numbers, a new scale modeling method, and a new airflow network zoning approach of high-rise shafts during fires. Different from previous studies, the analytical model and new scale modeling method consider heat transfer between the smoke and walls using thermal resistance between two sides of the walls, as well as interior structure resistance; therefore they are more reasonable and accurate. The new zoning approach for airflow network program considers temperature gradient so it can achieve the same accurate with fewer zones compared with traditional zoning approach.

Chapter 2 Literature Review

2.1. Introduction

Fires in high-rise buildings often lead to huge amount of losses, when the fires are not well controlled. It is reported that smoke movement in high-rise buildings kills approximately 75 percent of the fire victims in the United States. These fire deaths occur in areas remote from the room where the fire originates and are due to the toxic effects of the smoke as it migrates throughout a building (Gann et al. 1994; Beitel, Wakelin, and Beyler 2000). Caused by stack effect and wind, smoke spreads beyond fire sources and to other spaces through multiple paths, such as large space, floor piping hole, stairwells, elevator shafts and building envelopes (Su et al. 2011; Poreh and Trebukov 2000; Tamura 1994). Smoke can also spread through building equipment, such as the air-handling units and mechanical ventilation systems. Smoke movement throughout a high-rise building is, therefore, an important issue with respect to the life safety of people who are in a building when a fire occurs (Zhong et al. 2004; Hou et al. 2011; Luo et al. 2013). It also greatly impacts the firefighting efforts both in search and rescue as well as the attack on the fire (Beitel, Wakelin, and Beyler 2000).

Historically, a high-rise fire is found more likely to happen in the lower floors according to the statistics (Hall 2011), resulting in more non-fire floors to be exposed to smoke. The Winecoff Hotel fire at Atlanta, US (December 7, 1946) caused 119 deaths. The MGM Grand Hotel fire at Las Vegas, NV (November 21, 1980) led to the deaths of 85 people and the injuries of 600 people (Tamura 1994). It was reported that in the US between 2007 and 2011, 43% of fires in hotel buildings originated below the 2nd floor, and 73% below the 6th floor, and 37% of fires in office buildings originated below the 2nd floor, and 64% below the 7th floor. Driven by stack effect, the resultant smoke from fires may spread to the higher levels more easily via the vertical shafts, e.g.

stairs, elevators, light wells, ventilation ducts, than through leakage openings in the building structure. It was reported that smoke spread through shafts counts for about 95% or more of the upward movement of smoke in typical high-rise buildings (Tamura 1994). Therefore, much attention has been paid to the study of the smoke movement in vertical shafts, aiming to decrease the smoke inside shafts (Harmathy 1998; Mercier and Jaluria 1999; Shi et al. 2014a).

To prevent smoke spread to higher levels, the pressurization systems have become a popular option since the 1960s, which is intended to prevent the smoke leaking through closed doors into shafts by injecting clean air into the shaft enclosure as the pressure in the shaft is greater than the adjacent fire compartment (Lay 2014). However, the pressurization systems do not always work to prevent smoke spreads through shafts, especially for the high-rise shafts due to stack effect and floor-to-floor variations in flow resistance (Klote 2011). It was estimated that 35% of pressurization systems might fail to function as intended (Lay 2014).

As an alternative solution, the idea of using ventilation to exhaust smoke from the fire floor or keeping spaces tenable during high-rise fires attracts much attention. Many studies have been conducted on the experiments, mathematical models and applications of smoke ventilation in shafts. Ji and Shi did extensive experimental research to investigate transport characteristics of thermal plume in the ventilated stairwell with two or multiple openings (Jie Ji et al. 2015; Li et al. 2014; Ji et al. 2013; Shi et al. 2014a). Harmthy proposed the Fire Drainage System to remove the heat and induced convection flow from a fire through a series of shafts to reduce the spread of fire from the region of fire source (Lay 2014; Harmathy and Oleszkiewicz 1987). Design principles of this system were also introduced based on the assumption of constant gas temperature (Harmathy and Oleszkiewicz 1987) and the heat transfer between the gas and shaft walls was not considered. Similar to the Fire Drainage System, the Beetham Tower system was developed to use an air inlet

shaft to exhaust smoke from fire floor by stack effect but mechanical input was employed to enhance the performance (Lay 2014). Klote studied the ventilation control of stairwells in tall buildings by tenability analysis, computational fluid dynamics (CFD) and network modeling. It was found that the stairwell smoke control by ventilation is feasible (Klote 2011). The elevator hoistway shafts could also provide excellent paths to remove hot smoke out of the building, which gains wide acceptance even in the absence of supporting research (Klote et al. 2012). The International Building Code demands that hoistways of elevators and dumbwaiters penetrating more than three stories shall be provided with a means for venting smoke and hot gases to the outer air in case of a fire. Vents shall be located at the top of the hoistway and shall open either directly to the outer air or through non-combustible ducts to the outer air (International Code Council 2007). However, the hot smoke inside of the elevator hoistway shafts can also make the smoke flow from the elevator shaft to the building, especially on the upper floors of buildings (Klote 2004). Therefore, more attention needs to be paid to the elevator hoistway shafts design.

Analytical models, scaling method and numerical simulations are the commonly used approaches to study the smoke movement through high-rise shafts during fires. Related previous researches will be introduced in the following section in this chapter.

2.2. Analytical models

Hand calculation method that is based on the analytical models is essential to the fire smoke protection design, because it is fast and simple to obtain important parameters for early stage design. Generally, high-rise buildings could be simplified to three types of spaces, fire floor, non-fire floor and shafts, each of which is calculated separately. As mentioned in section 2.1, the shafts are very important for the fire smoke protection study, many researchers developed analytical models of smoke movement in the shafts. Sections 2.2.1 and 2.2.2 will introduce the analytical

models developed by these studies based on uniform temperature and non-uniform temperature, which do not consider heat transfer and consider heat transfer between smoke and shaft walls respectively.

2.2.1. Analytical model without considering heat transfer

Klote (1991) presented a general method for the evaluation of the neutral pressure level (*NPL*) for a space (e.g. a room or a shaft) connected to its surroundings by any number of openings based on the assumption that the temperature is uniform and the walls are adiabatic in the space. The analytical solutions of mass flow rate, $\dot{m}$, and the height of *NPL*, x_{np}, are derived as Eqs. (2-1) and (2-2) show. It was found that *NPL* between a space and its surrounding is a strong function of the size of openings (Eq. (2-2)). Further, the mass flow rate leaving a space due to stack effect strongly depends on the room temperature (Eq. (2-1)). The pressure distribution thereby could be derived as Eq. (2-3) shows (Chow and Zhao 2011).

$$\dot{m} = CA\sqrt{\frac{2\rho_a{}^2 g H_n (T - T_a)}{T}} \tag{2-1}$$

$$x_{np} = \frac{H}{\left[1 + \frac{T}{T_a}\left(\frac{A_l}{A_u}\right)^2\right]} \tag{2-2}$$

$$p_{ix} = p_{ox} + \left(\frac{1}{T_o} - \frac{1}{T_i}\right)\left(x - x_{np}\right) \tag{2-3}$$

However, normally the temperature inside the shaft could not be uniform. For a shaft with fire at the bottom, Zhang et al. (2008) believed that the temperature at the location close to the fire source is much higher than others in the shaft; while the temperature in the shaft above the fire floor achieves uniformity rapidly due to the strong heat exchange between the inside and the outside.

They proposed a two-zone model for predicting the location of the neutral plane inside the shaft of a building during fires, where the fire room and other spaces in the shaft are defined as two zones and in each zone the temperature is uniform. Eqs. (2-4) and (2-5) present the total mass flow rate into the shaft and the location of the *NPL*. It was found that the location of the neutral plane x_{np} strongly depends on the dimensions of the openings between the fire room and the surrounding.

$$m_{in} = \frac{2}{3} C W' H'_f{}^{3/2} \sqrt{2\rho_a g(\rho_a - \rho'_f)} + \frac{2}{3} C W (x_{np} - H_f)^{3/2} \sqrt{2\rho_a g(\rho_a - \rho_i)} \quad (2\text{-}4)$$

$$(x - x_{np})^{3/2} = (W' / W)(H'_f)^{3/2} T_c \times \sqrt{(T'_f - T_a)/[T_a T'_f (T_i - T_a)]} + (x_{np} - H_f)^{3/2} \sqrt{T_i / T_a} \quad (2\text{-}5)$$

It is simple to calculate by assuming the uniform temperature inside of the shaft or in the two zones of the shaft. However, it may lead to large errors in the prediction of smoke movement during a fire. Wang et al. illustrated the importance of temperature profiles on the prediction of smoke movement in high-rise buildings. They found that an accurate estimation of the temperature profile in a shaft is crucial for the prediction of smoke movement during a fire, because the smoke flow through a shaft is closely coupled to the heat transfer during a fire. An inaccurate estimation of temperature profile may result in the substantial errors as high as 80% (Wang, Black, and Zhao 2013). Therefore, it is necessary to develop analytical models that consider heat transfer between smoke and the boundaries.

2.2.2. Analytical model considering heat transfer

Yang et al. (2012) developed analytical models for the evaluation of stack effect in a shaft, counting for the heat transfer from shaft interior boundaries. Both the conditions with constant heat flux from shaft wall to the airflow and with constant shaft wall temperature were considered. Eqs. (2-6) ~ (2-9) provide the temperature profile and mass flow rate for constant heat flux, and Eqs. (2-10) and (2-13) for constant shaft wall temperature. According to the mass balance law,

$\dot{m}_{\text{out}}$ and $\dot{m}_{in}$ should be equal, so the *NPL* location x_{np} could also be obtained. The prediction capabilities of these analytical models were evaluated by using large eddy simulation (LES) for a hypothetical shaft. The results show that there are fairly good agreements between the predictions of the analytical models and the LES predictions in mass flow rate, vertical temperatures profile and pressure difference as well. Both the results of analytical models and LES prove that the neutral plane could locate higher than one half of the shaft height when the upper opening area is identical with the lower opening area. Further, it is also concluded that the analytical models perform better than Klote's model does in the mass flow rate prediction.

For constant heat flux:

$$\Delta T = \frac{Kx}{\dot{m}} \tag{2-6}$$

$$K = \frac{q''P}{C_p} \tag{2-7}$$

$$\dot{m}_{out} = C_d A_u \sqrt{2g \frac{T_a \rho_a \dot{m}}{KH + \dot{m} T_a} \rho_a \left[H - x_{np} - \frac{T_a \dot{m}}{K} \ln\left(\frac{KH + \dot{m} T_a}{KH_n + \dot{m} T_a} \right) \right]} \tag{2-8}$$

$$\dot{m}_{in} = C_d A_l \sqrt{2g\rho_a{}^2 \left[x_{np} - \frac{T_a \dot{m}}{K} \ln\left(\frac{Kx_{np} + \dot{m} T_a}{\dot{m} T_a} \right) \right]} \tag{2-9}$$

For constant shaft wall temperature:

$$\Delta T_w = \Delta T_{w,0} e^{-\frac{K' x}{\dot{m}}} \tag{2-10}$$

$$K' = \frac{hP}{C_p} \tag{2-11}$$

$$\dot{m}_{out} = C_d A_u \sqrt{2g \frac{T_a \rho_a}{T_{w.} - \Delta T_{w,0} e^{-K'H/\dot{m}}} \rho_a \left[\left(1 - \frac{T_a}{T_{w.}} \right) \left(H - x_{np} \right) - \frac{T_a \dot{m}}{K' T_w} \ln \left(\frac{T_{w.} - \Delta T_{w,0} e^{-K'H/\dot{m}}}{T_{w.} - \Delta T_{w,0} e^{-K'H_n/\dot{m}}} \right) \right]} \tag{2-12}$$

$$\dot{m}_{in} = C_d A_l \sqrt{2g\rho_a{}^2 \left[\left(1 - \frac{T_a}{T_{w.}} \right) x_{np} - \frac{T_a \dot{m}}{K' T_w} \ln \left(\frac{T_{w.} - \Delta T_{w,0} e^{-K'H/\dot{m}}}{T_a} \right) \right]} \tag{2-13}$$

Yang et al. (2013) also developed a model for analysis of convection induced by stack effect in a shaft with warm airflow expelled from adjacent space. The model can predict the vertical distributions of temperature, mass inflow rate, and neutral plane location as Eqs. (2-14) ~ (2-17) show.

$$T = \begin{cases} T_w - \left(\dot{m} T_w - \dot{m}_l T_l - \dot{m}_{in} T_a \right) e^{K'(H_1 - x)/\dot{m}} \; for \quad x \geq H_1 \\ T_a \; for \quad x < H_1 \end{cases} \tag{2-14}$$

$$\dot{m} = \begin{cases} \dot{m}_{in} + \dot{m}_l = \dot{m}_{out} for \quad x \geq H_1 \\ \dot{m}_{in} \; for \quad x < H_1 \end{cases} \tag{2-15}$$

$$\dot{m}_{out} = C_d A_u \sqrt{\frac{2g\dot{m} T_a \left[\left(1 - T_a / T_w \right) \left(H - x_{np} \right) - \left(T_a \dot{m} / K' T_w \right) \ln \dfrac{\dot{m} T_w - \left(\dot{m} T_w - \dot{m}_1 T_1 - \dot{m}_{in} T_a \right) e^{K'(H_1 - H)/\dot{m}}}{\dot{m} T_w - \left(\dot{m} T_w - \dot{m}_1 T_1 - \dot{m}_{in} T_a \right) e^{K'(H_1 - x_{np})/\dot{m}}} \right]}{\dot{m} T_w - \left(\dot{m} T_w - \dot{m}_1 T_1 - \dot{m}_{in} T_a \right) e^{K'(H_1 - H)/\dot{m}}}} \tag{2-16}$$

$$\dot{m}_{in} = C_d A_l \sqrt{2g\rho_a{}^2 \left[\left(1 - \frac{T_a}{T_w} \right) \left(H - x_{np} \right) - \frac{T_a \dot{m}}{K' T_w} \ln \frac{\dot{m} T_w - \left(\dot{m} T_w - \dot{m}_1 T_1 - \dot{m}_{in} T_a \right) e^{K'(H_1 - x_{np})/\dot{m}}}{\dot{m}_1 T_1 + \dot{m}_{in} T_a} \right]} \tag{2-17}$$

During a fire, heat transfer in the shaft is quite different from non-fire cases. Fire smoke temperature can be an order of magnitude higher than surrounding air at the bottom of a shaft and drop quickly at the higher floors. The elevated smoke temperature would cause exacerbated convective and radiant heat transfer, which could be further enhanced by increased radiant emittance of the smoke loaded with combustion products, e.g. carbon dioxide, water vapor and

soot. Meanwhile, both shaft surface temperature and heat flux would vary significantly with the height of a shaft. Therefore, the previous studies of natural ventilation are not applicable.

For high-rise fires, the studies by Sun et al. (2011) are probably most relevant. They developed a theoretical model for predicting the one-dimensional transient buoyant plume rise in a vertical shaft with convective heat transfer from hot up-rising flow to the side walls, including continuity equation (Eq.(2-18)) and energy equation (Eq.(2-19)). Eqs. (20) ~ (24) provide the solutions of mass flow rate, temperature and velocity profiles in the shaft under the condition that the constant number, *I* (Eq. (2-20)), is known, which can be obtained by experiment. In fact, the theoretical models cannot be solved directly without knowing the value *I*. The reason is that the momentum equation is not included in the model, leading to in non-closed form equations. Moreover, this theoretical model neglects radiant heat transfer by assuming that the shaft wall temperature was constant and equal to that of the exterior environment. As a result, the heat loss to the walls was exaggerated and the smoke temperature was underestimated in Sun et al. (2011).

Continuity equation:

$$\frac{\partial \rho}{\partial t} + \frac{\partial (\rho v)}{\partial x} = 0 \tag{2-18}$$

Energy equation:

$$\rho C_p \left(\frac{\partial T}{\partial t} + v \frac{\partial T}{\partial x} \right) = -k \frac{\partial^2 T}{\partial x^2} + \frac{h}{D} \left(T_a - T \right) \tag{2-19}$$

$$\frac{v}{T} = \frac{R\dot{m}}{Ap_a} = I \tag{2-20}$$

$$\Delta T = T - T_a = (T_i - T_a) e^{-\alpha \varphi} \tag{2-21}$$

where

$$\alpha = \frac{A_h h H}{D C_p \dot{m}} \tag{2-22}$$

$$v = \frac{R\dot{m}}{Ap_a}\left[\left(T_i - T_o\right)e^{-\alpha\varphi} + T_a\right] \tag{2-23}$$

$$\varphi = \frac{x}{H} \tag{2-24}$$

2.3. Scale modeling

Numerous studies have focused on the fire smoke movement inside high-rise large vertical spaces by means of computer simulation and experiments, in which experiments play an incredible important role. The experiment is done in the physical world and is more realistic (Klote et al. 2012); so the results are more reliable and computer simulation needs to be verified by it. Since full-size fire experiments are costly and often unpractical to be conducted in buildings, most of the experimental researches on smoke movement in high-rise buildings are conducted on sub-scaled physical models. The sub-scaled modeling methods to simulate fire smoke spread in buildings normally include the saltwater modeling and Froude modeling. The idea of saltwater modeling is to substitute turbulent buoyant salt water moving in fresh water for turbulent buoyant hot gas moving in cold gas (Steckler, Baum, and Quintiere 1986). The scale model is submerged in a tank of fresh water and the inject salter simulates a heat source. Since the density of salt water is higher than fresh water, the salt water tends to flow down whereas smoke tends to flow upward (Klote et al. 2012). Steckler, Baum, and Quintiere (1986) used salt water modeling to study fire-induced flows in multi-compartment structures. They developed the scaling laws relating salt water flows and hot gas flows, based on which 1/20 scale salt water experiments were conducted to simulate fire-induced flows in a single-story multi-room structure. The sub-scaled experimental results are in good agreement with available full-scale results. The saltwater modeling was also applied to the

smoke filling visualization experiments on the atria and balcony spill plumes. The details can be found in the work of Chow and Siu (1993) and Yii (1998), so they are not included here.

Froude modeling is probably the most common approach to scale modeling of smoke movement in buildings, and is widely used for design analysis, verification of CFD simulation and fire reconstruction. The Froude number, *Fr*, can be considered the ratio of inertial forces to buoyancy gravity forces, which is shown in Eq. (2-25). The scaling relations are listed in Eqs. (2-26) to (2-34).

$$Fr = \frac{U^2}{gl} \tag{2-25}$$

The scaling relations are:

$$x_m = x_f \left(\frac{l_m}{l_f} \right) \tag{2-26}$$

$$T_m = T_f \tag{2-27}$$

$$\rho_m = \rho_f \tag{2-28}$$

$$v_m = v_f \sqrt{\frac{l_m}{l_f}} \tag{2-29}$$

$$Q_m = Q_f \left(\frac{l_m}{l_f} \right)^{5/2} \tag{2-30}$$

$$\dot{m}_m = \dot{m}_f \left(\frac{l_m}{l_f} \right)^{5/2} \tag{2-31}$$

$$t_m = t_f \sqrt{\frac{l_m}{l_f}} \tag{2-32}$$

$$E_m = E_f \left(\frac{l_m}{l_f} \right)^{5/2} \tag{2-33}$$

$$\Delta p_m = \Delta p_f \left(\frac{l_m}{l_f} \right) \tag{2-34}$$

Based on Froude modeling, Ding et al. (2004) developed a 1:25 scale model to validate CFD simulations. Then, they carried out CFD simulations on a full size 8-storey building with a solar chimney on top of the atrium to investigate the possibility of using the same system for natural ventilation and smoke control in buildings. Froude modeling was also used to design experiments on 1:10 physical scale model. The results of the experiments were employed to validate CFD simulations. At last, both of the experimental and CFD results were used to investigate the hot smoky gases entering an atrium from a fire within an adjacent compartment, (Harrison 2004).

Quintiere used a 1:7 geometric scale model in fire based on Froude modeling as evidence in civil litigation case. It clarified the performance of a smoke control system which was operated in an actual fire incident in a department store atrium. The scaled model results confirmed a design flaw in the smoke control system. It was also found that the high velocity inlet air was shown to be responsible for mixing and de-stratifying the hot smoke in the atrium and dispersing it throughout the department store (Quintiere and Dillon 2008).

To study smoke movement inside high-rise buildings, 1:3 scaled building model was developed by University of Science and Technology of China, which was designed using Froude modeling. Extensive researches have been conducted on scaled building model. The topics include the influence of the staircase ventilation state on the flow and heat transfer of the heated room on the middle floor (Shi et al. 2014a), the effects of ventilation on the combustion characteristics in the compartment connected to a stairwell (Ji et al. 2016).

However, due to the neglect of heat exchange between fire smoke and the boundaries, it was found that sub-scaled experiments using Froude modeling may not obtain accurate temperature. Carey compared temperatures at different locations between a full compartments and a 1:8 scaled compartments designed based on Froude modeling. The accuracy of the model does vary based on the distance from the fire. Due to heat transfer between the gas and the boundary, the temperatures measured near the boundaries are not as accurate as the temperatures measured closer to the fire. For the measuring location 5.1 cm below the ceiling and 5.76 m away from the fire of 250 kW gas burner, temperature rise of full size model is 40°C but the difference between full model and 1:8 scaled model is up to 20°C (Allison C. Carey 2010). Chow carried out experiments of natural smoke filling process on both full-scale atrium and a 1:26.5 scale atrium. The experiments were designed according to Froude modeling. However, it was observed that there are quite large deviations between the temperatures measured in the scale model and the full-size atrium. Therefore, they suggested that the scaling law for temperature requires further examination (Chow and Lo 2008). During a high-rise fire, fire smoke temperature can be an order of magnitude higher than surrounding air at the bottom of large vertical spaces and drop quickly at the higher floor due to the heat exchange between the fire smoke and the boundaries (Qi, Wang, and Zmeureanu 2014b). It is necessary to consider the heat transfers when sub-scaling the large vertical spaces during fires.

2.4. Numerical modeling

Multizone network models are often used to calculate mechanically or naturally driven airflows between different spaces (e.g. rooms) in a building, as well as between the building and the outdoors (Wang and Chen 2008). Each space is defined as one zone with uniformly distributed air parameters, e.g. air temperatures and species concentrations (Chen 2009), so that a whole-building airflow analysis can be conducted within seconds. The simple and yet air quality (IAQ) analysis,

ventilation design, building safety and security analysis, e.g. fire smoke movement in buildings (Wang, Black, and Zhao 2013). CONTAM is one of the most popular multizone models, which was developed by the National Institute of Standards and Technology (NIST) (Walton and Dols 2013). It has been applied to many building types (Ng et al. 2012). Ng et al. (2012, 2013) used CONTAM for the airflow and IAQ analysis in different DOE (the US Department of Energy) reference buildings including restaurants, offices, schools, stores, hotels, hospitals and apartments. Jo et al. (2007), Miller and Beasley (2009) and Miller (2011) conducted CONTAM simulations to pressure distribution and smoke controls by the pressurization of the shafts in high-rise buildings.

However, CONTAM does not solve the energy conservation equation so the temperature in each zone has to be provided as an input from users, because it was originally developed without the intent for temperature predictions. With applications of CONTAM to more building types and various design problems, the lack of the energy equation has started to reveal its limitations, especially for buoyancy-driven flows in buildings, e.g. designs of natural ventilations or smoke control systems in high-rise buildings. Wang, Black, and Zhao (2013) simulated the fire smoke movement in a forty-storey building and found that the availability of temperature profile in the shaft is the key to the accuracy of the prediction. The addition of the thermal analysis capability to CONTAM thus becomes quite necessary.

There have been a few previous efforts to add the energy equation to CONTAM (Tang 2005; Tang and Glicksman 2005; McDowell, Emmerich, Thornton, Walton 2003; Gu 2011), many of which have not yet resulted in a final product. Among them, CONTAM97R (Axley 2001, Wang et al. 2012) is probably the most completed model, which was firstly developed in 1997 but not well verified and/or validated so it was never released. Some previous studies tried to evaluate the performance of CONTAM97R through experimental validations. Axley et al. (2012) compared

the measured airflow rates in a naturally ventilated building to the predictions, and found that the difference could be over 25%. Such difference is also commonly seen in other experimental validation studies with a discrepancy ranging between 25% and 50% (Mahdavi and Proglhof 2008, Haghighat and Li 2004). Although experimental validation may be an effective way to prove the validity of a numerical model, it is difficult to explain and isolate the causes for the discrepancies, once observed, of the measurements and the predictions. Apparently, it is not reasonable to attribute all the discrepancies to the computer model itself because there are many other contributing factors, e.g. measurement uncertainties, user inputs, simplifications and assumptions for the creation of the physical model of the problems. Therefore, experimental validation is somehow limited during the evaluation of mathematical formulation and numerical discretization of a computer model. In comparison, an analytical model provides a mathematical solution to the same set of conservation equations formulated in a numerical model. Therefore, a verification study based on analytical solutions is often conducted to evaluate the accuracy of a computer model (Oberkampf and Trucano 2002, McDermott et al. 2010). The analytical solutions could also help to identify causes of the discrepancies and to suggest necessary remedies.

Chapter 3 Analytical Model of Heat and Mass Transfer through Non-adiabatic High-rise Shafts during fires

The contents of this chapter are published in "Dahai Qi, Liangzhu Wang, Radu Zmeureanu. 2014. Analytical model of heat and mass transfer through non-adiabatic high-rise shafts during fires. International Journal of Heat and Mass Transfer 72: 585-594". The contents are slightly modified.

Abstract

Fire protection in high-rise buildings requires a good understanding of the physics of smoke spread so that control measures can be properly undertaken. The problem is often complicated by the coupled heat and mass transfer phenomena, especially when smoke spread through vertical shafts far from a fire origin. Numerical analysis is often challenging due to limited computer resources for such large structures. This study aims to develop an analytical model of the smoke movement through a high-rise shaft under two ventilation conditions: the shaft with a given constant smoke flow rate, and with the smoke purely driven by stack effect. A hand-calculation procedure is proposed to obtain the solution to the analytical model, and demonstrated in a case of a 40-storey building with a fire located at the 1st floor. The accuracy of the analytical model is confirmed by comparisons to a numerical simulation and three experiments in the literature. It was found that the calculated profiles of smoke temperatures and shaft wall temperatures depend on the temperature attenuation coefficient a, a non-dimensional parameter associated with the geometrical and thermal properties of the smoke and the shaft. The analytical solutions of the smoke temperatures and smoke flow rates were plotted at different fire floor temperatures in non-dimensional forms, which can be used for the design of shaft smoke controls. The effect of radiation heat transfer on the calculation results was also discussed through a sensitivity study of

the analytical model. It was found that the calculated smoke and shaft wall temperatures seem not quite sensitive to the radiation heat transfer in the case being studied.

3.1. Introduction

According to the National Fire Protection Association (NFPA) 101 Life Safety Code, a high-rise building is defined as a building with the height more than 23 m (roughly 7 stories) (NFPA 101 2012). Fires in high-rise buildings are often disastrous and cause huge amount of losses, if the buildings are not well protected against fires. The Winecoff Hotel fire at Atlanta, US (December 7, 1946) caused 119 deaths. The MGM Grand Hotel fire at Las Vegas, NV (November 21, 1980) led to the deaths of 85 people and the injuries of 600 people (Tamura 1994). The terrorist attack on the US World Trade Center on September 11, 2001 caused huge fires and subsequent building collapse accounting for the deaths of 2,783 people. Between 2005 and 2009 in the North America (Hall 2011), there were around 15,700 reported high-rise structure fires with the annually averaged losses of 53 people, 546 injuries, and $235 million in direct property damage. Historically, a high-rise fire is found more likely to happen in the lower floors according to the statistics (Hall 2011). It was reported that in the US between 2007 and 2011, 43% of fires in hotel buildings originated below the 2nd floor, and 73% below the 6th floor, and 37% of fires in office buildings originated below the 2nd floor, and 64% below the 7th floor. Driven by stack effect, the resultant smoke from fires may spread to the higher levels more easily via the vertical shafts, e.g. stairs, elevators, light wells, ventilation ducts, than through leakage openings in building structure. Here, the stack effect refers to buoyancy-driven airflows due to a difference of indoor/outdoor densities, which often occur in building chimneys and/or flue gas stacks. It was reported that smoke spread through shafts accounts for about 95% or more of the upward movement of smoke in typical high-rise buildings

(Tamura 1994). Therefore, much attention has been paid to the study of the smoke movement in vertical shafts.

The risk of high-rise fire smoke spreads is closely related to the location of neutral pressure level (*NPL*), where the shaft pressure is equal to that of the non-fire floor at the same height. Above a *NPL*, the shaft pressure is higher than the non-fire floor so smoke would enter the non-fire floor if there is a leakage (Klote 1991a). Klote presented a general method for the evaluation of the *NPL* for a space (e.g. a room or a shaft) connected to its surroundings by any number of openings based on the assumption that the temperature is uniform in the space (Klote 1991a). It was found that the *NPL* between a space and its surrounding is a weak function of the room temperature but a strong function of the size of openings. Further, the mass flow rate leaving a space due to stack effect strongly depends on the room temperature. To predict the quantity of smoke entering a shaft, Marshall (1986) developed an empirical equation based on the experiments in a 1/5 scale model of a fire compartment with a corridor and a 5-storey open shaft. Xiao, Tu, and Yeoh (2008) investigated numerically the effects of such dimensionless numbers as Grashof, Reynolds and Biot numbers on smoke flow rate and temperature field. However, for simplification, these studies and many of others often assumed adiabatic shaft walls and neglected heat transfer between smoke and shaft boundaries. In fact, the smoke temperature strongly depends on the heat exchange with the shaft walls and may vary significantly with the height (Black 2009; Sun et al. 2011). Wang, Black, and Zhao (2013) also found that an accurate estimation of the temperature profile in a shaft is crucial for the prediction of smoke movement during a fire, because the amount of smoke spreading through a shaft is closely coupled to the heat transfer during a fire.

Numerical simulations and experimental studies are the commonly used methods to study the coupled heat and mass transfer through building shafts. Popular numerical models used in the field

of building smoke control include but not limited to computational fluid dynamics (CFD), e.g. Fire Dynamics Simulator (McGrattan et al. 2013) and ANSYS FLUENT, and simpler models such as CONTAM (Dols and Polidoro 2015) and COSMO (i.e. COntrol of SMOke) (Black 2010). Black studied the smoke movement and control by using COSMO (Black 2009). Peppes, Santamouris, and Asimakopoulos (2001, 2002) conducted a series of experiments and CFD modeling studies, showing that the smoke mass flow rate and the heat transfer rate are a function of the average temperature difference between zones. However, both simulations and experiments are often costly, time consuming, and experience demanding. It is often impractical to model a whole high-rise building by CFD due to limited computer resources, or perform a costly full-scale field test. Sub-scale experiments may be possible but it is not a trivial job to maintain the similarity of scaled and full-size models. Therefore, designs of high-rise smoke controls often resort to hand calculation methods based on analytical models.

In the literatures, analytical solutions to the coupled heat and mass transfer through a high-rise shaft are relatively scarce. Some studies have touched upon the problem but were limited to non-fire scenarios. Yam, Li, and Zheng (2008) provided an analytical solution to the coupled thermal airflow problem in a naturally ventilated building. Yang et al. (2012, 2013) developed an analytical model of a naturally-ventilated shaft by assuming either constant temperature or heat flux at the interior surfaces of the shaft walls. It was found that the location of the neutral pressure level was strongly associated with the heat transfer at the shaft wall surfaces. During a fire, heat transfer in the shaft is quite different from non-fire cases. Fire smoke temperature can be an order of magnitude higher than surrounding air at the bottom of a shaft and drop quickly at the higher floors. The elevated smoke temperature would cause exacerbated convective and radiant heat transfer, which could be further enhanced by increased radiant emittance of the smoke loaded with

combustion products, e.g. carbon dioxide, water vapor and soot. Meanwhile, both shaft surface temperature and heat flux would vary significantly with the height of a shaft. Therefore, the previous studies of natural ventilation are not applicable. For high-rise fires, the studies by Sun et al. (2011) are probably most relevant. They developed an analytical model of the smoke plume rise in a shaft by neglecting radiant heat transfer, and by assuming that the shaft wall temperature was constant and equal to that of the exterior environment. As a result, the heat loss to the walls was exaggerated and the smoke temperature was under estimated (Sun et al. 2011).

This paper aims to develop an analytical model of the coupled heat and mass transfer of fire smoke through the vertical shafts of high-rise buildings. Analytical solutions are provided to the temperature profiles of the smoke and the shaft wall surfaces (both interior and exterior), the pressure distribution and the mass flow rate. We considered two scenarios of ventilation: a shaft with a mechanical exhaust system at a given constant smoke flow rate, and the other with only stack driven flow. For the case of mechanically ventilated shaft, the solution of the dimensionless temperature profiles of smoke and wall temperatures are derived as a function of a so-called temperature attenuation coefficient, which is a dimensionless number based on smoke mass flow rate, thermal and geometric properties of the shaft. When the smoke through the shaft is only driven by stack effect, a hand calculation method is reported for the prediction of pressure and temperature profiles, and smoke mass flow rate. The accuracy of the analytical model is confirmed by comparisons to a FDS simulation and three experiments in the literature. The method is then demonstrated for a 40-story building with a fire located at the 1st floor, in which radiation is neglected at first and its effect on the smoke movement is considered in a later section. This paper also discusses the effect of radiation heat transfer on the calculation results in a sensitivity study of the analytical model.

3.2. Building shaft with given smoke mass flow rate

For a mechanical smoke control system with a dedicated exhaust shaft (Klote et al. 2012), a ceiling exhaust fan maintains a constant smoke mass flow rate through the shaft. One of the worst scenarios is probably a fire located at the 1st floor and a bottom opening located at the ground level so that all floors could be exposed to smoke as shown in Fig. 3-1. To formulate the analytical model, we make the following assumptions:

- Smoke movement in the shaft is one-dimensional at steady state.
- The outdoor air temperature and the building temperature at non-fire floors are constant.
- Specific heat capacity of the smoke, C_p, is constant.
- The smoke is assumed to be incompressible and viscous but thermally expansible satisfying the ideal gas law.
- No smoke leaks through shaft wall Heat transfer coefficients (either due to convection or radiation) are constant and do not vary along the height of the shaft.

  The temperature of the fire floor is uniform and maintained at the fire smoke temperature (Tamura 1994 and Black 2009).

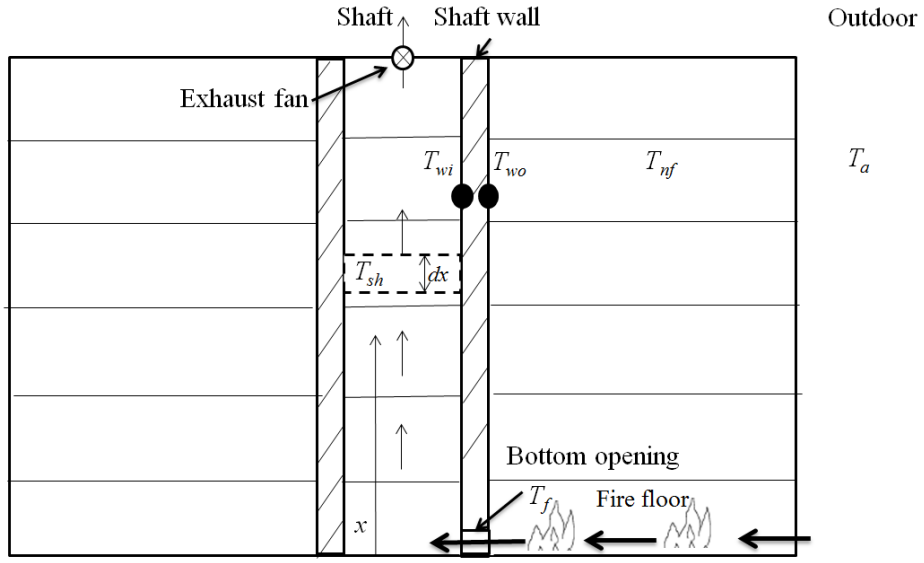

Figure 3-1 Schematic of a building with a ceiling exhaust fan with given flow rate

Applying the heat balance equation to the control volume inside the shaft spanning from the ground to any shaft height at x, we obtain Eq. (3-1).

$$\int_{T_f}^{Tshx} \dot{m} C_P dT_{sh} = -\int_0^x \frac{(T_{sh} - T_{nf}) P dx}{R_t} \tag{3-1}$$

where the thermal resistance

$$R_t = \frac{1}{h_{wi}} + \frac{W}{\lambda} + \frac{1}{h_{wo}} \tag{3-2}$$

Since h_{wi} and h_{wo} are assumed to be constant, R_t is constant. The solution to the smoke temperature at the height of x in the shaft, T_{shx}, can then be obtained by solving Eq. (3-1):

$$T_{shx} = T_{nf} + (T_f - T_{nf}) Exp\left(-\frac{Px}{\dot{m} C_P R_t}\right) \tag{3-3}$$

Eq. (3-3) can be written in a dimensionless form by defining a few dimensionless numbers as follows.

a) Dimensionless smoke temperature in the shaft:

$$\theta_{sh} = \frac{T_{shx} - T_{nf}}{T_f - T_{nf}} \tag{3-4}$$

b) Relative height:

$$\varphi = \frac{x}{H} \tag{3-5}$$

c) Temperature attenuation coefficient:

$$\alpha = \frac{PH}{\dot{m} C_P R_t} \tag{3-6}$$

Eq. (3-3) can then be rewritten in the non-dimensional form:

$$\theta_{sh} = Exp(-\varphi\alpha) \tag{3-7}$$

The temperature attenuation coefficient, α, is a dimensionless number that depends on smoke mass flow rate, thermal resistance between two sides of the shaft wall, and geometric features of the shaft (height and circumference of the shaft cross sectional area). It considers the heat transfer on both interior and exterior shaft walls, and solid wall conduction, which is different from the attenuation coefficient in the literatures (Sun et al. 2011), which only considered the convection on the interior shaft wall.

If we define the normalized temperature rise in the fire floor due to fire,

$$\eta = \frac{T_f - T_{nf}}{T_{nf}} \tag{3-8}$$

and the relative smoke temperature at the top of the shaft,

$$\gamma = \frac{T_{shH}}{T_{nf}} \tag{3-9}$$

which can be calculated from Eq. (3-3) for φ=1:

$$\gamma = 1 + \eta Exp(-\alpha) \tag{3-10}$$

For a control volume of the shaft located at the height of x, the heat fluxes through the shaft wall can be calculated from the heat transfer at the interior surface, through the wall, and at the exterior surface. Note that the heat transfer coefficients (h_{wi} and h_{wo}) do not vary along the height.

$$\dot{q}_x = \frac{T_{shx} - T_{nf}}{R_t} = h_{wi}(T_{shx} - T_{wix}) = \frac{\lambda}{W}(T_{wix} - T_{wox}) = h_{wo}(T_{wox} - T_{nf}) \tag{3-11}$$

From Eq. (3-11), the interior wall temperature of the shaft T_{wix} can be expressed as:

$$T_{wix} = T_{shx} - \frac{T_{shx} - T_{nf}}{h_{wi}R_t} \tag{3-12a}$$

Similarly, for the exterior shaft wall temperature, T_{wox}:

$$T_{wox} = T_{nf} + \frac{T_{shx} - T_{nf}}{h_{wo}R_t} \tag{3-12b}$$

The dimensionless interior shaft wall temperature can be obtained from Eq. (3-4) and Eq. (3-12a):

$$\theta_{wi} = \frac{T_{wix} - T_{nf}}{T_f - T_{nf}} = \left(1 - \frac{1}{h_{wi}R_t}\right)\theta_{sh} \tag{3-13}$$

Similarly, the dimensionless exterior shaft wall temperature is obtained as:

$$\theta_{wo} = \frac{T_{wox} - T_{nf}}{T_f - T_{nf}} = \frac{1}{h_{wo}R_t}\theta_{sh} \tag{3-14}$$

Sometimes the average values of temperatures are needed (e.g. for heat transfer coefficient calculations), which can be obtained by the integrations over the shaft height of Eq. (3-3) for the

average smoke temperature, $\overline{T_{sh}}$, Eq. (3-12a) for the average interior wall temperature, $\overline{T_{wi}}$, and Eq. (3-12b) for the average exterior wall temperature, $\overline{T_{wo}}$:

$$\overline{T_{sh}} = T_{nf}\left\{1+\frac{\eta}{\alpha}\left[1-Exp(-\alpha)\right]\right\} \tag{3-15}$$

$$\overline{T_{wi}} = T_{nf}\left[1+\frac{\eta}{\alpha}\left(1-\frac{1}{h_{wi}R_t}\right)\left(1-Exp(-\alpha)\right)\right] \tag{3-16}$$

$$\overline{T_{wo}} = T_{nf}\left[1+\frac{\eta}{\alpha}\frac{1}{h_{wo}R_t}\left(1-Exp(-\alpha)\right)\right] \tag{3-17}$$

To confirm the accuracy of the above analytical model of a building shaft with given mass flow rate, we compared the analytical solution of a high-rise building to a numerical simulation by FDS, which is a popular CFD model based on large eddy simulation (LES) for fire dynamics and smoke movement (McGrattan et al. 2013). The modeled shaft is with a height of 50 m, a cross section of 5 m × 1.6 m, and a wall thickness of 0.24 m. The conductive heat transfer coefficient is 10 W/(m^2·K), the smoke mass flow rate in the shaft is 12 kg/s and T_{sh0} is 973.15K. In FDS, a grid size of 0.32 m × 0.33 m × 0.33 m is adopted after a grid independence study. The FDS simulation takes 20 minutes on a 2.40 GHz processor and 4GB memory PC. Time-averaged temperatures of the shaft cross section for every 5 m are monitored in FDS, including T_{sh}, T_{wi} and T_{wo}. Both convective and radiative heat transfer are considered here, and the calculation method for the heat transfer coefficients is introduced in a later section of this paper. Fig. 3-2 compares the predicted temperature profiles by the analytical model and FDS. The largest average relative difference occurs at the interior wall surface, which is 3% (about 20 K). The discrepancy is not significant when considering many differences of FDS and the analytical model. Therefore, the accuracy of the above analytical model is confirmed.

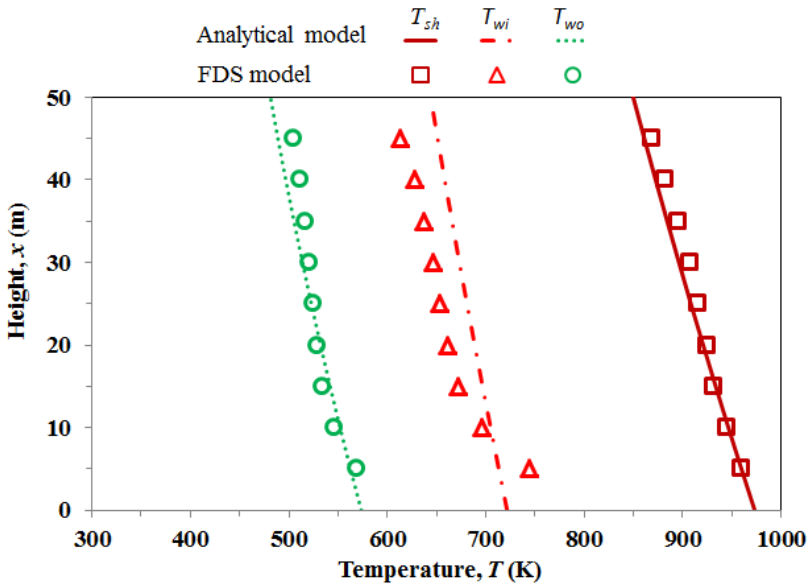

Figure 3-2 Comparison of the calculated temperatures by the analytical model and FDS

Meanwhile, a few major conclusions can be made from the analytical model. For a given smoke mass flow through a shaft, Eq. (3-7) illustrates that the smoke temperature is an exponential function of the product of dimensionless height and temperature attenuation coefficient. The exponential temperature profile is consistent to the predictions by some numerical models in the literatures. Wang, Black, and Zhao (2013) modeled a forty-storey building with four stairwell shafts by COSMO and found that the shaft temperature cannot be simplified as a linear profile but in fact follows a curve similar to an exponential distribution. It also shows that the temperature profile can become linear for small values of α by plotting Eq. (3-7) as shown in Fig. 3-3. When α is small enough, e.g. less than 0.3, the smoke temperature profile approaches linear. When α is large enough (e.g. $\alpha \geq 100$), the entire shaft temperature is almost uniform and close to the non-fire floor temperature, T_{nf}, and as well the temperature only decreases within the height of *0.05H*. This can be explained by that a large α value could indicate a small smoke mass flow or low thermal resistances of the walls so the effect of the fire smoke on the shaft temperature becomes

minimal. When α is very small (e.g. $\alpha \leq 0.05$), the smoke temperature also becomes uniform but close to fire floor temperature, T_f, due to the domination of a high smoke flow in the shaft or a high thermal insulation of the shaft walls. Therefore, Eq. (3-7) and its illustration in Fig. 3-3 provide the quantitative description of the transition of the shaft smoke temperature with the physical and geometrical properties of the shaft. One immediate application is the use of the temperature profile as the initial guess of the smoke/air temperatures in a shaft in a fire computer model or in a computer model of naturally ventilated buildings. Moreover, both interior and exterior shaft wall temperatures are a function of α as shown by Eqs. (3-13) and (3-14), which can also be used as initial guesses of boundary conditions in fire computer models.

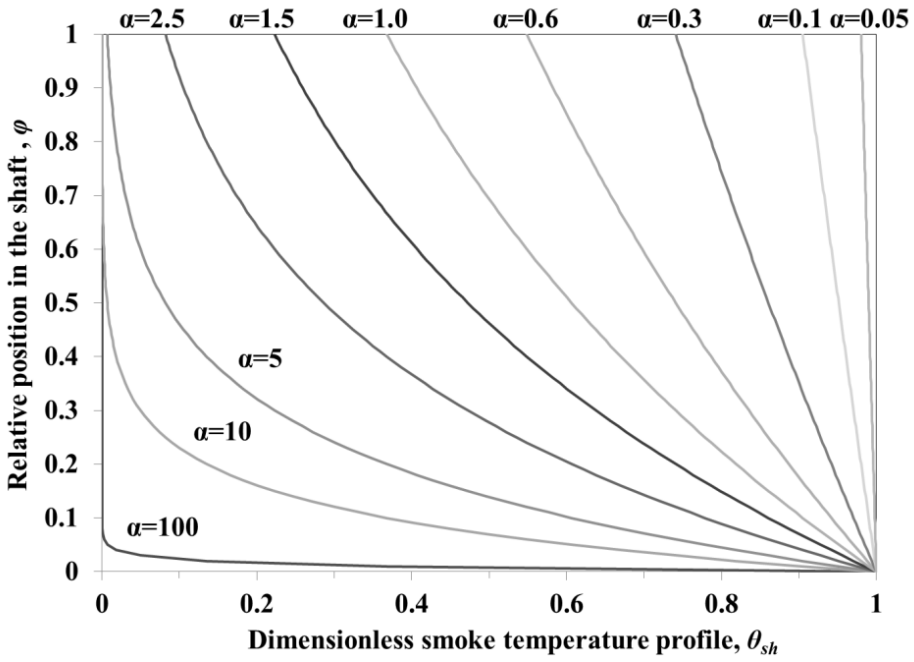

Figure 3-3 Dimensionless smoke temperature profile

The temperature at the top of the shaft, T_{shH}, is important for the selection of smoke exhaust fan installed at the shaft top (Klote et al. 2012) for the consideration of the safe operation of the fan. The EN 12101-3 standard of the European Committee for Standardization (EN 12101-3 Standard

2002) classifies smoke exhaust fans by temperatures, e.g. the type F200 fan must resist 200 ˚C for at least two hours. Eq. (3-10) shows that the shaft top temperature depends on fire and background temperature, and temperature attenuation coefficient, as plotted in Fig. 3-4. When $\alpha \geqslant 10$, γ equals to one, indicating that the smoke temperature at the shaft top is close to the non-fire floor temperature, T_{nf}, so the effect of fire is minimal. When α is small enough, e.g. less than 0.05, the whole shaft temperature is close to the fire floor temperature T_f. In the context of dimensions, for a shaft with the perimeter of P = 5 m and the height of H = 50 m, and the thermal resistance of R_t = 0.224 (m^2·K)/W, the temperature at the top of the shaft will approach the non-fire floor temperature for a smoke flow less than 1.1 kg/s, and reach the fire floor temperature for a smoke flow greater than 22.2 kg/s. If the EN 12101-3 type F200 fan is used in the same shaft, the allowable γ based on the safety smoke temperature of 200 ˚C will be about 1.6 as shown by the dashed line in Fig. 3-4. For a given exhaust fan (thus a given α), there always exists a maximally allowable fire temperature. For example, for an exhaust fan with a given flow rate of 1.6 kg/s (α = 0.7), the maximally allowable fire would be η = 1.2 (i.e. 374 ˚C), as illustrated by the circle in Fig. 3-3. This means that the F200 fan could only stands a fire smoke of 374 ˚C. The solution can be a change of another fan with higher temperature rating or an addition of another F200 fan to share the smoke flow rate. Therefore, Fig. 3-4 could be used in practice to evaluate the thermal performance of mechanical exhaust fans installed at the shaft top.

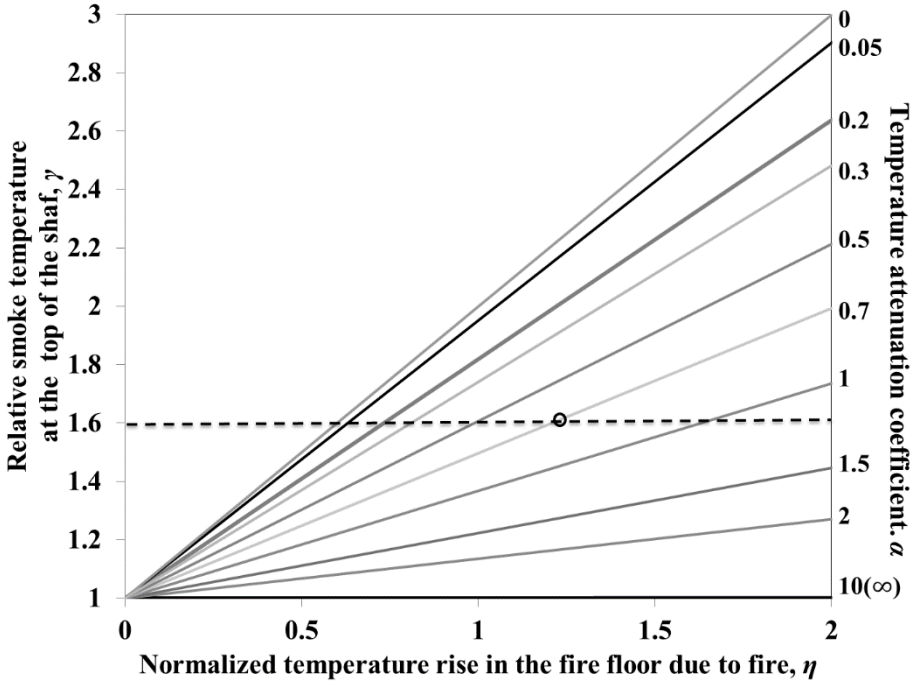

Figure 3-4 Relative smoke temperature at the top of the shaft

3.3. Building shaft with smoke driven by stack effect only

If a shaft has no mechanical exhaust system, the smoke flow in the shaft is only driven by stack effect as shown in Fig. 3-1, where the exhaust fan is replaced by an opening at the top. The smoke movement driven only by stack effect is also of particular interests because it helps to understand the transport route of the smoke and aids the deployment of active smoke control measures. In a stack-driven flow, the solution to temperature and pressure profiles, as well as mass flow rate through a shaft is a coupled problem of heat and mass transfer. The calculation of the temperature profiles is based on the same equations, Eqs. (3-7), (3-13) and (3-14), in the previous section. Here, we focus on how to obtain the pressure profile and the resultant smoke mass flow rate in the shaft.

For incompressible and viscous flow at steady state, the mechanical energy equation (Munson et al. 2009) for the control volume in Fig. 3-1 can be obtained.

$$dp + \frac{\rho}{2} dv^2 + \rho g dx + \rho g dh_L = 0 \tag{3-18}$$

where dh_L is the friction head loss

$$dh_L = f \frac{1}{D_h} \frac{v^2}{2g} dx \tag{3-19}$$

D_h is the hydraulic diameter of the shaft and can be calculated by Eq. (3-20).

$$D_h = \frac{4A_h}{P} \tag{3-20}$$

The friction factor of a shaft, f, can be calculated by an alternative form of the Colebrook formula for the fully rough region (Klote et al. 2012).

$$f = \frac{1}{\left[1.14 + 2\log_{10}\left(D_h / \varepsilon\right)\right]^2} \tag{3-21}$$

Integrating Eq. (3-18) from the ground level to any shaft height of x, we get

$$\int_{p_{sh0}}^{p_{shx}} dp + \int_{v_0}^{v_x} \frac{\rho}{2} dv^2 + \int_0^x \rho g dx + \int_0^x \rho g dh_L = \Delta p_{shx} + \Delta p_{dyx} + \Delta p_{elx} + \Delta p_{frx} \tag{3-22}$$

so the pressure at the height of x is:

$$p_{shx} = p_{sh0} - \Delta p_{dyx} - \Delta p_{elx} - \Delta p_{frx} \tag{3-23}$$

Where

$$\Delta p_{shx} = p_{shx} - p_{sh0} \tag{3-24}$$

$$\Delta p_{dyx} = \int_{v_0}^{v_x} \frac{\rho}{2} dv^2 = \frac{\dot{m}^2 R}{p_{a0} A_h^{\,2}} \left(T_{shx} - T_f\right) = \frac{\dot{m}^2 R\left(T_f - T_{nf}\right)}{p_{a0} A_h^{\,2}} \left[Exp\left(-\alpha x / H\right) - 1\right] \tag{3-25}$$

$$\Delta p_{elx} = \int_0^x \rho g\, dx = \int_0^x \frac{g p_{a0}}{R T_{shx}} dx$$
$$= \frac{g p_{a0} H}{R T_{nf}} \left\{ \frac{\dot{m} C_p R_t}{PH} \ln \left[\frac{(T_f - T_{nf}) + T_{nf} EXP\left(\frac{Px}{\dot{m} C_p R_t} \right)}{T_f} \right] \right\} \tag{3-26}$$
$$= \frac{g p_{a0} H}{R T_{nf}} \left\{ \frac{1}{\alpha} \ln \left[\frac{EXP(\alpha x / H) + \eta}{1 + \eta} \right] \right\}$$

$$\Delta p_{frx} = \int_0^x f \frac{1}{D_h} \frac{\rho v^2}{2} dx = \frac{f \dot{m}^2 R}{2 D_h A_h^{\,2} p_{a0}} \int_0^x T_{shx} dx$$
$$= \frac{f \dot{m}^2 R H T_{nf}}{2 D_h A_h^{\,2} p_{a0}} \left\{ \frac{x}{H} + \frac{\dot{m} C_p R_t}{PH} \frac{T_f - T_{nf}}{T_{nf}} \left[1 - EXP\left(\frac{-xP}{\dot{m} C_p R_t} \right) \right] \right\} \tag{3-27}$$
$$= \frac{f \dot{m}^2 R H T_{nf}}{2 D_h A_h^{\,2} p_{a0}} \left\{ \frac{x}{H} + \frac{\eta}{\alpha} \left[1 - EXP(-\alpha x / H) \right] \right\}$$

The smoke mass or volumetric flow rates through the bottom and the top openings of the shaft can be calculated by the orifice equation (Klote et al. 2012).

$$\dot{m}_b = C_d A_b \sqrt{2 \rho_f (p_f - p_{sh0})} = C_d A_b \sqrt{2 (p_f - p_{sh0}) p_{a0} / (R T_f)} \tag{3-28a}$$

$$\dot{m}_t = \dot{m}_b = C_d A_t \sqrt{2 \rho_{shH} (p_{shH} - p_{aH})} = C_d A_t \sqrt{2 (p_{shH} - p_{aH}) p_{a0} / \left(R T_{shH} \right)} \tag{3-28b}$$

$$Q_t = C_d A_t \sqrt{2 (p_{shH} - p_{aH}) / \rho_{shH}} \tag{3-28c}$$

where the outdoor pressure at the shaft top, p_{aH}, can be calculated by the lapse rate method (Munson et al. 2009) or here the hydrostatics for simplification:

$$p_{aH} = p_{a0} - \rho_a g H \tag{3-29}$$

Based on Eq. (3-28a), the pressure at the bottom of the shaft p_{sh0} can be calculated by

$$p_{sh0} = p_f - \frac{\dot{m}_b^{\,2}}{\left(C_d A_b \right)^2 (2 \rho_f)} = p_f - \frac{\dot{m}_b^{\,2} R T_f}{\left(C_d A_b \right)^2 2 p_f} \tag{3-30}$$

The fire floor pressure, p_f, can be obtained from Eq. (3-31). The neutral pressure level of the fire floor is assumed at the middle height as suggested by Tamura (1994).

$$p_f = p_a - \Delta p_f = p_a - g(x - x_{np})\rho_a \frac{(T_f - T_a)}{T_f} \tag{3-31}$$

The analytical model includes three equations: the heat balance equation of Eq. (3-1), the mechanical energy equation of Eq. (3-18), and the mass balance equation of Eqs. (3-28a), (3-28b). To combine these three equations into one equation, we take p_{shH}, p_{aH} and T_{shH} into Eq. (3-28b), and get

$$\begin{aligned} \dot{m} &= C_d A_t \sqrt{2(p_{shH} - p_{aH}) p_{a0} / (RT_{shH})} \\ &= C_d A_t \sqrt{\frac{2[(p_{sh0} - \Delta p_{dyH} - \Delta p_{elH} - \Delta p_{frH}) - (p_{a0} - \rho_a g H)] p_{a0}}{RT_{nf}\gamma}} \end{aligned} \tag{3-32}$$

where $\dot{m}=\dot{m}_b=\dot{m}_t$. p_{sh0}, Δp_{dyH}, Δp_{elH}, Δp_{frH}, and γ can be obtained from Eqs. (3-30), (3-25), (3-26), (3-27) and (3-9) respectively. Eq. (3-32) is an implicit function of $\dot{m}$ so it cannot be solved directly. The solution to such a coupled problem often needs an iterative procedure. Since most of the design methods in building smoke control rely on hand calculations, we propose an iterative method but following a hand calculation procedure to obtain the solution.

Given the superscript indicates the current iteration:

(i) Get R_t, p_{aH} and p_f by Eqs. (3-2), (3-29) and (3-31) respectively.

(ii) Get $\alpha^{(1)}$ by estimating smoke mass flow rate $\dot{m}_{bot}^{(1)}$, and calculate $\alpha^{(1)}$ by Eq. (3-6).

(iii) Get $p_{shH}^{(1)}$ by calculating $p_{sh0}^{(1)}$ using Eq. (3-30), calculate $\Delta p_{dyx}^{(1)}$, $\Delta p_{elx}^{(1)}$and $\Delta p_{frx}^{(1)}$ by Eqs. (3-25) ~ (3-27), and then calculate $p_{shH}^{(1)}$ by Eq. (3-23) when $x = H$.

(iv) Get $\dot{m}_t^{(1)}$ by calculating $T_{shH}^{(1)}$ using Eq. (3-7), and calculate $\dot{m}_t^{(1)}$ by Eq. (3-28b).

(v) If $|\dot{m}_t^{(1)}-\dot{m}_b^{(1)}|/\dot{m}_t^{(1)}$ is over a convergence threshold, let $\dot{m}_b^{(2)}= (\dot{m}_t^{(1)}+\dot{m}_b^{(1)})/2$, and then return to steps (ii) – (v) till the convergence is reached.

(vi) Obtain α, θ_{sh}, θ_{wi}, θ_{wo} and p_{shx} using Eqs. (3-6), (3-7), (3-13), (3-14) and (3-23), respectively.

To confirm the accuracy of the above analytical model, we employed the experiments in the literature based on a 1/3 scale stairwell (Ji et al. 2013). The stairwell physical model has 12 floors with a floor height of 1 m except 1.2 m for the ground floor, and with a cross sectional area of 1.5 m × 1.0 m (L × W). Three experiments were selected here for different sizes of Methanol fires located at the ground floor, differentiated by the square pool size of 10 cm × 10 cm, 20 cm × 20 cm and 30 cm × 30 cm. The measured corresponding smoke temperature at the ground level is 293 K, 310 K and 346 K, respectively, which were used as T_{sh0} in the analytical model. T_{nf} and T_a in the analytical model are set to the measured ambient temperature of 279.15 K. Fig. 3-5 compares the smoke temperatures and mass flow rates of the experiment and the analytical model. The largest temperature difference is 16 K for the pool size of 30 cm × 30 cm, and the largest relative difference of mass flow rate is 20% for 10 cm × 10 cm. So the results of the analytical model are close to those of the experiments.

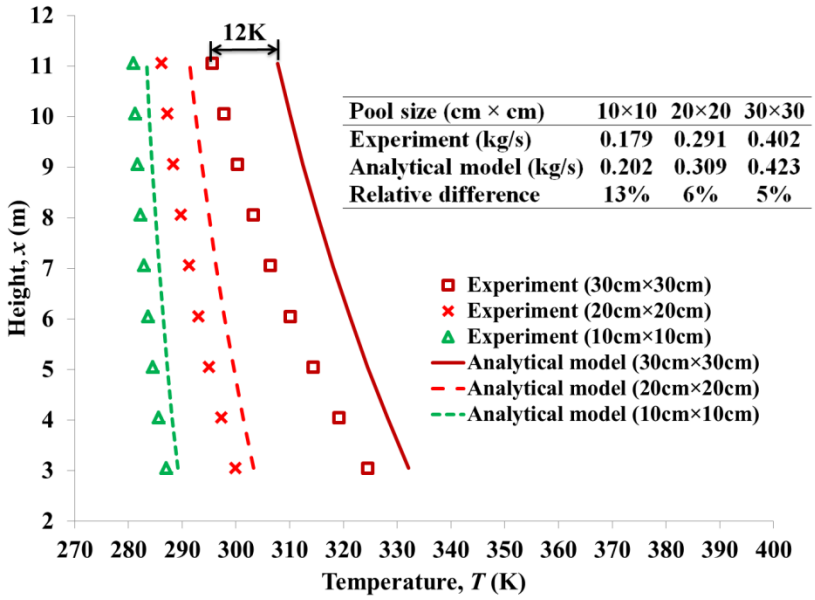

Figure 3-5 Comparison of smoke temperatures (lines) and mass flow rates (table) of the experiment (Ji et al. 2013) the analytical model

The above procedure of hand calculation method is demonstrated by a case study of a 40-storey concrete building with a shaft, which is similar to the building in Fig. 3-1 but without the exhaust fan. In the building, all the non-fire floors are assumed to have openings uniformly distributed above and below the mid-height without significant internal resistance as suggested by the literature (ASHRAE 2009). Therefore the pressures of the non-fire floors thus distribute hydrostatically as calculated by Eq. (3-33), which is not used to develop analytical model but calculate the non-fire floor pressure and study the NPL of the shaft in this case. Stronger stack effect in the shaft can be created by lower outdoor temperature. To model one of the worst scenarios of smoke spreads, the outdoor temperature is chose as 253.15 K, representing a winter condition. The analytical model can be applied to summer conditions, which were not included here due to page limit. Table 3-1 lists all the parameters for the calculation of the case study.

$$p_{nfx} = p_{a,H/2} - \rho_{nf} g\left(x - \frac{H}{2}\right) \tag{3-33}$$

In this case, for simplicity, radiation heat transfer was neglected but its effects on the calculation results will be discussed in a later section. The convective heat transfer coefficient h_{wc} at the shaft surfaces is obtained by combing natural and forced convection correlations (McGrattan et al. 2013) as Eq. (3-34) shows, which is employed by Fire Dynamics Simulator (FDS) to calculate convective heat transfer. The value of C_1 is 1.52 and 1.31 for a horizontal and vertical surface respectively in FDS, which has been verified and validated (McGrattan et al. 2013) for smoke flows and was employed in this case. While Musser, McGrattan, and Palmer (2001) and Qi, Wang, and Zmeureanu (2014b) suggested that C_1 is 4.05 and 3.08 for a horizontal and vertical surface respectively for indoor airflows by comparing the results of FDS and experiments.

$$h_{wc} = \max\left[C_1 |\Delta T_w|^{1/3}, \quad 0.037\frac{k}{l}\mathrm{Re}^{4/5}\,\mathrm{Pr}^{1/3}\right] \tag{3-34}$$

where

$$\mathrm{Re} = \frac{\rho v l}{\mu} \tag{3-35}$$

$$\mathrm{Pr} = \frac{\nu}{a} \tag{3-36}$$

For the shaft interior surface $h_{wc} = h_{wic}$, and for the shaft exterior surface $h_{wc} = h_{woc}$. For the interior surface, $|\Delta T_w| = |\Delta T_{wi}| = |\overline{T_{sh}} - \overline{T_{wi}}|$, which is the average temperature difference of the smoke and the shaft interior surface. h_{woc} can be calculated in the same way. Since the convective heat transfer coefficients depend on temperatures, h_{wc} and R_t should be updated at each iteration.

Table 3-1 Parameters of the case study of a 40-storey high-rise with a shaft (Fig. 3-1)

List of parameters	Values
A. Fire conditions	
Fire floor Temperature	300~1000 K
B. Atmospheric conditions	
Outdoor temperature	253.15 K
Outdoor pressure at the level of ground	101325 Pa
C. Building conditions	
Number of floor	40 [a]
Height of each floor	4 m [a]
Non-fire floor temperature	294.15 K
D. Shaft conditions	
Height	160 m [a]
Roughness	3.0 mm [b]
Cross section	2.66 m × 19.2 m [a]
Shaft wall width	0.24 m
Bottom opening area	1 m^2
Top opening area	1 m^2
Discharge coefficient	0.6
Material of shaft	Concrete
Conduction heat transfer coefficient	1.7 W/ (m·K) [c]

[a] Sizes of building and shaft are selected from Wang, Black, and Zhao (2013)
[b] Roughness of shaft is selected from Klote et al. (2012)
[c] Conduction heat transfer coefficient is selected from Guo et al. (2011)

The iterative procedure is demonstrated for the fire floor temperature of 475.15 K, based on which p_f is calculated as 101312.2 Pa by using Eq. (3-31). At the 1st iteration, $\dot{m}^{(1)}$ and $R_t^{(1)}$ is 0.1 kg/s and 0.34 (m^2·K)/W, respectively when both $h_{wic}^{(1)}$ and $h_{woc}^{(1)}$ are estimated to be 10 W/(m^2·K). Given a convergence threshold of 0.2%, five iterations are needed as shown in Table 3-2.

Table 3-2 Results of iteration by hand calculation

Iteration	$\dot{m}_b$ (kg/s)	R_t ((m^2·K)/W)	α	P_{shH} (Pa)	$\dot{m}_t$ (kg/s)	$\left\|\dot{m}_t^{(1)} - \dot{m}_b^{(1)}\right\| / \dot{m}_t^{(1)}$
1	0.10	0.34	204.32	99434	16.05	99.4%
2	8.08	2.52	0.34	99951	22.14	63.5%
3	15.11	0.51	0.91	99537	16.67	9.4%
4	15.89	0.58	0.78	99516	16.00	0.7%
5	15.95	0.56	0.78	99512	15.92	0.2%

We also collected the total numbers of iterations to reach convergence under different thresholds and for different fire temperatures as shown in Fig. 3-6. The calculation does not exceed eight iterations for the threshold of 0.2%, six for 1%, four for 5% and 10% for the fire temperature from 300 to 1000 K. Therefore, the hand calculation method can be used for practical engineering applications.

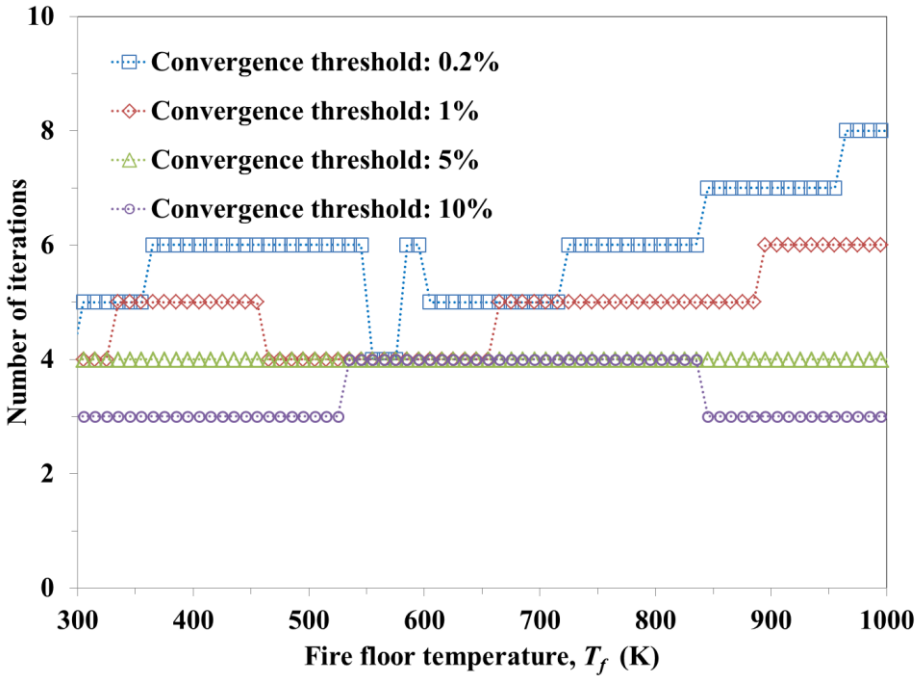

Figure 3-6 Numbers of iterations for different fire temperature and convergence thresholds

The analytical model not only provides a simple method for design calculations but also aids the understanding of high-rise smoke movement. A few observations were achieved in the following section.

Fig. 3-7 shows the variations of the smoke mass and volumetric flow rates with different fire temperatures in the case study. The volumetric flow rate Q increases with the fire temperature T_f because a stronger fire results in greater buoyancy/stack effect and thus more smoke entering the shaft. The mass flow rate $\dot{m}$, however, also depends on the smoke density, which decreases with the smoke temperature. As a result, there exists a maximum value of $\dot{m}$ as shown in Fig. 3-7. In the 40-storey building with specific shaft geometry and thermal properties, the maximum mass flow rate is 16.2 kg/s for the corresponding T_f of around 555 K. Most of the makeup air of the smoke could come from the outdoor through the fire floor and/or the non-fire floors due to mass balance. Excessive makeup air could accelerate fire growth. Therefore, the existence of such a

maximum fire temperature and the corresponding maximum smoke mass flow rate could be an important reference for the design of fire protection system, for the understanding of the effect of high-rise shaft on the burning conditions at the fire floor, and consequently for the design of active fire protection systems at the fire floor. The practical implications of the results are beyond the scope this paper but can be covered in another study later.

The analytical model also provides important information on the risk assessment of the smoke spread from the fire floor to higher floors mostly in terms of the location of the NPL. Fig. 3-8 shows the pressure profiles for the fire temperature of 375.15, 475.15 and 575.15 K. With the increase of fire temperature, the overall shaft smoke temperature increases so the pressure difference from the bottom to the top of the shaft becomes smaller. The location of NPL thus increases with the fire temperature. In the current case, the NPL is 78 m for the fire of 375.15 K, 84 m for 475.15 K, and 90 m for 575.15 K. Smoke could enter non-fire floors above the NPL so a higher NPL could result in a smaller section of non-fire floors subject to the smoke. However, with the increase of the fire temperature, the elevated pressure difference above the NPL (Fig. 3-8) could cause more smoke entry to these floors. Therefore, a detailed analysis should combine all these effects based on the results from the current analytical model, which is beyond the scope of this study but can be addressed in more details later.

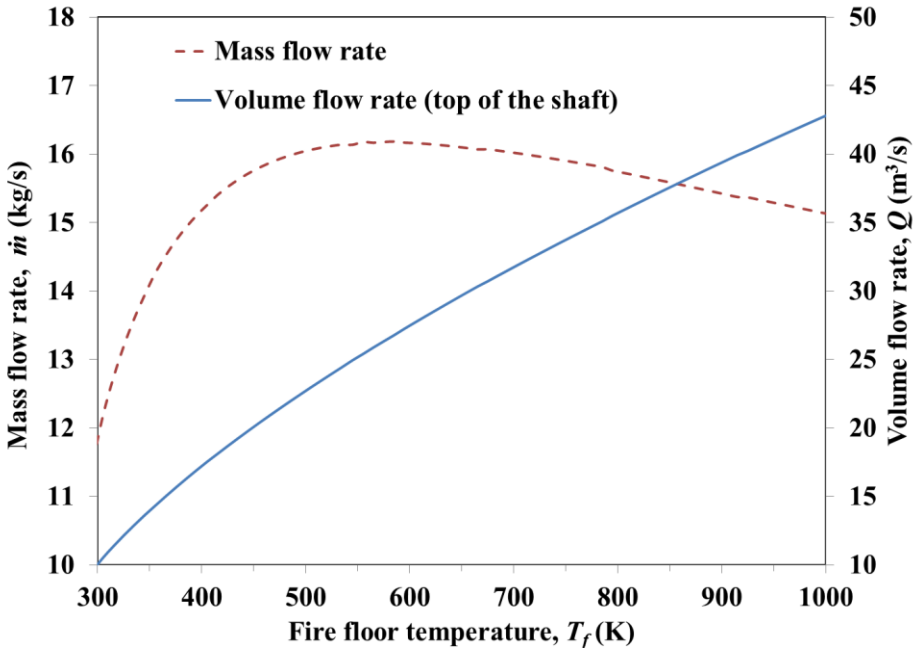

Figure 3-7 Variation of flow rate with different fire floor temperatures

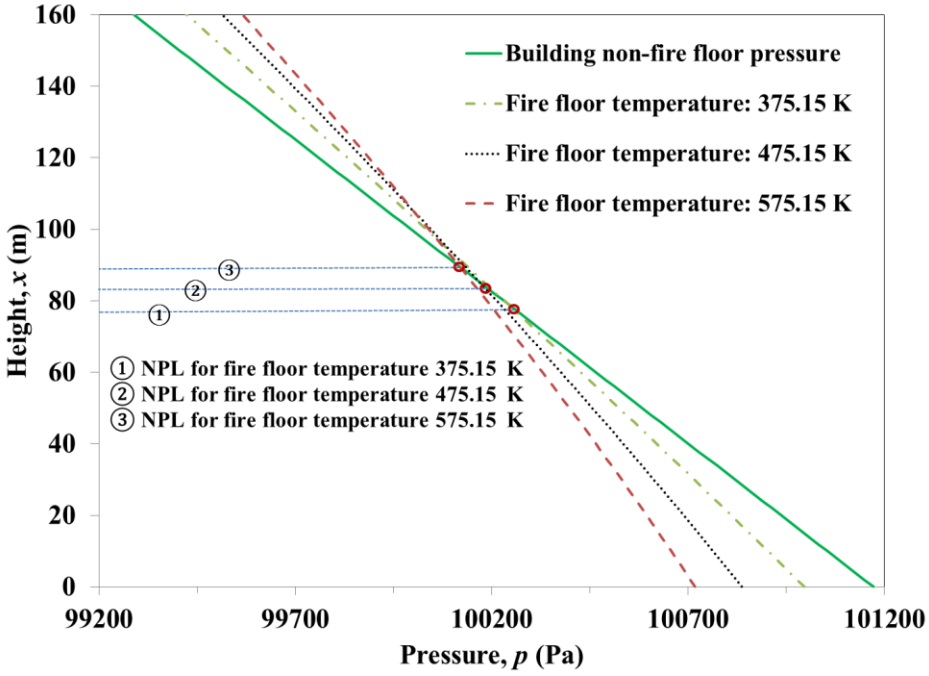

Figure 3-8 Pressure profiles for different fire floor temperatures

3.4. Discussion

The case study only considers convective heat transfer but neglect radiation, which could be significant during smoke spread. To apply the same method as convection, this study uses radiant heat transfer coefficient to calculate radiation. Compared to convective heat transfer coefficient, e.g. Eq. (3-34), radiant heat transfer coefficient depends on more factors, e.g. the geometry of the shaft, gas compositions, gas and wall temperatures. Previous studies of analytical solutions often neglected radiation (Sun et al. 2011; Ji et al. 2013), in which the effects of the neglecting were not provided either. In this study, we discuss the effect of radiant heat transfer on the temperature distributions with/without radiation through a sensitivity study of radiant heat transfer coefficients.

The same 40-storey building was used here for three different fire temperatures of 973.15 K (case 1), 773.15 K (case 2) and 573.15 K (case 3). The total heat transfer coefficients, h_{wi} and h_{wo} are the sum of convective heat transfer coefficient and radiant heat transfer coefficient as Eqs. (3-37) and (3-41) show. The convective heat transfer coefficients, h_{wic} and h_{woc} are still calculated by Eq. (3-34). For the radiation calculation, the smoke is assumed hot gas composed of water vapor and carbon dioxide so the radiant heat transfer coefficient at the shaft interior wall could be calculated by Eqs. (3-38) ~ (3-40) (Siegel and Howell 1993). The details about a_i, k_i, L_e, C_{CO_2}, and ε_g can be found in the literature(Siegel and Howell 1993). In real cases, a fire smoke can be loaded with many other gases and/or soot, causing a higher radiation heat transfer. However, the method presented here still applies if the radiant heat transfer coefficient can be provided. For the shaft exterior wall, when the surface temperature is high, the radiation to the surrounding air inside the building could become significant. The radiant heat transfer coefficient h_{wor} could be calculated by Eq. (3-42) (Hutcheon and Handegord 1983) with ε_w assumed one in this study.

$$h_{wi} = h_{wic} + h_{wir} \tag{3-37}$$

$$h_{wir} = \frac{\sigma\left[\varepsilon_g \overline{T_{sh}}^4 - a_g \overline{T_{wi}}^4\right]}{\overline{T_{sh}} - \overline{T_{wi}}} \tag{3-38}$$

where ε_g can be obtained from the weighted sum of gray gases model:

$$\varepsilon_g = \sum_{i=1}^{n} a_i - \sum_{i=1}^{n} a_i e^{-k_i p L_e} \tag{3-39}$$

$$a_g = a_{CO_2} = C_{CO_2} \varepsilon_{CO_2} \left(\frac{\overline{T_{sh}}}{\overline{T_{wi}}} \right)^{0.5} \tag{3-40}$$

$$h_{wo} = h_{woc} + h_{wor} \tag{3-41}$$

where $h_{wor} = \varepsilon_w \sigma \dfrac{\overline{T_{wo}}^4 - T_{nf}{}^4}{\overline{T_{wo}} - T_{nf}}$ (3-42)

Fig. 3-9 illustrates the temperature profiles for the highest fire temperature of 973.15 K (case 1), in which the results with/without radiation are mostly significant among all three cases. When the radiation is considered, the smoke temperature decreases due to a lower heat resistance, R_t. The temperature attenuation coefficient, α, increases accordingly so the temperature gradient at the shaft bottom becomes greater, compared to the case with convection only (see Eq. (3-7) and Fig. 3-3). For the exterior surface temperature of the shaft, $T_{wox} = T_{nf} + \dot{q}_x / h_{wo}$ (Eq. (3-11)). When radiation is considered, T_{wox} decreases because $\overline{\dot{q}_x} / h_{wo}$ is reduced from 142 K to 85.5 K (Table 3-3). The average wall temperature, $\overline{T_{wo}}$, thus decrease as shown in Fig. 3-9. The interior wall temperature also drops with the exterior due to the heat conduction through the wall.

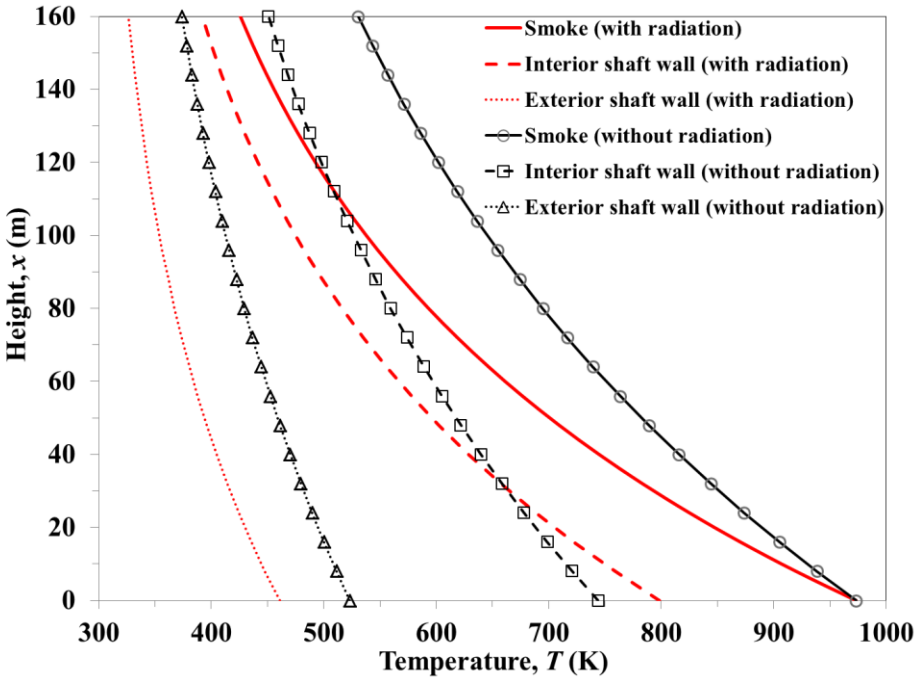

Figure 3-9 Comparison of temperature profiles with/without radiation for the fire temperature of 973.15 K (case1)

Table 3-3 Comparison of the results with/without radiation in case 1

	h_{wo} (W/(m^2·K))	$\dot{m}$ (kg/s)	T_f-T_{shH} (K)	$\overline{\dot{q}_x}$ (W/m^2)	$\overline{\dot{q}_x}/h_{wo}$ (K)
Without radiation	6.8	15.2	443	966	142
With radiation	14.3	15	547	1180	85.5

To quantify the difference of the predicted temperatures with radiation, $T_{c\&r}$, and without radiation, T_c, this study use normalized mean square error (NMSE) (ASTM D5157-97 2008).

$$NMSE = \frac{1}{\overline{T_c}\,\overline{T_{c\&r}}}\left[\frac{1}{n}\sum_{i=1}^{n}\left(T_{c,i} - T_{c\&r,i}\right)^2\right] \tag{3-43}$$

The calculated temperatures at every eight meters in the shaft were used to calculate the NMSE. Table 3-4 lists the NMSEs for T_{sh}, T_{wi} and T_{wo}. It shows that the largest difference is 1.8% for the

smoke temperature in case 1, which corresponds to an average temperature difference of 84 K. The difference seems insignificant in case 3, in which the average difference is 28 K. In all three cases, the difference with/without radiation is less than 2.2%, which is probably due to the use of Kelvin in the denominator in Eq. (3-43). The radiation also seems to affect the smoke and the exterior wall temperatures more than the interior wall temperature. This may be caused by the assumption that the air temperature near the exterior shaft wall temperature T_{nf} is constant so the radiation influenced T_{wo} more than T_{wi}.

Table 3-4 Deviation of temperatures profiles when radiation is considered and not considered

	For T_{sh}		For T_{wi}		For T_{wo}	
Case	NMSE (%)	Average temperature difference (K)	NMSE (%)	Average temperature difference (K)	NMSE (%)	Average temperature Difference (K)
Case 1 (973.15 K)	1.8	84	0.6	29	2.2	59
Case 2 (773.15 K)	1.0	54	0.4	24	1.4	45
Case 3 (573.15 K)	0.4	28	0.2	17	0.7	29

The radiant heat transfer coefficient at the shaft interior wall h_{wir} accounts for the major temperature decrease of the smoke when radiation is considered. Therefore, we studied the sensitivity of h_{wir} with a variation of $\pm 20\%$, $\pm 50\%$ and $\pm 100\%$ for case 1. Table 3-5 shows the calculated NMSEs of the predicted temperatures in different cases. It is found that the change of

h_{wir} affects the smoke and the interior wall temperatures more than the exterior as expected. In this case, the over-estimations of h_{wir} generally cause fewer changes than the under-estimations when the radiation was considered. The largest variation (0.57%) occurs when h_{wir} is 100% under-estimated in this case, corresponding to an average temperature deviation of only 46 K. Therefore, the temperature predictions seem not quite sensitive to the change of radiant heat transfer coefficient in this case.

Table 3-5 NMSEs of predicted temperatures for different radiant heat transfer coefficients

Case	Temperature profile	Variations of radiant heat transfer coefficient h_{wir} (%)					
		-100%	-50%	-20%	20%	50%	100%
Case 1 (973.15 K)	For T_{sh}	0.57	0.09	0.01	0.01	0.04	0.12
	For T_{wi}	0.54	0.08	0.01	0.01	0.04	0.11
	For T_{wo}	0.10	0.02	0.00	0.00	0.01	0.02

Note that among other cases when radiation is considered, heat transfer coefficients may vary significantly along the shaft height, because radiation is the fourth order of absolute temperatures. In this case, the assumption that heat transfer coefficients do not vary along the height may not be applicable. However, the limitation could be overcome by dividing the shaft into several vertical sub-sections, for each of which the foregoing analytical model can be applied with different heat transfer coefficients.

3.5. Conclusion

This study developed an analytical model for the smoke spread through a vertical shaft in a high-rise building during fires when the shaft is with a given constant smoke flow rate and with the

smoke purely driven by stack effect. The associated equations include heat and mass balance, and mechanical energy equations, which form a coupled smoke heat and mass transfer problem through the shaft. This study presented the hand calculation method to solve the coupled problem and demonstrated it in a case study of the smoke spread in a 40-storey building. The effects of the radiant heat transfer on the calculated temperature profiles were also discussed. The study reached the following major conclusions:

(1). The temperature attenuation coefficient, α, is an important parameter for the solutions of the coupled problem, because the temperature profiles of smoke and shaft wall are both shown to be exponential functions of α.

(2). The analytical solution provides the important information for the risk assessment of the smoke spread from the fire floor to higher floors, including shaft top temperature, maximum mass flow rate and corresponding fire floor temperature, and location of *NPL*.

(3). In the case study of the 40-storey building, only a few hand calculation iterations were needed to obtain the analytical solution so the analytical model is very practical for real design problems.

(4). The effect of radiation on temperature calculations increases with fire temperatures. The sensitivity study of the radiant heat transfer coefficient shows that the overestimation of the radiation generally affects the temperature calculations less than the underestimation. Generally, the temperature calculations seem not quite sensitive to the change of the radiant heat transfer coefficients at the shaft interior wall in the case studied.

Some limitations about the current analytical solution were also noted. The current solution does not consider the situation when heat transfer coefficients vary significantly along the shaft height. The limitation could be overcome by dividing the shaft into several vertical sub-sections, for each

of which the analytical model can be applied with variable heat transfer coefficients with the height of the shaft.

Chapter 4 Dimensionless Analytical Solutions for Steady-state Heat and Mass Transfer through High-rise Shafts

Abstract

Analytical solutions in terms of dimensionless numbers for the smoke spread through high-rise shafts during fires are essential to provide a fundamental understanding of smoke transport physics, which is a complex coupled heat and mass transfer problem. Existing solutions are often dimensional based on simplification of the problem such as assuming adiabatic conditions. In order to obtain the dimensionless analytical solutions, energy balance equation, mechanical energy equation and mass balance equation were established for high-rise smoke spread under both mechanical and natural venting conditions. Experiments were deigned and conducted on two different size and material shafts, and the measured results were compared to the dimensionless analytical solutions. It was found that the dimensionless analytical solutions could predict temperature profiles, mass flow rate and neutral plane level accurately. The effect of the adiabatic assumption on the accuracy was also discussed. For example, due to the adiabatic assumption, the error of the calculated mass flow rate required during mechanical venting to maintain a high-rise shaft smoke free was found to increase with a dimensionless number, ω, defined by the geometrical and thermal properties of the shaft.

4.1. Introduction

Fires in high-rise buildings are often disastrous, causing many injuries, fatalities and huge economic losses. Such notorious fires as the Winecoff Hotel fire at Atlanta, US (December 7, 1946) caused 119 deaths, and the MGM Grand Hotel fire at Las Vegas, NV (November 21, 1980) led to the deaths of 85 people and 600 injured (Tamura 1994). A most recent high-rise fire, the 63-story

Address Downtown Dubai Hotel fire, occurred on New Year's Eve of 2016, and continued to generate smoke on the next day even after the fire was put down ("Dubai Hotel Fire Could Have Been Worse" 2016; Chappell 2016). Although luckily no deaths seem reported, the estimated repairs and business interruption exceeds $100 million dollars. Smoke generated from fires often spreads quickly throughout a building, often even faster than the fire itself, especially in a high-rise building, carrying toxic gases responsible for the majority of fatalities (Gann et al. 1994) with elevated temperatures causing spread damages of upholsteries and structures.

In typical high-rise buildings, about 95% or more of the upward movement of smoke attributes to the spreads through shafts (Tamura 1994), e.g. stairs, elevators, light wells, ventilation ducts. High-rise smoke control using pressurization systems becomes a popular option since the 1960s: by injecting clean air with mechanical fans into a shaft enclosure such that the pressure in the shaft is greater than the adjacent fire compartment, the pressurization systems are intended to prevent smoke leaking from its sources (Lay 2014). However, the pressurization systems have been found not to always work as expected, especially for high-rise shafts with strong stack effect, also known as chimney effect where shafts act like chimneys and smoke tends to spreads upwards due to buoyancy, and floor-to-floor variations in flow resistance (Klote 2011). It was estimated that 35% of pressurization systems might fail to function as intended (Lay 2014). A pressurization system often acts against the stack effect so its performance heavily relies on the strength of the stack effect, which could be subject to many variants, e.g. fire strengths and ambient weather conditions. An alternative approach is the use of shafts as smoke venting routes through which the smoke would be properly channeled to spread upwards, and eventually be exhausted at the top of the shafts to the outside of a building. Instead of fighting against the stack effect, this method of shaft

smoke ventilation takes advantage of naturally-generated stack effect due to buoyancy, aided by mechanical fan systems when necessary, and thus gains much attentions lately.

These shaft smoke ventilation systems allow fire smoke to spread through expectedly well-engineered routes of shafts so it is critical to understand the dynamic and thermal properties of the smoke along its route to the exit points, specifically smoke flow rates, smoke temperature and pressure distributions. Previous studies have been conducted using various experimental, mathematical and numerical techniques. Ji and Shi performed extensive experiments to investigate the transport characteristics of thermal plume in a ventilated stairwell with two or multiple openings (Jie Ji et al. 2015; Li et al. 2014; Ji et al. 2013; Shi et al. 2014a). Harmthy proposed a Fire Drainage System to remove the heat and induced convection smoke flow from a fire through a series of shafts to reduce the spread of fire from the region of fire source (Lay 2014; Harmathy and Oleszkiewicz 1987). Design principles of this system were also introduced based on the assumption of constant gas temperature (Harmathy and Oleszkiewicz 1987) but the heat transfer between the smoke and the shaft walls was not considered, i.e. under adiabatic conditions. Similar to the Fire Drainage System, the Beetham Tower system was developed to use an air inlet shaft to exhaust smoke from the fire floor aided by a mechanical fan system (Lay 2014). Klote studied the smoke ventilation control of stairwells in tall buildings by a tenability analysis based on computational fluid dynamics (CFD) and multizone network modeling. It was concluded that the stairwell smoke ventilation is a feasible approach (Klote 2011). Qi et al. (Qi, Wang, and Zmeureanu 2014a) developed an analytical model of smoke movement in high-rise shafts. Different from other analytical models, heat transfer between smoke and the shaft boundaries was considered. Based on the analytical model, a hand calculation method and empirical equations

were developed for the calculation of temperature distribution, mass flow rate and pressure inside the shaft (Qi, Wang, and Zmeureanu 2014b; Qi, Wang, and Zmeureanu 2016).

However, most of the previous studies were conducted on specific buildings and shafts. As a result the generalization of the conclusions to other cases may need further verifications. Therefore, there exists a gap of research that the solutions to smoke flow rates, temperature and pressure distributions, preferably expressed in dimensionless analytical forms, should be developed for a better understanding of the thermal aerodynamics of shaft smoke ventilations. The dimensionless solutions could also benefit the research on the similitude and scale modeling analysis of a high-rise building, for which the sheer size of the structure often makes full-size tests impractical.

This paper reported the development of dimensionless analytical solutions of smoke spread in non-adiabatic high-rise shafts during fires. Conservation equations of thermal energy, mechanical energy, and mass were developed in dimensionless forms for both mechanical and natural smoke ventilations. A series of experiments were then conducted on two scaled shafts with different dimensions and materials, and used to validate the developed dimensionless analytical solutions by comparing temperature distribution, mass flow rate, pressure distributions, and neutral plane levels (*NPL*). As an example of demonstration, we applied the dimensionless analytical solution developed in this study to calculating the minimum mechanical venting rate required to maintain a full-size high-rise shaft free of smoke, and compared to the result if the conventional adiabatic assumption is used. The comparison helps to show the impact of the adiabatic assumption on the accuracy of the calculation.

4.2. Theory

Smoke spread inside high-rise shafts may be generalized by the schematic in Fig. 4-1. When mechanical smoke ventilation is used, a fan is installed at the top of the shaft. In comparison, the fan is replaced by an opening at the top for natural venting/ventilation of the smoke. The objective of this section is to develop dimensionless analytical solutions for these two venting systems, for which the following assumptions are used:

- A fire is located at the first floor of the building with a fire strength defined by the fire temperature.
- Smoke movement in the shaft is one-dimensional at steady state.
- The outdoor air temperature and the building temperature at non-fire floors are constant.
- Specific heat capacity of the smoke, C_p, is constant.
- The smoke is assumed to be incompressible and viscous but thermally expansible satisfying the ideal gas law.
- No smoke leaks through shaft walls.
- Heat transfer coefficients (either due to convection or radiation) are constant and do not vary along the height of the shaft.
- The temperature of the fire floor is uniform and maintained at the fire smoke temperature (Qi, Wang, and Zmeureanu 2014a).
- The smoke flow inside the shaft could be assumed as one-dimensional steady-state flow (Qi, Wang, and Zmeureanu 2014a; Li et al. 2014).
- The friction loss of the flow due to interior shaft wall is neglected (Qi, Wang, and Zmeureanu 2016).

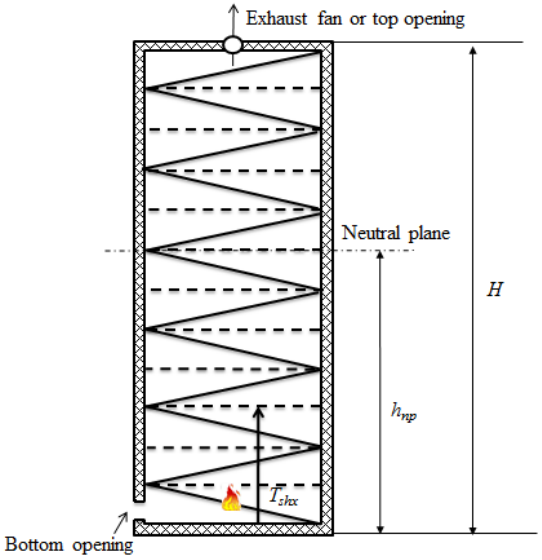

Figure 4-1 Schematic of a high-rise shafts during fires

4.2.1. Mechanical smoke venting

Smoke spread inside a shaft of mechanical smoke venting is governed by the conservation equations of heat or energy (Eq. 4-1), mechanical energy (Eq. 4-2a), and mass balance (Eq. 4-3a) in dimensional forms.

- Energy balance equation

$$\dot{m}C_P dT_{shx} + \frac{(T_{shx} - T_a)Pdx}{R_t} = 0 \tag{4-1}$$

- Mechanical energy equation

$$dp_{shx} + \rho_{shx} g dx = 0 \tag{4-2a}$$

Integrate Eq. (4-2a) from bottom to a vertical height of x and Eq. (4-2b) is obtained.

$$p_{shx} = p_{sh0} - \Delta p_{elx} \tag{4-2b}$$

where

$$\Delta p_{elx} = \int_0^x \rho_{shx} g dx = \frac{g p_{a0} H}{R T_a} \left\{ \frac{1}{\alpha} \ln \left[\frac{e^{(\alpha x / H)} + \eta}{1 + \eta} \right] \right\} \tag{4-2c}$$

- Mass balance equation

$$\dot{m}_t = \dot{m}_b = \dot{m} \tag{4-3a}$$

where $\dot{m}_b$ can be calculated by the orifice equation:

$$\dot{m}_b = C_d A_b \sqrt{2\rho_a (p_{a0} - p_{sh0})} = C_d A_b \sqrt{2(p_{a0} - p_{sh0}) p_{a0} / (R T_a)} \tag{4-3b}$$

For mechanical venting, mass flow rate is controlled by mechanical fan, so p_{sh0} is calculated by Eq. (4-3b)

To convert the conservation equations into dimensionless forms, a series of dimensionless numbers are defined as follows.

- Dimensionless temperature, θ_{sh}

$$\theta_{sh} = \frac{T_{shx} - T_a}{T_{sh0} - T_a} \tag{4-4}$$

- Dimensionless fire temperature, η

$$\eta = \frac{T_{sh0} - T_a}{T_a} \tag{4-5}$$

- Temperature attenuation coefficient, α

$$\alpha = \frac{PH}{\dot{m} C_P R_t} \tag{4-6}$$

where $R_t = \frac{1}{h_{wi}} + \frac{W}{\lambda} + \frac{1}{h_{wo}}$

- Dimensionless mass flow rate, ψ

$$\psi = \frac{\dot{m}_b}{C_d A_b \rho_a \sqrt{gH}} \tag{4-7}$$

- Geometry and thermal factor, ω

$$\omega = \frac{PH}{C_d C_p R_t A_b \rho_a \sqrt{gH}} = \alpha\psi \tag{4-8}$$

- Relative height, φ

$$\varphi = \frac{x}{H} \tag{4-9}$$

Please note that the dimensionless numbers in Eqs. (4-4) ~ (4-9) are defined based on the non-dimensionalizing process of the conservation equations.

Solving the energy balance equation by the integration over the height of the shaft, we obtained the dimensionless solution to the smoke temperature.

$$\theta_{sh} = \frac{T_{shx} - T_a}{T_{sh0} - T_a} = e^{(-\varphi\alpha)} \tag{4-10a}$$

From Eq. (4-10a), the dimensionless interior shaft wall surface temperature, θ_{wi}, can then be obtained based on the equation of heat fluxes at the interior surface and through the wall (Qi, Wang, and Zmeureanu 2014a).

$$\theta_{wi} = \left(1 - \frac{1}{h_{wi} R_t}\right)\theta_{sh} = \left(1 - \frac{1}{h_{wi} R_t}\right)e^{(-\varphi\alpha)} \tag{4-10b}$$

One of the most important smoke control parameters for pressure distribution is the neutral plane level (*NPL*) of pressure (the unit of height), where the shaft internal pressure, p_{shxnp}, is equal to that of the building floor at the same height, $p_{a,np}$ (Eq. 4-11). Here, the dimensionless *NPL* is defined

by the relative neutral plane level, φ_{np}, which can be obtained by combining Eqs. (4-2b), (4-3a), (4-3b) and (4-11) when $x = x_{np}$.

$$p_{a,np} = p_{a0} - \rho_a g x_{np} \tag{4-11}$$

$$\varphi_{np} = \frac{1}{2}\left(\frac{\omega}{\alpha}\right)^2 + \frac{1}{\alpha}\ln\left[\frac{\eta + e^{(\alpha\varphi_{np})}}{\eta+1}\right] = \frac{1}{2}\psi^2 + \frac{\psi}{\omega}\ln\left[\frac{\eta + e^{(\frac{\psi}{\omega}\varphi_{np})}}{\eta+1}\right] \tag{4-12}$$

For mechanical smoke venting, mechanical fan is used so the smoke mass flow rate is a known value, which is not the case for natural smoke venting as explained next.

4.2.2. Natural smoke venting

Natural smoke venting takes advantage of stack effect to drive and exhaust smoke through shafts. Dimensionless smoke and wall temperatures can be calculated by Eqs. (4-10a) and (4-10b), respectively. According to the previous study by Qi et al. (Qi, Wang, and Zmeureanu 2016), the relative *NPL*, φ_{np}, for natural smoke venting can be expressed as

$$\varphi_{np} = \frac{1}{1 + \left(\frac{\rho_a - \overline{\rho}_{shl}}{\rho_a - \overline{\rho}_{shu}}\right)\gamma\phi^2} \tag{4-13}$$

where ϕ is the ratio of bottom opening area to top opening area, A_b / A_t

and

$$\overline{\rho}_{shl} = \frac{\Delta p_{el,x_{np}}}{g x_{np}} = \frac{1}{x_{np}}\int_0^{x_{np}} \rho_{shx} dx \tag{4-14}$$

$$\overline{\rho}_{shu} = \frac{1}{H - x_{np}} \int_{x_{np}}^{H} \rho_{shx} dx \tag{4-15}$$

Take Eqs. (4-14) and (4-15) into Eq. (4-13), the dimensionless solution of *NPL* could be obtained:

$$\varphi_{np} = \frac{1}{1 + \left\{ \frac{1 - \frac{1}{\alpha\varphi_{np}} \ln\left[\frac{\eta + e^{(\alpha\varphi_{np})}}{\eta + 1}\right]}{1 - \frac{1}{\alpha(1-\varphi_{np})} \ln\left[\frac{\eta + e^{(\alpha)}}{\eta + e^{(\alpha\varphi_{np})}}\right]} \right\} \gamma\phi^2} \tag{4-16}$$

To obtain the mass flow rate, we apply the orifice equation to the top opening of the shaft as Eq. (4-17) shows.

$$\dot{m}_t = C_d A_t \sqrt{2\rho_{shH}(p_{shH} - p_{aH})} = C_d A_t \sqrt{2(p_{shH} - p_{aH}) p_{a0} / (RT_{shH})} \tag{4-17}$$

By combining Eqs. (4-2b), (4-3a), (4-3b), (4-8) and (4-17) when $x = H$, the dimensionless mass flow rate, ψ , for natural venting can be derived.

$$\psi^2 = \left(\frac{\omega}{\alpha}\right)^2 = \frac{2\left[1 - \frac{1}{\alpha} \ln\left(\frac{\eta + e^{\alpha}}{1 + \eta}\right)\right]}{\left(1 + \phi^2\gamma\right)} \tag{4-18}$$

Where γ is the dimensionless smoke temperature at the top of the shaft, $T_{shH}/T_a = 1 + \eta e^{(-\alpha)}$.

Table 1 summarizes the dimensionless solutions for both mechanical and natural venting. A few observations can be made here:

- The temperature profile, θ_{sh}, is the function of α, in which α is only associated with the geometrical and thermal properties of the smoke and the shaft

- The relative *NPL* equations are implicit but can be solved easily by common iterative methods, such as fixed-point iterations.
- The *NPL* for mechanical venting, φ_{np}, depends on the dimensionless numbers ψ, η and α. For a specific mechanical venting shaft with known fire strength, ψ and η are known and ω could be calculated by Eq. (4-8), so α could be calculated which equals to ω/ψ, and therefore θ_{sh} and φ_{np} could be obtained according to Eqs. (4-10a) and (4-12).
- For a specific natural venting shaft with known fire strength, ψ, ϕ and η are known and ω could be calculated by Eq. (4-8), so α and φ_{np} could be obtained by solving Eqs. (4-16) and (4-18), which is listed in Table 4-1.

Table 4-1 Dimensionless analytical solutions

	Mechanical venting	Natural venting
Dimensionless smoke temperature	$\theta_{sh} = e^{(-\varphi\alpha)}$	
Dimensionless interior shaft wall surface temperature	$\theta_{wi} = \left(1 - \frac{1}{h_{wi}R_t}\right)e^{(-\varphi\alpha)}$	
Dimensionless mass flow rate	$\psi = \frac{\omega}{\alpha}$	$\psi^2 = \left(\frac{\omega}{\alpha}\right)^2 = \frac{2\left[1-\frac{1}{\alpha}\ln\left(\frac{\eta+e^{\alpha}}{1+\eta}\right)\right]}{\left(1+\phi^2\gamma\right)}$
Relative neutral plane level	$\varphi_{np} = \frac{1}{2}\psi^2 + \frac{1}{\alpha}\ln\left[\frac{\eta+e^{(\alpha\varphi_{np})}}{\eta+1}\right]$ $= \frac{1}{2}\psi^2 + \frac{\psi}{\omega}\ln\left[\frac{\eta+e^{(\frac{\psi}{\omega}\varphi_{np})}}{\eta+1}\right]$	$\varphi_{np} = \frac{1}{1+\left\{\frac{1-\frac{1}{\alpha\varphi_{np}}\ln\left[\frac{\eta+e^{(\alpha\varphi_{np})}}{\eta+1}\right]}{1-\frac{1}{\alpha\left(1-\varphi_{np}\right)}\ln\left[\frac{\eta+e^{\alpha}}{\eta+e^{(\alpha\varphi_{np})}}\right]}\right\}\gamma\phi^2}$

4.3. Experiments

To validate the dimensionless analytical solutions, two series of experiments were designed and conducted independently using two sub-scaled shafts, one at Concordia University (Concordia shaft), and the other at the University of Science and Technology of China (USTC shaft) as shown in Fig. 2. Made of 3 mm acrylic panels, the Concordia shaft has eight floors with the 0.5 m height for the first floor and 0.3 m for the rest of floors, which is 1/10 scale of the full size. The USTC shaft is a 12-floor and 12.2 m high structure, which is 1/3 scale of the full-size with internal stairs (Ji et al. 2013). The cross sectional area of the shaft is 1.5×1 m^2 with half of the shaft wall made of 12-mm fire-resistant glass, and the other half made of 2-mm steel plates. A small opening was drilled at each floor for observing the flow direction using smoke tracer sticks to estimate the location of *NPL*.

To measure temperature, thermocouple arrays were placed evenly in the vertical centerline at each floor in both the USTC and Concordia shafts. Interior shaft wall surface temperatures were also measured in the Concordia shaft. The velocities of the airflow at the bottom openings of the shafts were measured by hot-wire anemometers. For the USTC shaft, the internal pressure was difficult to be captured steadily due to the existence of turbulent flows mostly from the internal stairs. The *NPL* was thus estimated by using artificial smoke tracer sticks: the smoke produced from the sticks would enter the shaft under *NPL* and exit above the *NPL* so its location can be determined. For the Concordia shaft, the fire source was simulated by a propane gas burner at the center of the ground floor. The fire strength was controlled by a gas flow controller. At each floor, two small holes were drilled to measure the pressure distribution inside the shaft. Pressures were measured by handheld manometer at the drilled holes with accuracy of ±0.05% full scale and then *NPL* was

determined in the Concordia shaft. Smoke tracer sticks were also used to find *NPL* location in the Concordia shaft

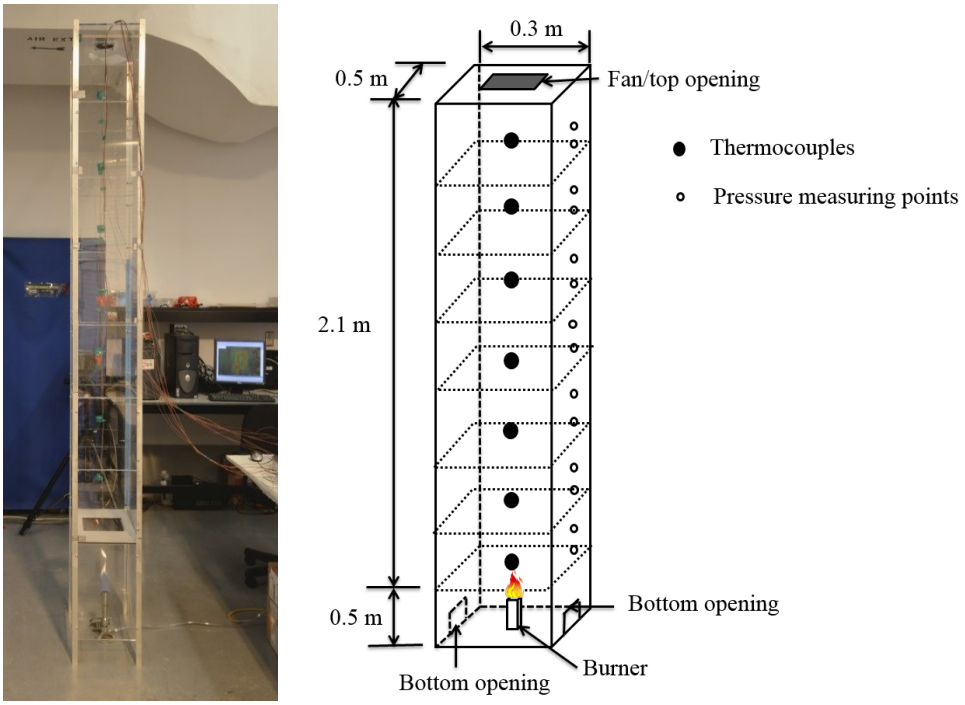

(a) Concordia shaft

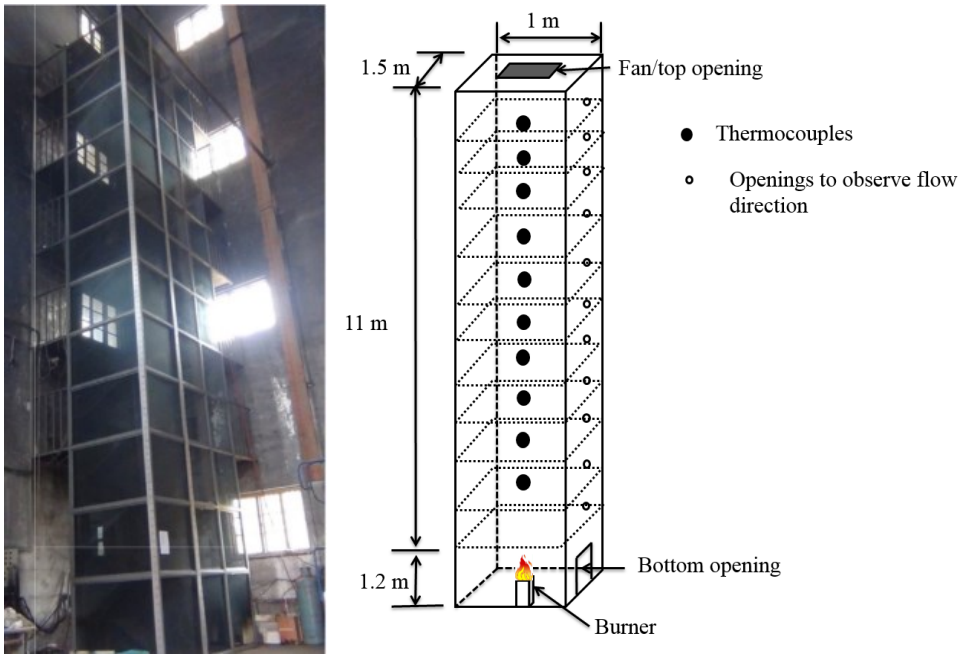

(b) USTC shaft

Figure 4-2 Schematic of the experimental setup

Table 4-2 Experiments design

	Geometry and thermal factor, ω	Dimensionless fire temperature, η	Dimensionless mass flow rates, ψ
	Mechanical venting		
Concordia shaft[1]	0.15	0.29	0.33~0.61
	0.15	0.35	0.4~0.63
USTC shaft[2]	0.3	0.12	0.17~0.35
	0.3	0.16	0.27~0.39
	Natural venting		
Concordia shaft[3]	0.08	0.10	/
	0.11	0.18	/
	0.12	0.28	/

[1] C_d=0.65(Dols and Polidoro 2015), R_t = 0.5 (m^2·K)/W
[2] C_d=0.23(Ji et al. 2013), R_t = 0.27 (m^2·K)/W
[3] C_d=0.65(Dols and Polidoro 2015), R_t = 0.5~0.7 (m^2·K)/W

Fire strength in terms of dimensionless fire temperature, η, and dimensionless mass flow rates, ψ, were reported in Table 4-2. Nine experiments were conducted for the Concordia shaft and 24 experiments were conducted on the USTC shaft for mechanical venting. For natural venting, three experiments were performed on the Concordia shaft. Note that the USTC tests were conducted independently before the dimensionless analytical solutions in this study were developed mostly at Concordia, so many dimensionless numbers were with different values, and they were not intentionally made to be the same.

4.4. Results and discussion

4.4.1. Mechanical smoke venting

4.4.1.1. Temperature distribution

Figure 4-3 compares the measured and predicted dimensionless smoke temperature, θ_{sh}, and/or interior wall temperature, θ_{wi}, for different fire temperature, η, and different shafts defined by the geometry and thermal factor, ω. The dimensionless smoke mass flow rate, ψ, and the temperature attenuation coefficient, α, are also reported in the figures. Because the USTC tests did not measure interior wall temperatures so only the smoke temperatures were shown in Figs. 4-3(c) and 4-3(d). Figure 4-3 shows that the predicted temperature profiles by the dimensionless model agreed well with the measurements from both shafts. In Figure 4-3, it is also observed that for both the experiments and the theoretical solutions, with the increase of the mechanical venting rate (ψ), the vertical temperature gradients of smoke and interior wall surface become smaller, indicating decreased value of the temperature attenuation coefficient, α, which is also consistent with Eq. (4-8).

In fact, α is in a form of the Stanton number, *St*, with an extra term of the wall-floor area ratio, PH/A_c (Eq. 4-19). Therefore, for a given shaft with PH/A_c as a constant, α is only determined by *St* as defined by Eq. (4-20). When the mechanical venting rate is increased, both α and thus *St* become smaller for a given shaft. Since Stanton number is the ratio of the heat loss of the smoke over the thermal capacity of the smoke, a smaller *St* indicates less heat loss from smoke or more smoke thermal capacity, which explains the decrease of vertical temperature gradient in the shaft when the mechanical venting rate (ψ) is increased.

$$\alpha = \frac{PH}{A_h} St \tag{4-19}$$

$$St = \frac{1/R_t}{\rho v C_p} \tag{4-20}$$

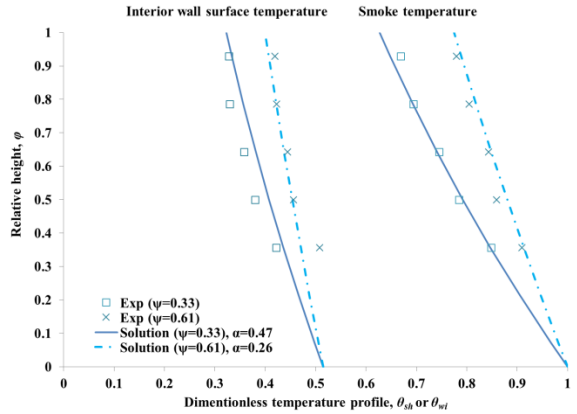

(a) Concordia Shaft (ω=0.15, η=0.29)

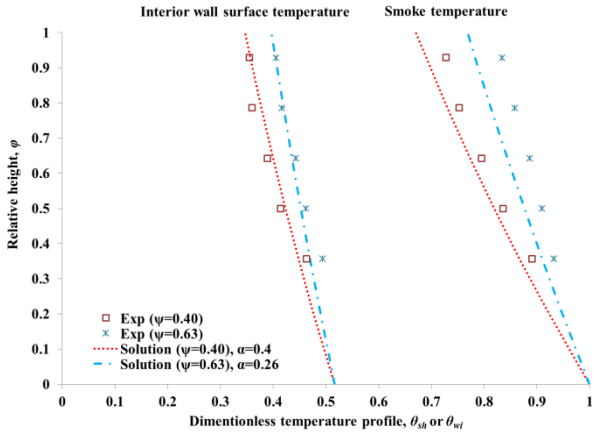

(b) Concordia Shaft (ω=0.15, η=0.35)

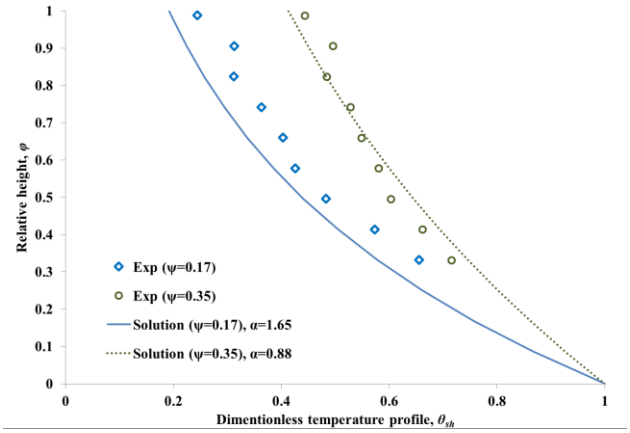

(c) USTC shaft (ω=0.3, η=0.12)
(only smoke temperature)

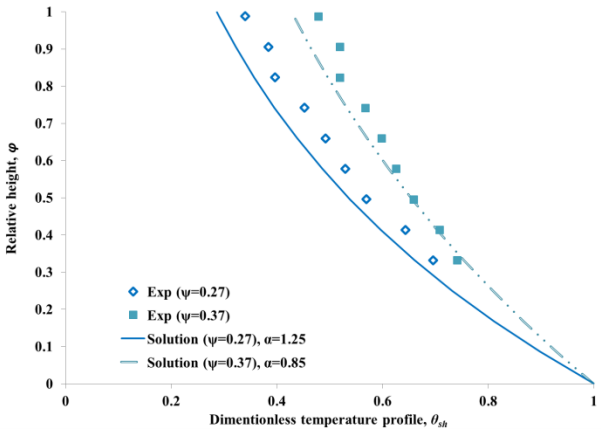

(d) USTC shaft (ω=0.3, η=0.16)
(only smoke temperature)

Figure 4-3 Comparison between measured and predicted temperature distribution for mechanical venting

4.4.1.2. Neutral plane level

According to Eq. (4-12), φ_{np} only depends on the dimensionless mechanical venting flow rate, ψ for a specific shaft with known fire strength, i.e. ω and η are known. As a result, Fig. 4-4 shows that with the increase of mass flow rate, ψ, the *NPL* increases, which is understandable because the fan expels more smoke from the shaft causing an overall lower pressure and thus higher *NPL* in the shaft. It can also be noticed that for the same shaft, i.e. a fixed value of ω, a higher fire temperature, η, leads to lower *NPL*, which means more building floors will be potentially exposed

to potential smoke leaking from the shaft. Therefore, bigger fan is needed to increase *NPL* of the building. Here once again, the predicted φ_{np} compares generally well with the experimental results for both shafts.

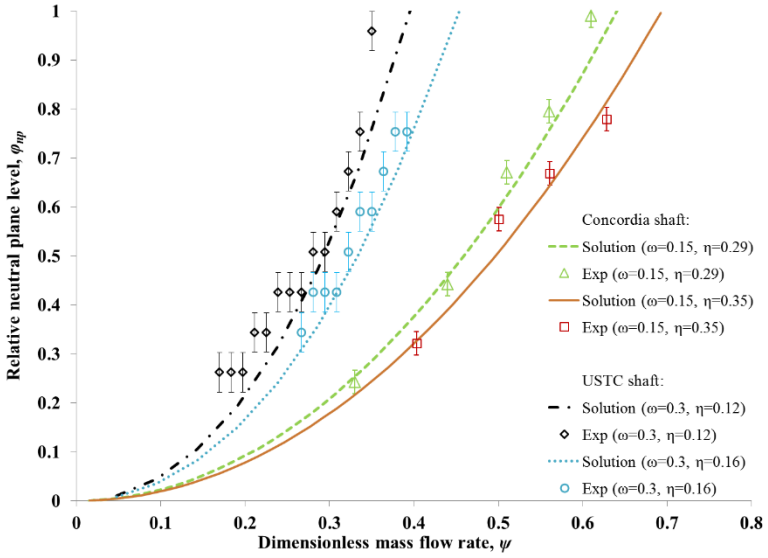

Figure 4-4 Comparison between measured and predicted dimensionless *NPL* for mechanical ventilation

4.4.2. Natural smoke venting

For natural smoke venting for a specific shaft with known fire strength, i.e. ω and η are known, the smoke flow rate is unknown but can be determined by solving Eqs. (4-8) and (4-18), in which the dimensionless smoke flow rate, ψ, and the temperature attenuation coefficient, α, are unknown. These two combined equations can be solved numerically or more simply plotted in Fig. 4-5 (thanks to dimensionless forms of the solutions). For example, for the Concordia shaft, $\omega = 0.08$, and $\eta = 0.1$. Then, the predicted mass flow rate, $\psi = 0.28$, and the temperature attenuation coefficient, $\alpha = 0.32$ after reading directly in Fig. 4-5. The temperature profiles of the smoke and wall surfaces can then be determined by using Eqs. (4-10a) and (4-10b).

Figure 4-5 and Fig. 4-6 compare the dimensionless mass flow rate and smoke temperature predicted by the analytical solutions and the measurements. The predicted results are quite close to the experimental data in both cases. Some other interesting observations are also made here:

- From Fig. 4-5, as the fire strength (represented by η) increases, dimensionless mass flow rate, ψ, increases.
- Accordingly, temperature attenuation coefficient, α, decreases slightly for the given shaft, i.e. fixed ω. This means the change of fire strength here had minor impact on the changes of temperature gradient, especially for the region with $\alpha < 1$ as shown in Fig. 4-5. This is consistent with the temperature profile results in Fig. 6: the change of temperature and its gradient seem insignificant for both shafts.
- Figure 4-5 also shows that for a given fire (η is fixed), ψ is not quite sensitive to a wide range of ω, i.e. the region when $\omega < 0.12$ for the Concordia shaft. Therefore, ψ is only determined by the fire strength, η, which could be used to simplify calculation of mass flow rate.

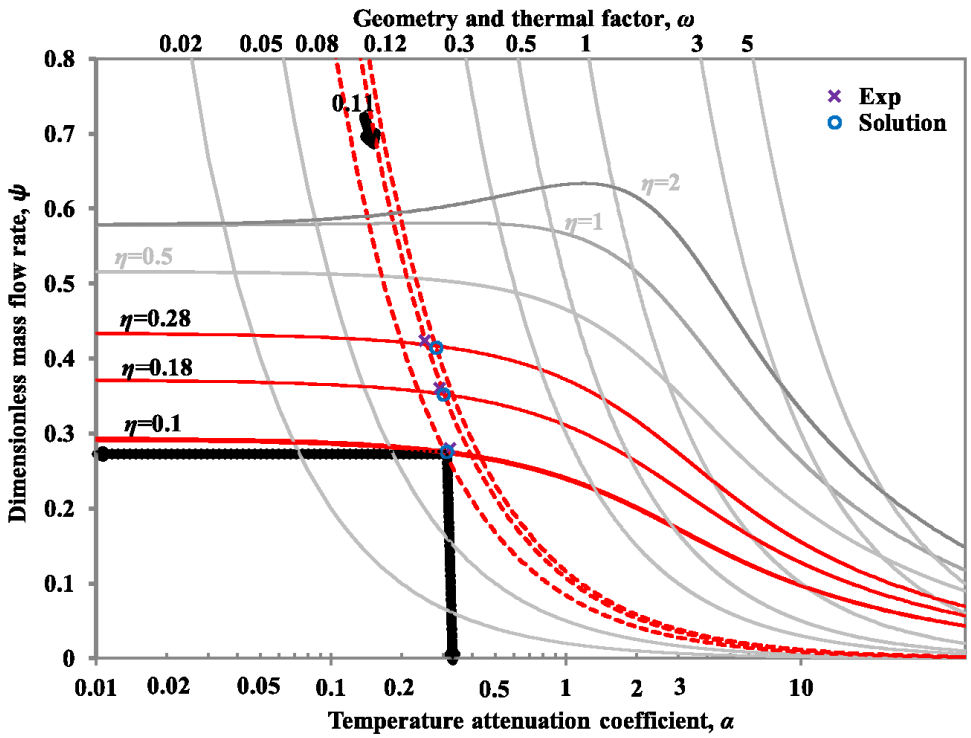

Figure 4-5 The predicted and measured dimensionless smoke flow rates, ψ, under different temperature attenuation coefficients, α, for different shaft properties (ω), and fire temperatures (η) during the natural venting of Concordia shaft.

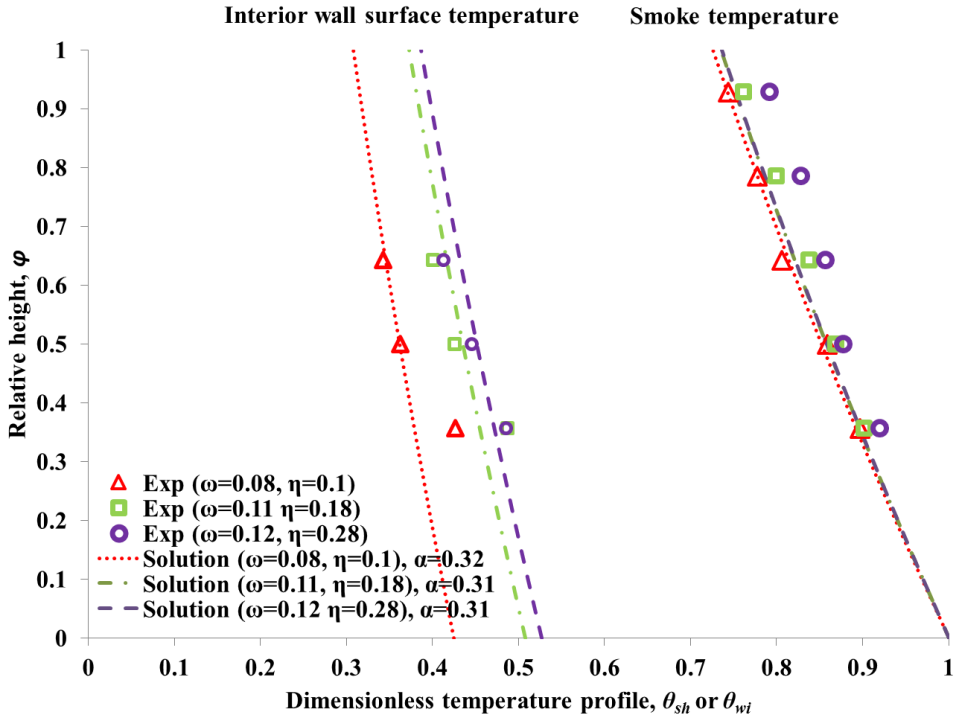

Figure 4-6 Temperature distributions predicted by dimensionless analytical solutions and measured by experiments for natural venting of Concordia shaft.

Due to the minor change of α with the increase of fire strength as it indicated by Fig. 4-6, the fire strength has little influence on the relative *NPL* for natural venting. This is consistent with the previous study by Li et al. (2014). Table 4-3 compares φ_{np} of measured and predicted relative *NPL* for natural venting. When the fire strength, η, increases from 0.1 to 0.28, the measured φ_{np} is around 0.46±0.05 is close to the predicted one by dimensionless model, which is around 0.44.

Table 4-3 Measured and predicted relative *NPL* by dimensionless analytical model for natural venting of Concordia shaft.

	Measured results	Predicted by dimensionless model
Relative *NPL*	0.46 ± 0.05	0.44

4.5. Discussion

For simplicity, many previous studies often assumed a shaft to be adiabatic (Zhang et al. 2008; Klote et al. 2012), for which the literature found that the error of the predicted *NPL* location could be significant (Yang et al. 2012). An inaccurate prediction of *NPL* could cause a poorly designed or even failed mechanical venting system, because the mechanical fan is expected to achieve a *NPL* as high as possible, preferably to the top of the shaft so there would be zero chance that non-fire building floors could be potentially exposed to toxic smoke from the shaft.

In this section, with the help of the dimensionless analytical solutions developed here, we are able to discuss about the errors from the adiabatic assumption. The required mechanical venting rate to keep a shaft smoke free can be found by letting $\varphi_{np} = 1$ in Eq. (4-12) to obtain Eq. (4-21), from which the dimensionless fan flow rate required to achieve the highest *NPL* (the top of the shaft) can be calculated based on geometrical and thermal parameters of the shaft, i.e. ω, and fire strength, i.e. η. For comparison, the required fan flow under the adiabatic assumption can also be derived: for Eq. (4-21) under the adiabatic assumption, setting the geometry and thermal factor of a shaft, $\omega = 0$, and finding its limit, we can obtain Eq. (4-22) if the adiabatic assumption is applied. It shows that Eq. (4-22) is only a function of fire strength, η, regardless of the shaft geometrical and thermal properties. The relative error of the adiabatic assumption can then be defined by Eq. (4-23) when compared to the non-adiabatic situation.

$$1 = \frac{1}{2}\psi_{non-ad}^2 + \frac{\psi_{non-ad}}{\omega}\ln\left\{\frac{\eta + e^{\frac{\omega}{\psi_{non-ad}}}}{\eta + 1}\right\} \tag{4-21}$$

$$\psi_{ad} = \sqrt{\frac{2\eta}{\eta + 1}} \tag{4-22}$$

$$\text{Relative error} = \frac{\dot{m}_{ad} - \dot{m}_{non\text{-}ad}}{\dot{m}_{non\text{-}ad}} = \frac{\psi_{ad} - \psi_{non\text{-}ad}}{\psi_{non\text{-}ad}} \quad (4\text{-}23)$$

where "ad" is for "adiabatic" and "non-ad" for "non-adiabatic".

Equation 4-23 is plotted for a wide range of building parameters (ω) and fire (η) as shown in Fig. 4-7. Here are a few interesting observations:

- With the increase of ω, the error due to adiabatic assumption increases. It can be explained by that: a greater P, H or smaller values of R_t increase ω, and thus more heat loss from smoke to shaft wall. So neglecting heat transfer leads to more error under the adiabatic assumption.
- With the decrease of η, the error also increases. Therefore, for a shaft with bigger ω and/or smaller η, the adiabatic assumption leads to more errors.

Here, to put the analysis in the context of real buildings, consider a 40-storey high-rise stairwell with the detailed specification shown in Table 4. If all the infiltration area is lumped as a part of the bottom opening area, which is often done to consider leakages on shaft walls, ω is around 1.5. The relative error of the adiabatic assumption is about 18% for a fire with η = 2, corresponding to a high-rise fire of 5 MW. The error of 18% means an overestimation of 18% of the mechanical venting fan capacity in terms of mass flow rate to keep the high-rise shaft smoke free.

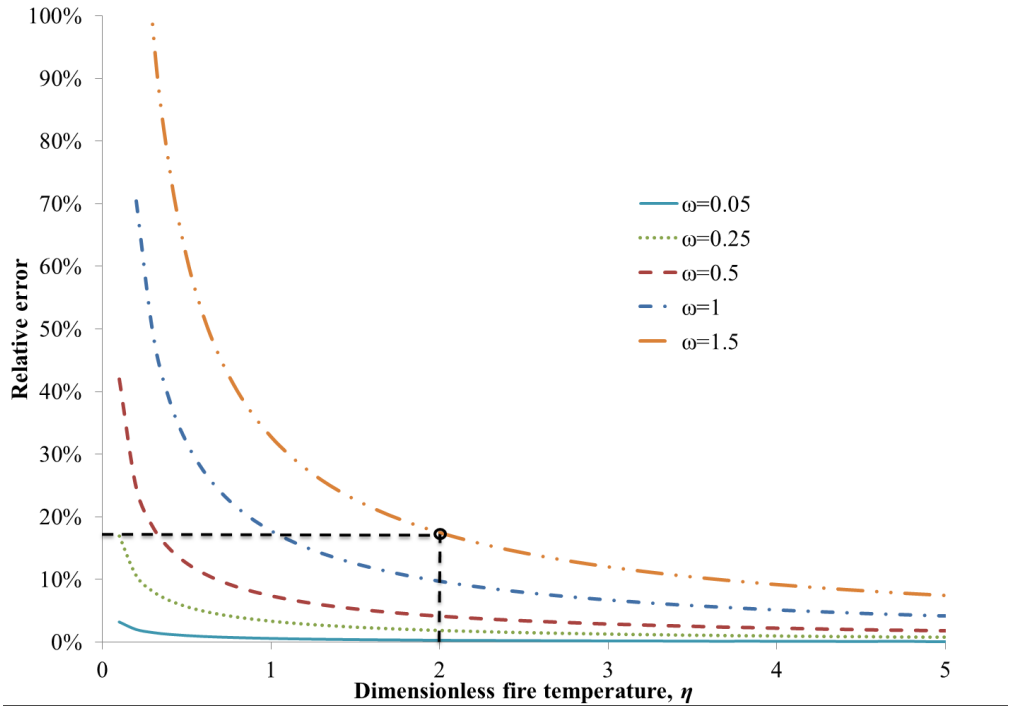

Figure 4-7 The relative error caused by the adiabatic assumption for the required mechanical venting rate achieving a shaft smoke free using the dimensionless NPL from this study as a baseline (non-adiabatic).

Table 4-4 Parameters of a 40-storey high-rise stairwell for demonstration

List of parameters	Values
Height	160 m
Cross section	4 m × 5 m
Shaft wall width	0.24 m
Heat transfer coefficient on the shaft wall surface	10 W/ (m^2·K)
Conduction heat transfer coefficient	1.7 W/ (m·K)
Door size (height × width)	2.13 × 1.22 m
Crack width around the perimeter	1 mm
Area ratio of openings	0.000014 m^2/m^2 (for tight stairwell) (Klote et al. 2012)

4.6. Conclusion

This study derived dimensionless analytical solutions of steady-state smoke flow in non-adiabatic high-rise shafts. Based on energy balance equation, mechanical energy equation and mass balance equation, dimensionless analytical solutions for both mechanical venting and natural ventilating

were developed. Experiments were designed and conducted on two different size and material shafts, the results of which were used to validate the dimensionless models. To compare with the solutions based on adiabatic assumption, the required mechanical venting to achieve a shaft free of smoke was discussed and compared to the result without the assumption. This study reached the following major conclusions:

(1) When compared to the two sub-scale tests, the developed dimensionless model accurately predict temperature distribution, mass flow rate and neutral plane level for both mechanical and natural venting.

(2) By defining the dimensionless number, ω, which equals to ψ times α, the coupled problem of smoke movement inside shaft driven by stack effect can be solved by only two equations, which much simplifies the calculations that cannot be achieved by previous studies.

(3) For the natural venting, with the increase of fire strength, smoke flow rate through the shaft increases accordingly whereas the temperature gradient does not change significantly, thus leading to minor change of *NPL*.

(4) The temperature attenuation coefficient, α, is in a form of the Stanton number, *St*, which is the ratio of the heat loss of the smoke over the thermal capacity of the smoke. When the mechanical venting rate (ψ) is increased in a shaft, *St*, becomes smaller, indicating less heat loss from smoke or more smoke thermal capacity, and thus the vertical temperature gradient decreases.

(5) The adiabatic assumption, which is commonly used in the literature, is found to lead to an overestimation of the mechanical venting rate necessary to keep a high-rise shaft free of smoke. The resultant error depends on the dimensionless number, ω, describing the geometry and thermal properties of the shaft: the adiabatic assumption causes more errors for bigger values of ω.

In summary, the dimensionless analytical solution developed by this study therefore provides insights on the smoke spread in high-rise building shafts. It can be potentially used for further studies on similarities and scale modeling of these phenomena for high-rise buildings.

Chapter 5 The Effects of Non-uniform Temperature Distribution on Neutral Plane Level in Non-adiabatic High-rise Shafts during Fires

The contents of this chapter are published in "Dahai Qi, Liangzhu Wang, Radu Zmeureanu. 2016. The effects of non-uniform temperature distribution on neutral plane level in non-adiabatic high-rise shafts during fires. Fire Technology. Springer US. doi:10.1007/s10694-015-0554-2". The contents are slightly modified.

Abstract

The location of neutral plane level (*NPL*) is an important factor for the evaluation of risks of smoke spreads in high-rise buildings. The current method to determine the location of *NPL* assumes uniform temperature distribution inside a shaft, which causes concerns over accuracy of the predicted *NPL* for high-rise shafts with non-uniformly distributed temperatures during fires. To address the effect of temperature distribution on *NPL* location, this paper introduces a method to calculate temperature distribution and its associated *NPL* location based on a coupled model of smoke temperature profile, flow rate and pressure distribution inside a shaft. The measured data from a 1/3 scale experiment is used to validate the method and used to develop two empirical equations for *NPL* locations in terms of dimensionless numbers: one empirical equation based on shaft top temperature and the second based on shaft bottom temperature. A sensitivity study of the empirical equations is then conducted to evaluate the applicability of the developed equations when compared to the existing *NPL* method. It was found that for the existing *NPL* equation based on uniform temperature assumption may under-/overestimate the *NPL* locations. For non-adiabatic shafts, the effects of non-uniform temperature distribution on *NPL* should be considered and the suggested empirical equations can predict *NPL* locations with a reasonable accuracy.

5.1. Introduction

In the last decades, a large number of high-rise buildings have been constructed all over the world, and the number is still increasing rapidly especially in cities with fast economic growth, e.g. 130 high-rise projects were under construction in the first quarter of 2014 at Toronto, Canada (CBC news 2014). Building fire safety is a major challenge for high-rise buildings. Driven by stack effect, the toxic smoke resulting from fires can spread to higher levels rapidly via vertical shafts, such as stairwells and elevator hoist ways. In the United States, fire smoke accounts for approximately 75% of the victims of building fires due to the toxic effects of the smoke migrating throughout the building (Gann et al. 1994; Beitel, Wakelin, and Beyler 2000). Therefore, the study of smoke movement in shafts and its associated risks on building occupants are among the major tasks of high-rise building fire protection (Lie and McGuire 1975; Hadjisophocleous and Jia 2009; Wang, Zalok, and Hadjisophocleous 2011; Shi et al. 2014b).

Smoke spread via a shaft is directly determined by the pressure distribution inside the shaft and from an engineer's point of view, neutral plane level (*NPL*), where the shaft internal pressure is equal to that of the building floor at the same height. Due to buoyancy, fire smoke seeks any possible route to spread to the rest of a building despite summer or winter seasons. If fire smoke enters a shaft by any means, the temperature inside the shaft is generally higher than the air temperature of the floors. As a result, above a *NPL*, the shaft pressure is higher than that of the floor so smoke would enter the building floor if there is a leakage. Accordingly the flow direction would be reversed under the *NPL*. Therefore, the major objective of a shaft smoke management plan is to identify and control the location of *NPL* to prevent smoke from entering building floors via shafts. A number of studies have been focused on *NPL*. To determine the *NPL* location, Klote (1991) assumed a uniform temperature inside a shaft and proposed a simple equation Eq. (5-1)

(hereafter as Klote's equation) widely used to determine *NPL* location (Karlasson and Quintiere 2002; Tamura 1994; Klote et al. 2012). T_i in Eq. (5-1) is the uniform temperature, which can be obtained by averaging the smoke temperature, T_{shx}, over the shaft height (Figure 5-1). If smoke temperature is non-uniform as a result of smoke's heat transfer with the surroundings, e.g. shaft walls (Ji et al. 2015; Black 2009; Sun et al. 2011; L. Wang, Black, and Zhao 2013), the applicability of the Klote's equation would be questioned.

$$\frac{h_{np}}{H} = \frac{1}{1+\left(\frac{T_i}{T_a}\right)\left(\frac{A_b}{A_t}\right)^2} \tag{5-1}$$

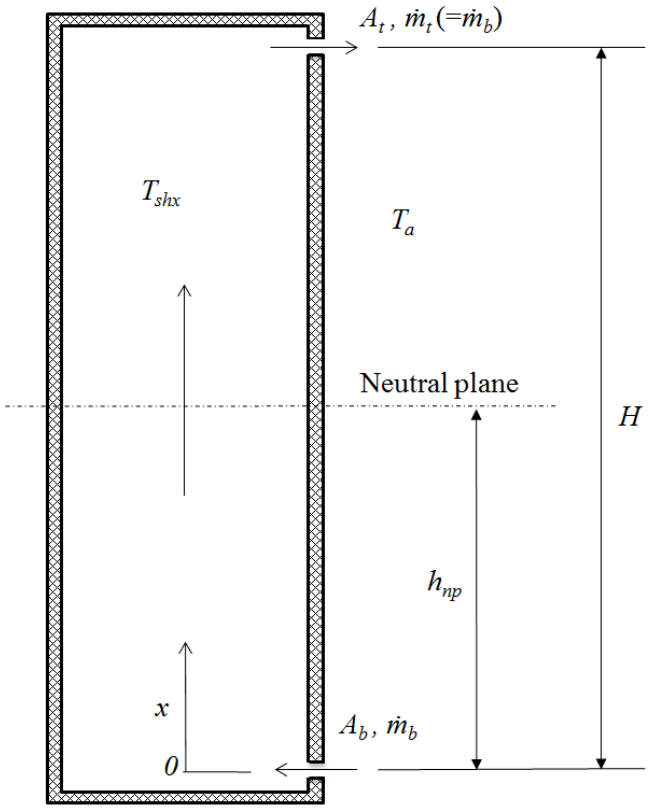

Figure 5-1 Schematic of a shaft.

Black (2009, 2010) considered the effect of temperature distributions on the *NPL* numerically with a computer program COntrol of SMOke (COSMO) for specific buildings and found that taller buildings tend to have lower *NPL* on a percentage basis relative to building height. Li et al. (2014) conducted experiments in a 1/3 scale stairwell with three vents located at the top, bottom and mid-height location, respectively. Temperature distributions were recorded and the *NPL* was calculated accordingly. It was found that *NPL* is closely related to the location of the middle vent, which directly affected shaft temperature distributions, and the smaller heat release rate results in the slight lower *NPL*. Both of these previous studies are based on specific buildings and no general equation/formulation was provided to improve the Klote's equation. Although it is always possible to conduct a numerical simulation or an experiment for a specific building, a general formulation of *NPL*, especially in the form of dimensionless parameters similar to the Klote's equation, would be preferred.

The distribution of smoke temperature in high-rise shafts is often non-uniform and found to be an exponential function of relative height (Yang et al. 2013; Qi, Wang, and Zmeureanu 2014a) . From scaled building model experiments, Li et al. (2014) found that the vertical temperature difference can be over 55 K for a 12.2-m high shaft. A simplification of the temperature profile as a uniform temperature may affect the predicted smoke flow rate, pressure distribution, and eventually the location of *NPL*. It was found that the uniform temperature assumption may overestimate the smoke flow rate in a shaft by over 70% (Wang, Black, and Zhao 2013). Qi, Wang, and Zmeureanu (2014a) developed a mathematical model of smoke movement inside non-adiabatic shafts during fires, considering non-uniform distribution of temperatures. It was found that the calculated profiles of smoke temperatures and shaft wall temperatures depend on the temperature attenuation coefficient, α, a non-dimensional parameter associated with the geometrical and thermal properties

of the smoke and the shaft. The *NPL* can be obtained by the mathematical model however a few number of iterations are needed, which may not be quite straightforward and practical for actual designs and analyses in the field of fire protection preferring simpler formulations. The literature search also shows that there are no existing studies on the evaluation of the applicability of the uniform temperature assumption to determine the *NPL*, and the effects of the temperature distribution and potentially other factors on the *NPL* location in a high-rise shaft.

Therefore, this study aims to take into account the effects of non-uniform smoke temperature distribution on the location of *NPL* in high-rise shafts when compared to the existing model (i.e. Klote's equation), which is based on the uniform temperature assumption, and develop a *NPL* formulation, e.g. an empirical equation, that do not need iterations when used. Apparently, Klote's equation applies to adiabatic shafts where there is no heat transfer between smoke and shaft walls. Therefore, this study focuses on non-adiabatic shafts and it is based on dimensionless numbers so it can be generalized to a broad range of cases. First, a method is reported to determine smoke temperature profile, flow rate and pressure distribution inside non-adiabatic shafts and validated by the measured data from a 1/3 scale experiment from the literature. Empirical equations for *NPL* in terms of associated dimensionless numbers are then developed by regression analysis from the experimental data. To evaluate the effects of the temperature distribution on *NPL*, a sensitivity study of the developed empirical equations is conducted for different shaft bottom temperatures, ambient temperatures and shaft heights. The applicability and limitations of the existing Klote's *NPL* model are also identified.

5.2. Theory

Because smoke temperature profile affects pressure distribution and consequently *NPL* location, we need to find a method to determine the distribution of smoke temperature in a non-adiabatic

shaft first. For a buoyancy-driven smoke spread in Figure 5-1, the method in fact needs to solve a coupled thermal and smoke flow problem. Smoke enters the shaft through the bottom opening and leaves through the top opening. The corresponding opening areas are A_b and A_t. To formulate the coupled equations, we make the following assumptions:

- Smoke movement in the shaft is one-dimensional at steady state.
- Similar to Klote's method, smoke temperature at shaft bottom, T_{sh0}, is higher than T_a.
- Specific heat capacity of the smoke, C_p, is constant.
- The smoke is assumed to be incompressible and viscous but thermally expansible satisfying the ideal gas law.
- No smoke leaks through shaft walls.
- Heat transfer coefficients (either due to convection or radiation) are constant and do not vary along the height of the shaft.
- The effect of wall friction on pressure drop along the shaft height is neglected.

The above coupled thermal airflow problem can be solved by applying mass, heat and mechanical energy conservation equations developed by the authors (Qi, Wang, and Zmeureanu 2014a). To avoid repetition, this paper summarizes the final equations of smoke temperature (Eq. 5-2) and pressure profiles (Eq. 5-9). The average temperature of smoke, $\overline{T_{sh}}$, wall interior and exterior surface temperatures, $\overline{T_{wi}}$ and $\overline{T_{wo}}$, are also presented in Eqs. (5-3) ~ (5-5).

$$T_{shx} = T_a + (T_{sh0} - T_a)Exp(-\alpha x/H) \tag{5-2}$$

$$\overline{T_{sh}} = T_a\left\{1 + \frac{T_{sh0} - T_a}{T_a \alpha}[1 - Exp(-\alpha)]\right\} \tag{5-3}$$

$$\overline{T_{wi}} = T_a\left[1+\frac{T_{sh0}-T_a}{T_a\alpha}\left(1-\frac{1}{h_{wi}R_t}\right)\left(1-Exp(-\alpha)\right)\right] \tag{5-4}$$

$$\overline{T_{wo}} = T_a\left[1+\frac{T_{sh0}-T_a}{T_a\alpha}\frac{1}{h_{wo}R_t}\left(1-Exp(-\alpha)\right)\right] \tag{5-5}$$

Where

$$\alpha = \frac{PH}{\dot{m}C_pR_t} \tag{5-6}$$

$$R_t = \frac{1}{h_{wi}} + \frac{W}{\lambda} + \frac{1}{h_{wo}} \tag{5-7}$$

Heat transfer through the shaft wall is closely related to the thermal resistance between two sides of the wall, R_t, (Eq. (5-7)), which is determined by heat transfer coefficients on the interior and exterior shaft wall surfaces (h_{wi} and h_{wo}), as well as thermal conductivity of the wall, *k*. Both h_{wi} and h_{wo} are the effective heat transfer coefficients, which include both convective and radiant heat transfer portions. The radiant heat transfer depends on many factors, e.g. the geometry of the shaft, gas composition, gas and wall temperatures. Details about the calculation method of radiant heat transfer coefficient can be found in the reference Qi, Wang, and Zmeureanu (2014a). A sensitivity study by Qi, Wang, and Zmeureanu (2014a) also found that the results are not quite sensitive to the radiant heat transfer portion. Therefore, in this study, only convective heat transfer, h_{wc}, is considered on shaft wall surfaces, which is also the same as the previous studies did (Sun et al. 2011; Ji et al. 2013). h_{wc} is determined by Eq. (5-8), which combines natural and forced convections and C_w is 3.08 suggested by Qi, Wang, and Zmeureanu (2014a). ΔT_w is the temperature difference between the average smoke/air and surface temperatures of shaft wall, which can be calculated using Eqs. (5-3) ~ (5-5).

$$h_{wc} = \max[C_w \,|\, \Delta T_w \,|^{1/3}, \quad 0.037(k/l)\,\mathrm{Re}^{4/5}\,\mathrm{Pr}^{1/3}] \tag{5-8}$$

$$p_{shx} = p_{sh0} - \Delta p_{elx} \tag{5-9}$$

where

$$\Delta p_{elx} = \int_0^x \rho g dx = \frac{g p_{a0} H}{R T_a} \left\{ \frac{1}{\alpha} \ln \left[\frac{(T_{sh0} - T_a) + T_a Exp(\alpha x / H)}{T_{sh0}} \right] \right\} \tag{5-10}$$

Mass flow rate through the top and bottom openings of the shaft is calculated by Eqs. (5-11) and (5-12).

$$\dot{m}_t = \dot{m}_b = C_d A_t \sqrt{2(p_{shH} - p_{aH}) p_{a0} / (R T_{shH})} \tag{5-11}$$

$$\dot{m}_b = C_d A_b \sqrt{2\rho_a (p_{a0} - p_{sh0})} \tag{5-12}$$

To obtain the temperature attenuation coefficient, α, temperature profile, T_{shx}, pressure profile, p_{shx}, and mass flow rate, $\dot{m}$, the above coupled equations need to be solved by iterations. Detailed calculation steps are shown in Figure 5-2, where $\dot{m}_b$ and R_t are updated in each iteration and taken into the next iteration until the results converge. However, iterative calculations are not quite straightforward or practical for designs and analyses in the field of fire protection, which often relies on simpler formulations, e.g. empirical equations , without the need of iteration, such as the Klote equation for *NPL*, the upper-layer gas temperatures equations (McCaffrey, Quintiere, and Harkleroad 1981), and the equations of plume front locations developed by Cannon and Zukoski (Ji et al. 2015). Therefore, it would be meaningful to obtain a *NPL* formulation, e.g. in an empirical format, that consider non-uniform temperature distribution inside shaft. To achieve this, the first step is to identify the key physics parameters that can represent the non-uniform temperature distribution inside shaft. Then based on the key parameters, empirical equations will be developed.

The following work of this section is to derive a dimensionless form of *NPL*, based on which the key parameters can be determined.

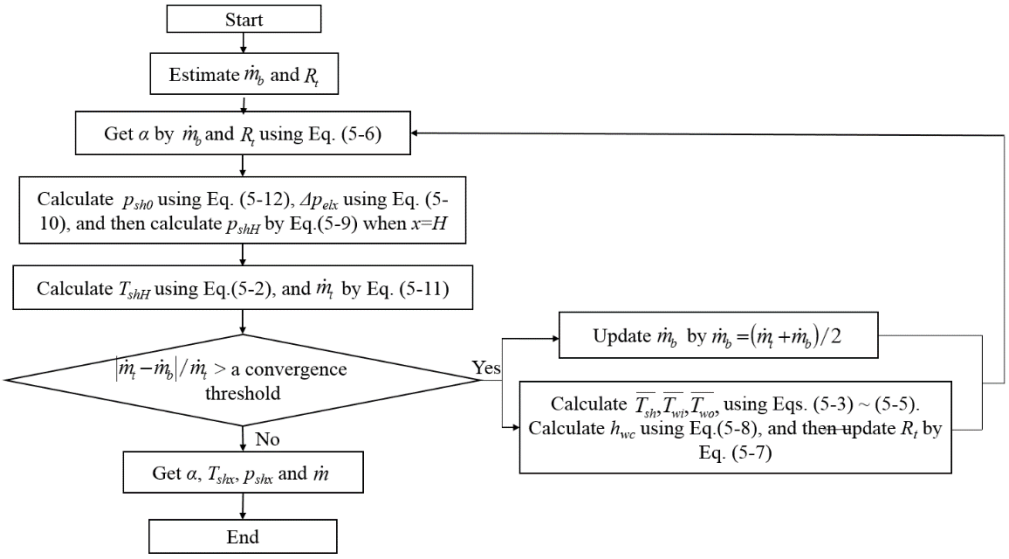

Figure 5-2 Iteration method to solve the coupled equations Eqs. (5-2) ~ (5-12).

The ambient pressure at the height of the *NPL*, $p_{a,np}$, is calculated by

$$p_{a,np} = p_{a0} - \rho_a g h_{np} \tag{5-13}$$

Based on these equations, new formulations of *NPL* can be derived by the following steps. First, we define an average smoke density below the *NPL*, $\overline{\rho}_{shl}$, and that above the *NPL*, $\overline{\rho}_{shu}$.

$$\overline{\rho}_{shl} = \frac{\Delta p_{el,h_{np}}}{g h_{np}} = \frac{1}{h_{np}} \int_0^{h_{np}} \rho_{shx} dx = \frac{1}{h_{np}} \int_0^{h_{np}} \frac{p_{a0}}{R T_{shx}} dx \tag{5-14}$$

$$\overline{\rho}_{shu} = \frac{1}{H - h_{np}} \int_{h_{np}}^{H} \rho_{shx} dx = \frac{1}{H - h_{np}} \int_{h_{np}}^{H} \frac{p_{a0}}{R T_{shx}} dx \tag{5-15}$$

Then take Eqs. (5-13) ~ (5-15) into Eq. (5-9) when $x = h_{np}$ and apply $\bar{\rho}_{shl}$ and $\bar{\rho}_{shu}$ to calculate pressure change below and above the *NPL*, an analytical equation of *NPL* in a dimensionless form, Eq. (5-16), is obtained.

$$\frac{h_{np}}{H} = \frac{1}{1 + \left(\frac{\rho_a - \bar{\rho}_{shl}}{\rho_a - \bar{\rho}_{shu}} \right) \frac{T_{shH}}{T_a} \left(\frac{A_b}{A_t} \right)^2} \tag{5-16}$$

Since the temperature profile is obtained by solving the coupled equations by following the procedure in Figure 5-2 and both of $\bar{\rho}_{shl}$ and $\bar{\rho}_{shu}$ depend on h_{np}/H, Eq. (5-16) is an implicit function of h_{np}/H, to find which it still needs iterations. One solution to avoiding iterations is to develop an empirical form of Eq. (5-16), which will be introduced in a later section of this study. Because Eq. (5-16) calculates the relative *NPL*, h_{np}/H, based on the smoke temperature at the shaft top, T_{shH}, we name Eq. (5-16) as the *NPL* equation based on shaft top temperature. For practical field applications, where a *NPL* needs to be determined, Eq. (5-16) shows that it is possible to measure T_{shH} at the top of a shaft to obtain the *NPL*.

For the cases, where T_{shH} is not available from measurements, the determination of the shaft top temperature, T_{shH}, is often not straightforward because it depends on the dimensionless number, α, and smoke mass flow rate, $\dot{m}$, as indicated by Eqs. (5-2) and (5-6). Therefore, it is preferable to express Eq. (5-16) in terms of other parameters, such as the smoke temperature at the shaft bottom, T_{sh0}, which is often known as the fire temperature at the fire floor and can be obtained from the nominal temperature-time curve (ISO 834 1975) or be related to HRR using the MQH method (McCaffrey, Quintiere, and Harkleroad 1981).

Therefore, to replace T_{shH} in Eq. (5-16) by T_{sh0}, we first reformulate Eqs. (5-11) and (5-12):

$$\dot{m} = \dot{m}_t = C_d A_t \sqrt{2\rho_{sh0}(H - h_{np})(\rho_a - \rho_{sh0})g} \tag{5-17}$$

$$\dot{m} = \dot{m}_b = C_d A_b \sqrt{2h_{np}\rho_a(\rho_a - \rho_{sh0})g} \tag{5-18}$$

Combining Eqs. (5-17) and (5-18), we obtain Eq. (5-19) by defining an effective area term, A^*.

$$\dot{m} = C_d A^* \sqrt{2[(H - h_{np})\rho_{sh0} + h_{np}\rho_a](\rho_a - \rho_{sh0})g} \tag{5-19}$$

where

$$A^* = \frac{1}{\sqrt{1/(A_t)^2 + 1/(A_b)^2}} \tag{5-20}$$

Combining Eqs. (5-2), (5-6) and (5-19), we finally obtain h_{np}/H as a function of T_{sh0} in Eq. (5-21), which is named here as the *NPL* equation based on shaft bottom temperature as a comparison to Eq. (5-16).

$$\frac{h_{np}}{H} = \frac{1}{1 + \left(\frac{\rho_a - \overline{\rho}_{shl}}{\rho_a - \overline{\rho}_{shu}}\right)\left[1 + \frac{T_{sh0} - T_a}{T_a} Exp\left(\frac{-PH/(C_p R_t)}{C_d A^* \sqrt{2[(H - h_{np})\rho_{sh0} + h_{np}\rho_a](\rho_a - \rho_{sh0})g}}\right)\right]\left(\frac{A_b}{A_t}\right)^2} \tag{5-21}$$

Both Eqs. (5-16) and (5-21) are implicit functions of the relative *NPL*, h_{np}/H, which cannot be solved directly.

For similar situations, empirical equations based on experimental data are often derived. For example, based on measured data, Li and Ji et al. derived the equation of the pressure difference between the shaft internal pressure at the *NPL* and the external pressure at the bottom opening (Li et al. 2014; Ji et al. 2013).

$$\Delta p_a = \frac{3463D}{T_a \beta} \ln \frac{1 + \alpha^* Exp\left(\beta \frac{h_{np}}{D}\right)}{1 + \alpha^*} \tag{5-22}$$

Based on the measured data, they are able to calculate the *NPL* of the stairwell (Li et al. 2014). In the following section, we compare the *NPL* results from this paper to their results. Meantime, Eqs. (5-16) and (5-21) will be further simplified to empirical forms by using the measured data from Ji et al. (2013) in a later section.

5.3. Validation

The *NPL* location in either Eqs. (5-16) or (5-21) can be found by solving the coupled equations introduced above. In this section, to confirm the accuracy of these equations, we employed steady state experimental data from a 1/3 scale stairwell (Ji et al. 2013). The stairwell physical model is with 12 floors and a floor height of 1 m except 1.2 m for the ground floor. The cross sectional area of the shaft is 1.5 m^2 with half of the shaft wall made of 12-mm fire-resistant glass and the other half made of 2-mm steel plates. There are two openings in the shaft: a 0.54 m^2 at the top and a 0.35 m^2 opening at the bottom. Two experiments in the literature were selected here for different sizes of methanol fires located at the ground floor, differentiated by the square pool size of 15 × 15 cm^2 and 25 × 25 cm^2. The measured corresponding smoke temperature at the ground level is 298 K and 324 K, respectively, which were used as T_{sh0} in the coupled equations T_a is set to the measured ambient temperature of 279 K.

The measured temperature distribution and mass flow rate will be used to compare with the predicted results from this paper. Since *NPL* is not measured in the experiment, the calculated *NPL* based on measured data following the method by Li et al. (2014) (Eq. 5-22) as introduced in the previous section will be used to compare with the results from this study.

Figure 5-3 compares the smoke temperature rise in the experiment and this study. The major discrepancy of smoke temperature rise is around 1 K for the pool size of 25 × 25 cm^2. Table 5-1

compares the mass flow rates and *NPL*. The largest relative difference of mass flow rate and *NPL* is 13% and 4%, respectively, for the pool size of 15 × 15 cm^2. Considering the complexity of the problem and the relative simplicity of the equations, these discrepancies are not significant and the predicted results by the coupled equations are acceptable.

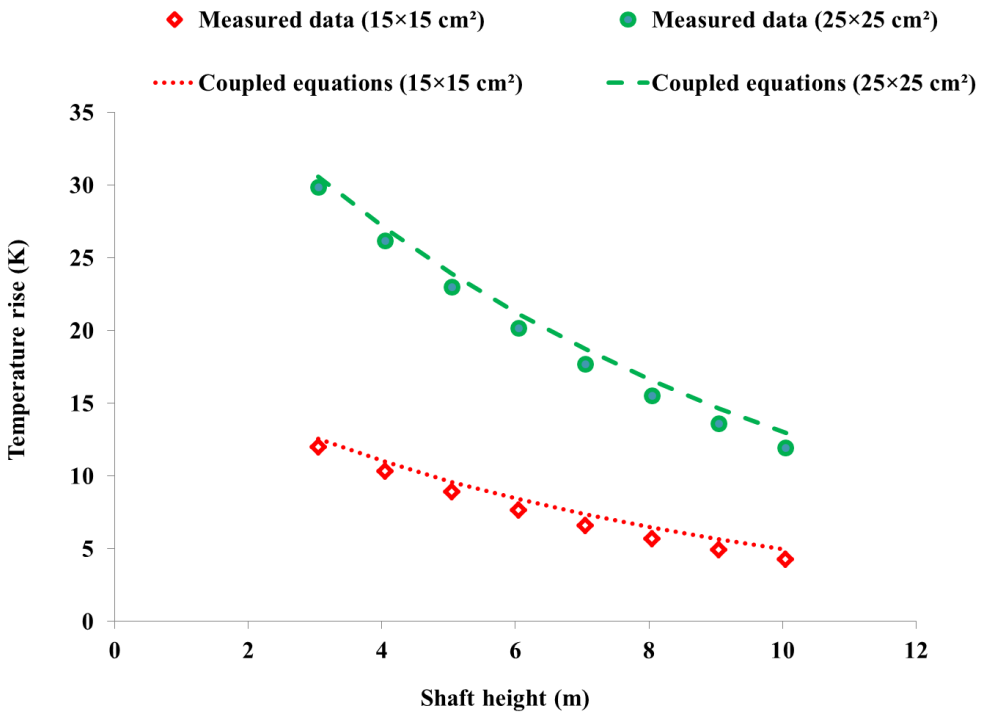

Figure 5-3 Comparison of predicted temperature distribution by coupled equations with the measured data (Ji et al. 2013) for different pool size

Table 5-1 Comparison of predicted mass flow rate and relative *NPL* by coupled equations with measured data (Ji et al. 2013) for different pool sizes

	Pool size	15×15 cm^2	25×25 cm^2
Mass flow	Ji et al. (2013)	0.252	0.336
rate (kg/s),	This study	0.220	0.328
$\dot{m}$	Relative difference	13%	2%

	Calculated from Ji et al. (2013)	0.526	0.554
h_{np}/H	This study	0.507	0.560
	Relative difference	4%	1%

5.4. Empirical formulations

According to the validation study, coupled equations that consider the effect of non-uniform temperature distribution can predict *NPL* with reasonable accuracy. Meanwhile, to avoid the iterations needed to solve these coupled equations, this section develops empirical formulations of *NPL* that consider the effect of non-uniform temperature distribution based on Eqs. (5-16) and (5-21).

5.4.1. NPL based on shaft top temperature

The *NPL* equation based on shaft top temperature, Eq. (5-16), is simplified to Eq. (5-23), a similar form to the Klote's equation (Eq. 5-1).

$$\frac{h_{np}}{H} = \frac{1}{1 + C_1 \left(\frac{T_{shH}}{T_a} \right)^{N_1} \left(\frac{A_b}{A_t} \right)^2} \tag{5-23}$$

The coefficients C_1 and N_1 in Eq. (5-23) can be determined by correlation analysis using experimental data. Here, we use the experiment for the pool sizes of 10 × 10 cm^2, 15 × 15 cm^2, 20 × 20 cm^2, 25 × 25 cm^2 and 30 × 30 cm^2 from the literature Ji et al. (2013) to obtain the coefficients, C_1 and N_1. The measured corresponding smoke temperatures at the bottom opening are 293 K, 298 K, 310 K, 324 K and 346 K, and the temperatures at the top opening are 281 K, 282 K, 286 K, 288 K and 295 K. Figure 5-4 finds that

C_1 = 2.36 and N_1 = -5.13.

The linear correlation coefficient, r, is 0.82, greater than 0.8 indicating a strong correlation (Chan 2003).

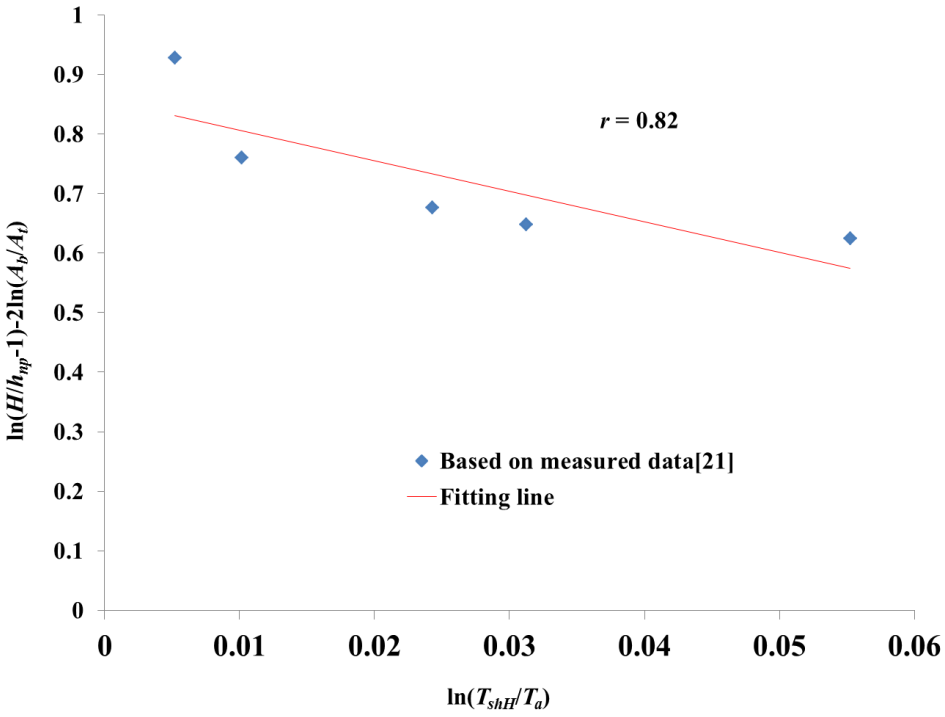

Figure 5-4 Correlation for empirical equation based on shaft top temperature.

Different from Klote's equation, the empirical equation (Eq. 5-23) considers heat transfer between smoke and shaft wall, which is represented by shaft top temperature, T_{shH}, instead of the uniform temperature, T_i, in Eq. (5-1). As indicated in Eq. (5-2), T_{shH} is related to smoke inflow temperature, T_{sh0}, ambient temperature, T_a, and temperature attenuation coefficient, α, in which the temperature attenuation coefficient, α, is an index representing smoke temperature distribution inside the shaft (Qi, Wang, and Zmeureanu 2014a) and it is also a function of overall thermal resistance, R_t, of the shaft as shown in Eqs. (5-6) and (5-7). A small α indicates a small decrease of the smoke temperature from bottom to top of the shaft because of large thermal resistance of shaft wall; hence

T_{shH} is close to T_{sh0}. A large α indicates large reduction of the smoke temperature inside the shaft because of low thermal resistance, and T_{shH} is much lower than T_{sh0}. Therefore, in Eq. (5-23), heat transfer through the shaft boundary is closely related to T_{shH}/T_a, which is a dimensionless number considering non-uniform temperature distribution for a non-adiabatic shaft. Meanwhile, the obtained constants C_1 and N_1 are based on the measured data from the literature, which may be limited and affected by variations of the parameters, e.g. heat transfer coefficient of the shaft wall, which will be investigated by a sensitivity study of 70 cases in section 5.5 of this paper.

5.4.2. NPL based on shaft bottom temperature

For other scenarios, e.g. when design smoke control systems, T_{shH} is unknown and hard to be estimated, the empirical equation based on T_{shH} cannot be used. It is necessary to seek an alternative empirical equation that only uses known parameters, such as the parameters relating to the shaft structure and design fire. Here, we simplified Eq. (5-21) into Eq. (5-24), where C_1 and N_1 are the same values as Eq. (5-23), and the coefficient, C_2, can be determined by the correlation of the experimental data.

$$\frac{h_{np}}{H} = \frac{1}{1+C_1\left(1+\frac{T_{sh0}-T_a}{T_a}Exp(-C_2\frac{P\sqrt{H}}{C_d A^*\sqrt{\rho_a{}^2-\rho_{sh0}{}^2}})\right)^{N_1}\left(\frac{A_b}{A_t}\right)^2} \tag{5-24}$$

Based on the measured data from the literature Ji et al. (2013), Figure 5-5 finds that

$C_2 = 0.0037$

with r of 0.81.

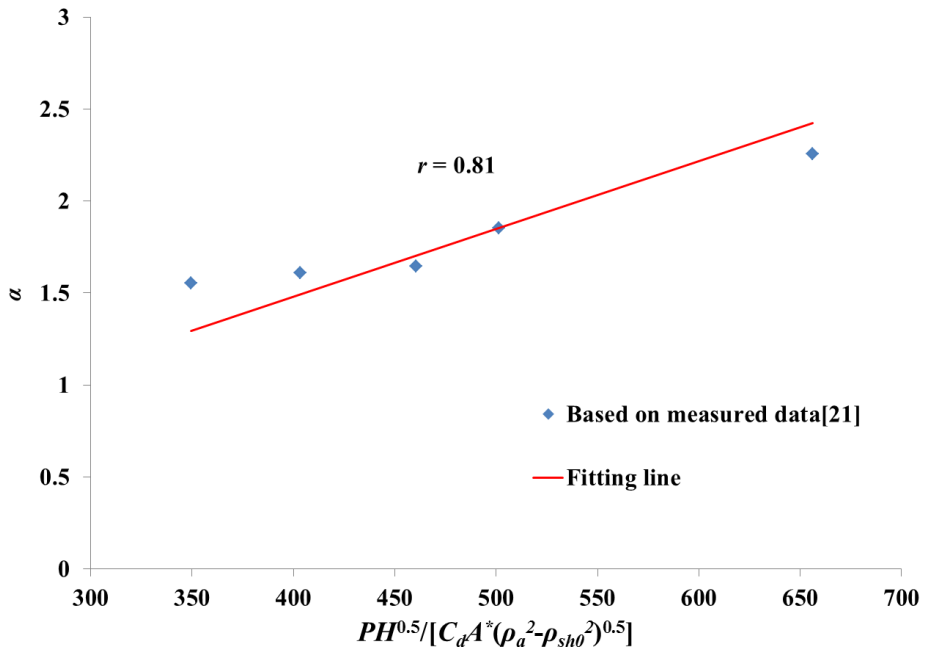

Figure 5-5 Correlation for empirical equation based on shaft bottom temperature.

It should be noted that due to limited data available from the literature, the values of C_1, N_1 and C_2 obtained in this section may be only applicable to the cases with the similar conditions as those of the 1/3 scale experiment. Therefore, it is suggested that readers use the constants, C_1, N_1 and C_2 with caution. It is also suggested that more experiments be conducted to verify and improve these constants, if necessary, which would be the future work but not the focus at the current stage. The main contributions of this paper are to determine the key parameters that consider non-uniform temperature distribution inside the shaft and to obtain the empirical equations (Eqs. 5-23 and 5-24) with these key parameters. Based on the correlation equations developed here, other researchers will be able to improve the actual values of the constants if more data are available.

Considering the fact that the empirical equations for the *NPL*, Eq. (5-23) and Eq. (5-24) with C_1 = 2.36, N_1 = -5.13 and C_2 = 0.0037 are based on limited number of experimental data, a sensitivity study was conducted to confirm its applicability to other ranges of data than the experiments, which

will be presented in the following section. Such a study also helps to compare the applicability and limitations among the Klote's equation (Eq. 5-1), the coupled equations in the theory section (Eqs. 5-2 ~ 5-12), and the empirical equations (Eqs. 5-23 and 5-24).

5.5. Sensitivity study

The sensitivity study includes 70 cases with different fire loads (i.e. represented by smoke entrance temperatures), shaft structures (top and bottom opening areas), and ambient temperatures as listed in Table 5-2, where each parameter varies between ± 20%, except the ambient temperature, T_a; 0% represents the experimental conditions (Table 5-3). The ranges of the thermal resistance of the shaft wall, R_t, calculated by the coupled equations, are also shown in Table 5-2.

Table 5-2 Key parameters for sensitivity study

Parameters	A_b (m^2)	A_t (m^2)	T_a (K)	T_{sh0} (K)*	R_t ((m^2·K)/ W)
Case 1~25	0.28~0.42 (Table 5-3)	0.54	279	293 ~ 346	0.097 ~ 0.18
Case 26~50	0.35	0.43~0.65 (Table 5-3)	279	293 ~ 346	0.099 ~ 0.18
Case 51~70*	0.35	0.54	251~307 (Table 5-3)	293 ~ 346	0.086 ~ 0.32

Note: *293K, 298K, 310K, 324K and 346K.

Table 5-3 Variation parameters

Variation of parameters	A_b (m^2)	A_t (m^2)	T_a (K)
-20%	0.28	0.43	/
-10%	0.31	0.48	251
-5%	/	/	265
0%	0.35	0.54	279
5%	/	/	293

10%	0.38	0.59	307
20%	0.42	0.65	/

Figure 5-6 compares the *NPL* by different methods. For the method based on uniform temperature distribution assumption (Klote's equation), T_{shH} is the uniform temperature, T_i, and for the method of empirical equation based on T_{sh0}, T_{shH} is calculated by Eq. (5-2). It is found that the predicted relative *NPL* by the empirical equations are reasonably close to that of the couple equations. The predicted relative *NPL* by the Klote's equation is also presented in Figure 5-6. Compared to the results of the coupled equations, the *NPL* is often overestimated by the Klote's equation, indicating that fewer building floors are exposed to smoke and therefore the risk of smoke is underestimated.

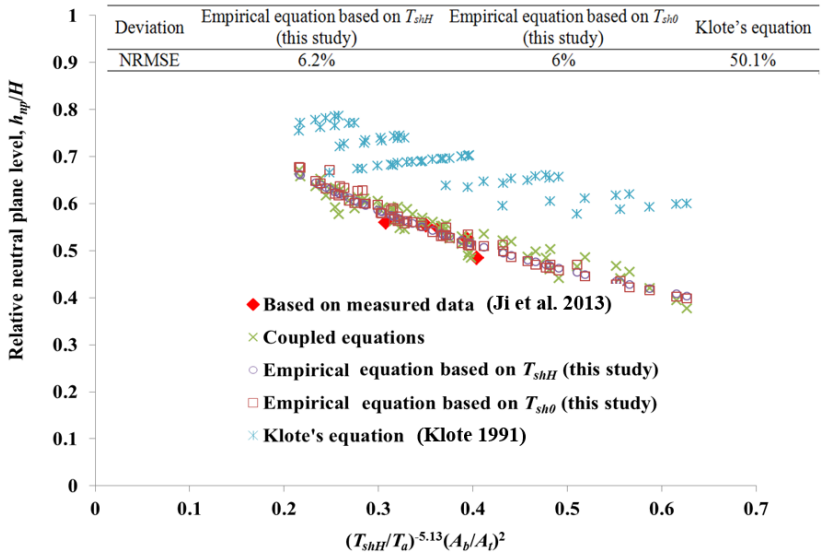

Figure 5-6 Comparison of predicted relative NPL.

For a quantitative comparison, *NRMSE* (Zhao and Wang 2014) in Eq. (5-25) is used. Using the results from the coupled equations as a baseline, the *NRMSE* is found to be 6.2%, 6% and 50.1% for the empirical equations based on T_{shH}, T_{sh0}, and Klote's equation, respectively. It shows that

the empirical equations perform better than the Klote's equation for a non-adiabatic shaft during fires. Considering the thermal resistance of the shaft wall varies from 0.086 to 0.32 (m^2·K)/W as is shown in Table 5-2, the small values of *NRMSE* for the empirical equations confirms that the correlated number C_1 and N_1 are not strongly dependent on the heat transfer conditions through the shaft wall for the cases studied in this paper.

$$NRMSE = \frac{1}{P_{coup,\max} - P_{coup,\min}} \left[\frac{1}{n} \sum_{i=1}^{n} \left(P_{ek,i} - P_{coup,i} \right)^2 \right]^{\frac{1}{2}} \tag{5-25}$$

5.6. Discussion

When the smoke temperature in a shaft is not uniform, such key parameters as fire strength (as indicated by inflow smoke temperature), shaft opening areas, ambient temperatures, and shaft heights may have different effects on the *NPL* location. To better understand the underlying physics, this section compares the predicted *NPL* by the empirical equations from this study and Klote's equation for different categories of parameters. In the following discussion, except the parameter that is considered for its effect, other parameters are kept the same as that of the experiment in the literature Ji et al. (2013).

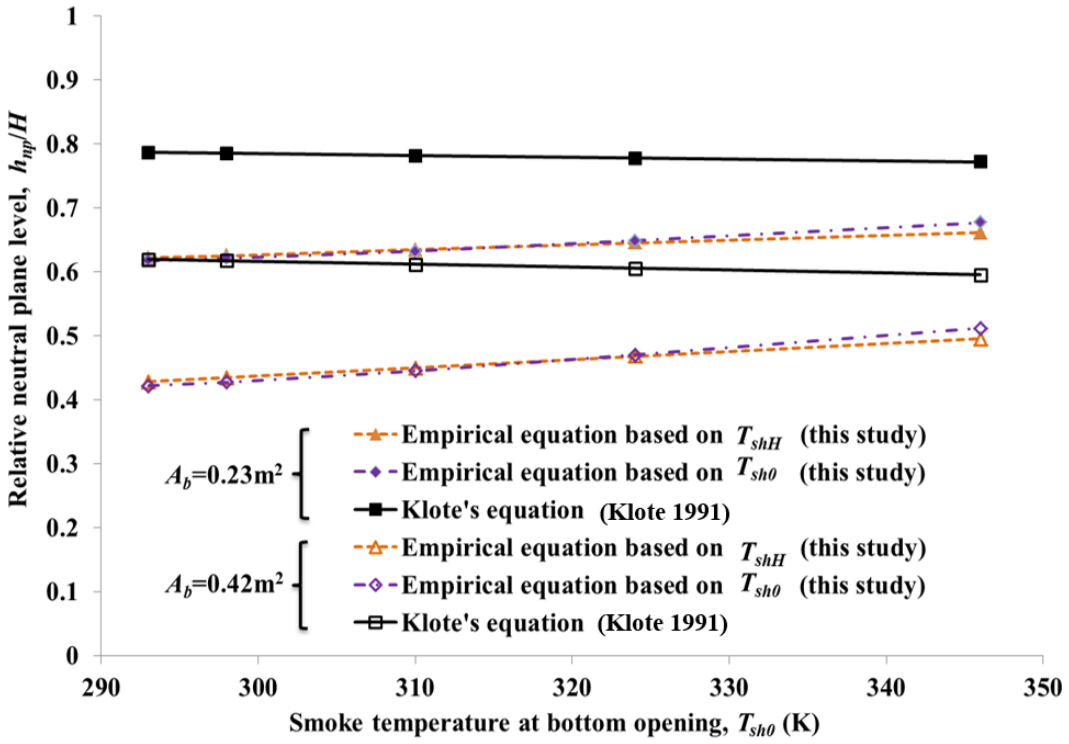
Relative neutral plane level, h_{np}/H
1
0.9
0.8
0.7
0.6
0.5
0.4
0.3
0.2
0.1
0
290
300
310
320
330
340
350
Smoke temperature at bottom opening, T_{sh0} (K)
A_b=0.23m²
Empirical equation based on T_{shH} (this study)
Empirical equation based on T_{sh0} (this study)
Klote's equation (Klote 1991)
A_b=0.42m²
Empirical equation based on T_{shH} (this study)
Empirical equation based on T_{sh0} (this study)
Klote's equation (Klote 1991)

(a)

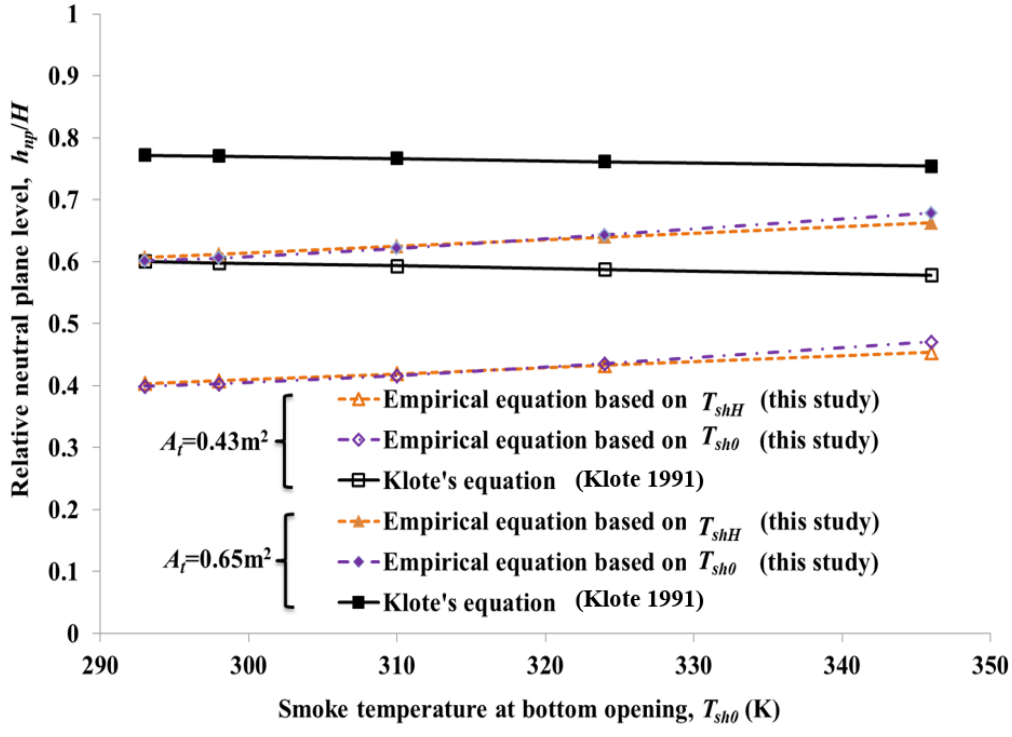
Relative neutral plane level, h_{np}/H
1
0.9
0.8
0.7
0.6
0.5
0.4
0.3
0.2
0.1
0
290
300
310
320
330
340
350
Smoke temperature at bottom opening, T_{sh0} (K)
A_f=0.43m²
Empirical equation based on T_{shH} (this study)
Empirical equation based on T_{sh0} (this study)
Klote's equation (Klote 1991)
A_f=0.65m²
Empirical equation based on T_{shH} (this study)
Empirical equation based on T_{sh0} (this study)
Klote's equation (Klote 1991)

(b)

Figure 5-7 Effects of shaft bottom temperature and (a) bottom opening area and (b) top opening area on predicted relative *NPL*.

Figure 5-7 compares the results among predicted *NPL*, T_{sh0}, A_b (Figure 5-7a) and A_t (Figure 5-7b). For all formulations, Figure 5-7(a) shows that the predicted *NPL* decreases with the increase of A_b, which is intuitive because a larger opening at the fire floor creates higher smoke risk in the shaft. In comparison, Figure 5-7(b) illustrates that the *NPL* increases with A_t for all three equations, which is also reasonable because a larger opening at the shaft top exhausts more smoke from the shaft itself and thus creates less risk of smoke spread to the building. It also shows that with the increase of fire strength (as indicated by an elevated shaft bottom temperature, T_{sh0}), the Klote's equation shows a slight decrease of *NPL*. Under the same conditions, the predicted *NPL* by the empirical equations in this study increases slightly, which is consistent with the study by Li et al. (2014).

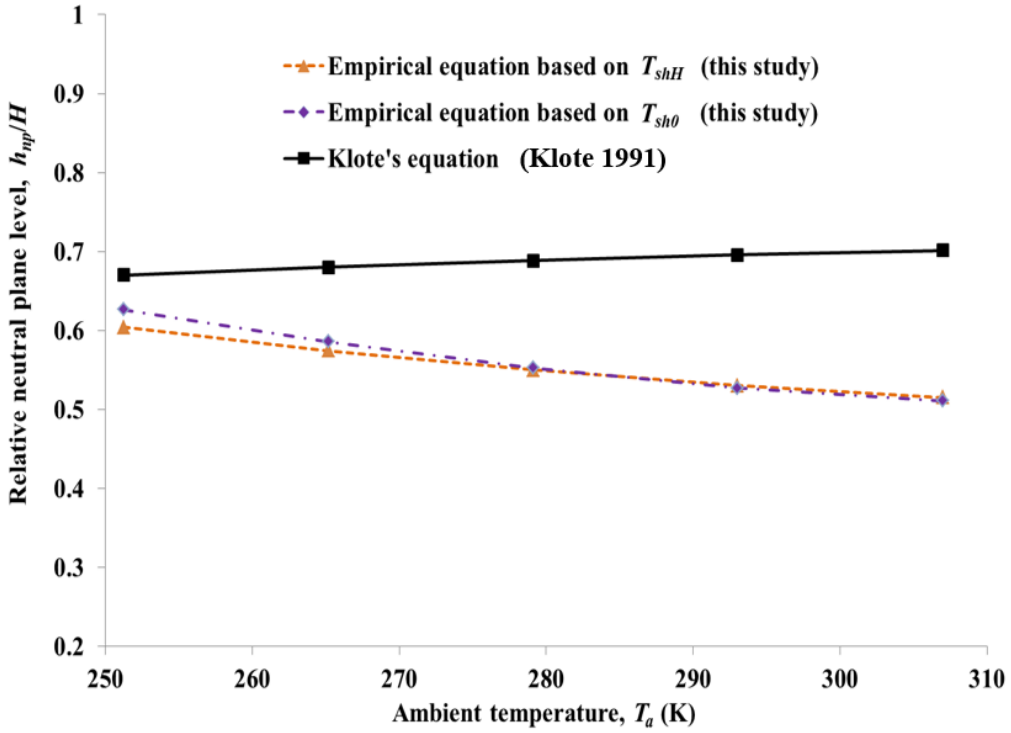

Figure 5-8 Effect of ambient temperature on predicted relative *NPL* when T_{sh0}=324 K.

Figure 5-8 shows the effect of ambient temperature on *NPL*. With the decrease of ambient temperature, T_a, the predicted *NPL* by the empirical equations increases. This is because the increased T_a contributes to a decreased value of T_{shH}/T_a. This is consistent with the calculated *NPL* based on the measured data by Ji et al. (2013) as shown in Figure 5-6. In comparison, the Klote's equation shows the opposite trend due to the assumption of the uniform temperature.

The effect of shaft height on *NPL* is shown in Figure 5-9. It is found that the *NPL* by the empirical equations are reversely proportional to the shaft height, *H*, which means higher buildings leading to lower *NPL* and thus more smoke threats. This conclusion is consistent with that found by Black (2009). However, the Klote's equation shows that the relative *NPL* is independent of the shaft height.

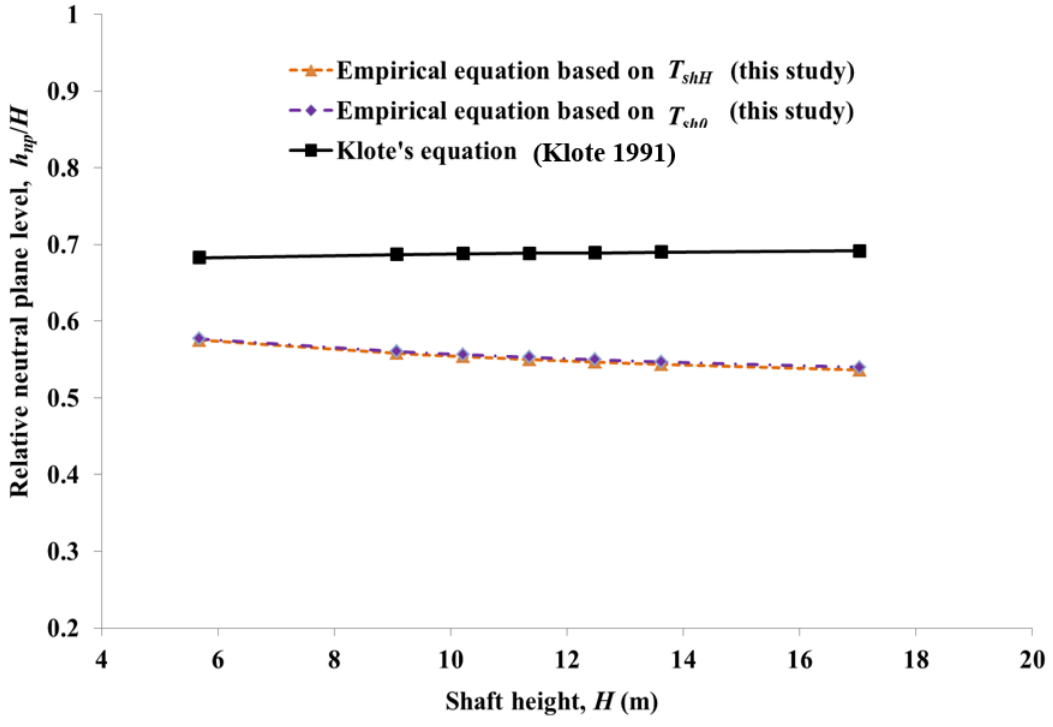

Figure 5-9 Effect of shaft height on predicted relative *NPL* when T_{sh0}=324 K.

5.7. Conclusion

To study the effects of non-uniform smoke temperature distribution on the location of *NPL*, the coupled equations of temperature distribution, flow rate and pressure distribution were reported for non-adiabatic shafts and validated by experimental data. Empirical equations based on dimensionless numbers were developed for *NPL* through regression analysis. A sensitivity study of the developed empirical equations was conducted by comparing with the predicted results of the coupled equations. The applicability and limitations of the conventional *NPL* model that is based on uniform temperature assumption (the Klote's equation) were evaluated by comparing with the empirical equations. The study reached the following major conclusions:

(1). For non-adiabatic shafts, the effects of non-uniform temperature distribution on *NPL* should be considered. The provided case study shows that the uniform temperature assumption leads to over-estimated *NPL*, and the relation between shaft bottom/top temperature and *NPL* predicted based on this assumption is inconsistent to that of the experiments.

(2). Non-uniform temperature distribution inside of the shaft can be represented by a dimensionless number, T_{shH}/T_a, which is a ratio of shaft top temperature to ambient temperature. This dimensionless number is a function of temperature attenuation coefficient, α, which indicates smoke temperature profile inside the shaft.

(3). The sensitivity study found that the developed empirical equations, which include the dimensionless number in terms of T_{shH} and T_{sh0}, can predict *NPL* accurately. The existing equation may either underestimate or overestimate the *NPL* locations.

It is noted that readers should use the obtained constants C_1, N_1 and C_2 of the empirical equations with caution due to limited data used to develop these constants. The main purpose of this paper

is therefore not to provide general applicable values of C_1, N_1 and C_2, but present *NPL* empirical equations that can benefit other researchers to understanding the underlying physics regarding the *NPL* in high-rise shafts and to developing their own correlations when more data are available. The limitations of the current study are also noted: the experimental data are limited and the *NPL* locations were not directly measured from the experiments. Further studies with more quality experimental data and measured *NPL* locations should be done in the future.

Chapter 6 Scale Modeling of Steady-state Smoke Spread in Large Vertical Spaces of High-rise Buildings

Abstract

Large vertical spaces are essential parts of modern high-rise buildings, providing much convenient and comfortable environment to people. However, driven by stack effect, smoke flows often spread through the large vertical spaces, which becomes a major challenge for high-rise fire protections; therefore it is necessary to conduct researches of smoke movement inside the large vertical spaces. Experimental studies on sub-scaled models play an important role in the fire smoke research. Froude modeling method is probably the most common approach to design sub-scaled experiments. However recent studies have found that Froude modeling may not obtain accuracy temperature on the sub-scaled experiments, especially for the temperature near the building boundaries where there exists heat transfer between smoke and the boundaries. In this paper, a new modeling method is developed by deriving dimensionless groups from differential governing equations that include energy balance and mechanical energy equations for both mechanical and natural venting systems, in which heat transfer is concerned in the energy balance equation. The resistance of the inside shaft structure is also concerns by discharge coefficient, C_d. To verify the new modeling method, experiments were designed on three different size shafts using both Froude modeling and new modeling methods. The results, including temperature profile, relative neutral plane level and mass flow rate, are compared between the two modeling methods, and it was found that the new modeling method can achieve much more accurate results.

6.1. Introduction

In the recent decades, large vertical spaces, elevator shafts, and tall atriums, have been widely used in high-rise buildings to achieve comfortable environment and energy conservation. For example,

the tall atriums applied in the high-rise buildings 1 Bligh Street (Austria) and Palais Royale (India) could benefit more compartments in the buildings by receiving natural sunlight and make full use of and natural ventilation to save energy (Wood and Ruba 2013; Colaco, Dravid, and Kasilwal 2012). However, due to the difference of indoor/outdoor densities of buildings, the buoyancy-driven smoke and toxic flows often spread from fire origins to upper part of the buildings, threating to people's lives and properties, and therefore become a major challenge for high-rise fire protections.

Statistics have shown that about more than 95 % of the upward movement of smoke in typical high-rise buildings is through the large vertical spaces (Tamura 1994). Numerous studies have focused on the fire smoke movement inside high-rise large vertical spaces by means of computer simulation and experiments, in which experiments play an incredible important role. The experiment is done in the physical world and more realistic (Klote et al. 2012); so the results are more reliable and computer simulation needs to be verified by it. Since full-size fire experiments are costly and often unpractical to be conducted in buildings, most of the experimental researches on smoke movement in high-rise buildings are conducted on sub-scaled physical models. Froude modeling is probably the most common approach to scale modeling of smoke movement in buildings, and is widely used for design analysis, verification of CFD simulation and fire reconstruction. Ding et al. (Ding et al. 2004) studied the possibility of using the same system for natural ventilation and smoke control in buildings by carrying out CFD simulations of full size 8-storey building with a solar chimney on top of the atrium. A 1/25 scale model, designed based on Froude modeling, is developed to validate CFD simulations. To investigate the hot smoky gases entering an atrium from a fire within an adjacent compartment, Harrison used Froude modeling to design experiments on 1/10th physical scale model, the results of which were applied to validate

CFD simulations (Harrison 2004). Quintiere applied scaling technique to clarify the performance of a smoke control system which operated in an actual fire incident in a department store atrium. The scale model results confirmed a design flaw in the smoke control system. The high velocity inlet air was shown to be responsible for mixing and destratifying the hot smoke in the atrium and dispersing it throughout the department store (Quintiere and Dillon 2008). To study smoke movement inside high-rise buildings, 1/3 scaled building model was developed using Froude modeling, on which extensive researches were conducted on the influence of the staircase ventilation state on the flow and heat transfer of the heated room on the middle floor (Shi et al. 2014a), the effects of ventilation on the combustion characteristics in the compartment connected to a stairwell (Ji et al. 2016).

However, several studies found that sub-scaled experiments using Froude modeling may not obtain accurate temperature. Carey compared temperatures at different locations between a full compartments and a 1/8 scaled compartments designed based on Froude modeling. It was found that the accuracy of the model does vary based on the distance from the fire. Due to heat transfer between the gas and the boundary, the temperatures measured near the boundaries are not as accurate as the temperatures measured closer to the fire. For the measuring location 5.1 cm below the ceiling and 5.76 m away from the fire of 250 kW gas burner, temperature rise of full size model is 40°C but the difference between full model and 1/8 scaled model is up to 20°C (Allison C. Carey 2010). Chow carried out experiments of natural smoke filling process on both full-scale atrium and a 1/26.5 scale atrium. The experiments were designed according to Froude modeling. However, it was observed that there are quite large deviations between the temperatures measured in the scale model and the full-size atrium. Therefore, they suggested that the scaling law for temperature requires further examination (Chow and Lo 2008). The large deviation is probably

caused by the negligence of heat transfer between the smoke/gas and the boundaries. During a high-rise fires, fire smoke temperature can be an order of magnitude higher than surrounding air at the bottom of large vertical spaces and drop quickly at the higher floor due to the heat exchange between the fire smoke and the boundaries (Qi, Wang, and Zmeureanu 2014a; Qi, Wang, and Zmeureanu 2015). Therefore it is necessary to consider the heat transfers when sub-scale the large vertical spaces during fires.

Smoke spread in high-rise vertical spaces is often either driven naturally by buoyancy due to the temperature difference of the smoke and the ambient, and/or mechanically by air moving devices, such as fans. This paper investigated both ventilation means starting by examining the differential forms of the governing conservation equations including heat balance equation, mechanical energy equation and continuity equation. Compared to previous work of scaling analysis, this study did not start the analysis with general and full-form partial differential equations but instead use a simplified form of analytical solutions to the heat and mass transfer in high-rise shafts. The new method helps to provide a better and more straightforward route to developing the required dimensionless groups suitable for the current specific problem. To verify the new scaling model, experiments were conducted in three shaft models with scale ratio of 1:1/3:1/4 and different materials for both mechanical and natural movement of the fire smoke. The performance of the similarity of the new model was then compared to the traditional Froude modeling method.

6.2. Governing equations and dimensionless groups

A scaling method is based on dimensionless groups/dimensionless variables (Munson et al. 2009). To obtain the dimensionless groups, governing equations that describe the phenomenon of interests are expressed in terms of dimensionless variables in this section.

Smoke movement inside the large vertical spaces can be modeled using one-dimensional forms of the governing equations at steady state (Qi, Wang, and Zmeureanu 2015; Qi, Wang, and Zmeureanu 2014b; Ji et al. 2013). In this paper, a shaft in Fig. 6-1 is employed to represent a typical large vertical space in high-rise building. At the top of the shaft, a fan is used to exhaust smoke from the shaft when mechanically-driven smoke spread system applies, while during naturally-driven, the exhaust fan is replaced by an opening. The following sections, section 6.2.1, and 6.2.2, report the derived dimensionless equations and groups for mechanically and naturally driven, respectively.

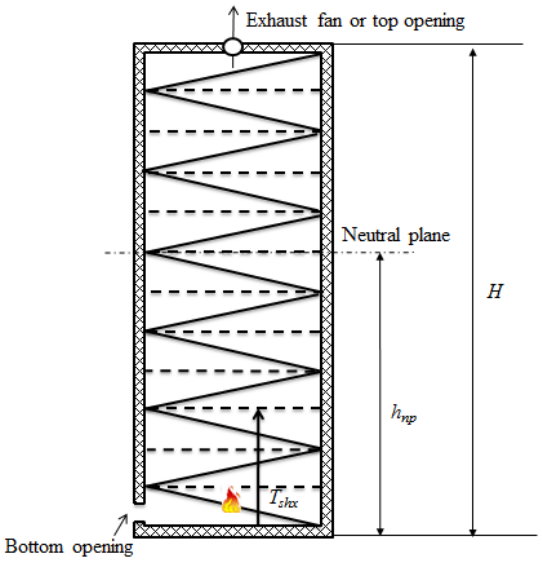

Figure 6-1 Schematic of a high-rise shaft during fires

6.2.1. Mechanical smoke venting

The dimensional governing equations of heat balance, and mechanical energy balance along the vertical direction of the shaft, and at the bottom of the shaft are listed in Eqs. (6-1) ~ (6-3), respectively.

Heat balance equation:

$$\dot{m}C_P dT_{shx} + \frac{(T_{shx} - T_a)Pdx}{R_t} = 0 \tag{6-1}$$

Mechanical energy balance equation along the height of shaft:

$$dp_{shx} + \rho_{shx} g dx = 0 \tag{6-2}$$

Mechanical energy equation at the bottom opening of shaft:

$$dp + \frac{\rho_a}{2} dv^2 = 0 \tag{6-3}$$

To nondimensionalize the above equations, the following dimensionless parameters are defined.

Dimensionless temperature:

$$\hat{T}_{shx} = \frac{T_{shx} - T_a}{T_f - T_a} = \theta_{shx} \tag{6-4}$$

Dimensionless height or relative height:

$$\hat{x} = \frac{x}{H} = \varphi \tag{6-5}$$

Dimensionless smoke velocity:

$$\hat{v} = \frac{v}{v_b / C_d} \tag{6-6}$$

where v_b is the velocity of air at bottom opening.

Dimensionless pressure:

$$\hat{p} = \frac{p - p_{a0}}{\rho_a g H} \tag{6-7}$$

Based on the Buckingham Π theorem, Eqs (6-1) ~ (6-3) can then be converted to their dimensionless forms accordingly.

Dimensionless heat balance equation:

$$d\hat{T}_{shx} + \Pi_1 \hat{T}_{shx} d\hat{x} = 0 \tag{6-8}$$

Dimensionless mechanical energy balance equation along the shaft:

$$d\hat{p}_{shx} + \frac{1}{\left(\Pi_2 \hat{T}_{shx} + 1\right)} d\hat{x} = 0 \tag{6-9}$$

Dimensionless mechanical energy equation at the bottom opening:

$$d\hat{p} + \frac{1}{2}\Pi_3{}^2 d\hat{v}^2 = 0 \tag{6-10}$$

Where the Π terms are defined here.

$$\Pi_1 = \frac{PH}{\dot{m} C_P R_t} = \alpha \tag{6-11}$$

$$\Pi_2 = \frac{T_f - T_a}{T_a} = \eta \tag{6-12}$$

$$\Pi_3 = \frac{v_b}{C_d \sqrt{gH}} = \frac{\dot{m}}{C_d A_b \rho_a \sqrt{gH}} = Fr / C_d \tag{6-13}$$

$$\Pi_1 \cdot \Pi_3 = \frac{PH}{C_d R_t A_b \rho_a \sqrt{gH}} \tag{6-14}$$

It should be noted that in the mechanical energy equation, Eq. (6-2), C_d is the discharge coefficient for the flow resistance at the top/bottom openings, and we did not directly express the flow frictions from shaft walls and/or stairs in staircases, and the change of velocity due to density. These wall/stair frictions can be lumped and combined into the discharge coefficient of the top/bottom openings under the assumption of the frictions distributed evenly throughout the shaft. Using this

concept, Ji et al. calculated the C_d value to be around 0.23 for the wall/stair frictions in their natural-ventilated 12.2-m scaled stairwell (Ji et al. 2013). Similarly, we derived the C_d formulation for mechanically-driven system in Eq. (6-15).

$$C_d = \left(\frac{1}{2} \rho_a v_b^2 \Big/ \Delta p \right)^{1/2} \tag{6-15}$$

where

$$\Delta p = \frac{3463D}{T_a \beta} \ln \frac{1 + \alpha^* e^{\left(\beta \frac{H}{D}\right)}}{1 + \alpha^*} \tag{6-16}$$

6.2.2. Natural smoke venting

Compared to mechanically-driven system, smoke flow rate is driven naturally by buoyancy due to the temperature difference inside/outside a shaft, and becomes an unknown parameter to be solved. Therefore the formulations and the dimensionless groups are slightly different, although the conservation equations of Eqs. (6-1) ~ (6-3) remain the same as the mechanically-driven.

For naturally-driven smoke spread, mechanical energy equation at the top opening of shaft is needed:

$$dp + \frac{\rho_{shH}}{2} dv^2 = 0 \tag{6-17}$$

Dimensionless mechanical energy equation at the top opening:

$$d\hat{p} + \frac{1}{2} \Pi_3^2 \Pi_4^2 \Pi_5^2 d\hat{v}^2 = 0 \tag{6-18}$$

where

$$\Pi_4 = \rho_a / \rho_{shH} = T_{shH} / T_a = 1 + \eta e^{(-\alpha)} = \gamma \tag{6-19}$$

$$\Pi_5 = \frac{A_b}{A_t} \tag{6-20}$$

In fact, Π_1 is the temperature attenuation coefficient, α , Π_2 is the normalized temperature rise, η, and Π_4 is the relative smoke temperature rise at the top of shaft, γ, as used in a previous study by Qi et al. (Qi, Wang, and Zmeureanu 2014a), who defined these numbers directly from their analytical solutions of shaft smoke flow instead of the similarity analysis as in this study.

Here, Π_5 is the ratio of bottom and top opening area. Using Ji et al.'s method (Ji et al. 2013), C_d can be for naturally-driven by Eq. (6-21).

$$C_d = \left[\left(\frac{1}{2} \rho_a v_b^2 + \frac{1}{2} \rho_{shH} v_{shH}^2 \right) \Big/ \Delta p \right]^{1/2} \tag{6-21}$$

6.3. Scale modeling method

Using the dimensionless groups obtained in section 6.2, a new modeling method for both mechanical and natural venting can be developed. For comparison, Froude modeling method is also summarized here.

6.3.1. Froude modeling method

For both mechanically-driven and naturally-driven smoke spread Eqs. (6-22) ~ (6-24) provide the Froude modeling method for scaling. For mechanically-driven smoke spread, the fan mass flow rate is determined by Eq. (6-24). Froude modeling requires no scaling for temperature, which means T_{shx}/T_a . and relative neutral plane level (*NPL*), φ_{np}, should be conserved with the full scale experiments.

Geometry similarity:

$$x_m = x_f \frac{H_m}{H_f} \tag{6-22}$$

Heat release rate:

$$E_m = \left(\frac{H_m}{H_f} \right)^{5/2} E_f \tag{6-23}$$

Mass flow rate:

$$\dot{m}_m = \dot{m}_f \frac{H_m^{5/2}}{H_f^{5/2}} \tag{6-24}$$

6.3.2. New modeling method

- Mechanical venting

As mentioned earlier, the issue with the Froude modeling is that heat transfer is not properly modeled so temperature similarity cannot be maintained as expected: the scaled temperature is often significantly different from the full-size value. Therefore, one of the major objectives here for the new scaling method is to maintain the same $\hat{T}_{shx}$ and $\hat{p}$, Π_1, Π_2, Π_3 need to be maintained according to Eqs. (6-8) ~ (6-10).

Since $\Pi_1 \cdot \Pi_3$ is only decided by the features of the shaft and ambient air density as shown in Eq. (6-15) and is easier to be calculated without considering the mass flow rate, $\dot{m}$, we use $\Pi_1 \cdot \Pi_3$ instead of Π_1. As a result parameters, $(\Pi_1 \cdot \Pi_3), \Pi_2$ and Π_3, need to be conserved. The new scaling method on the basis of $(\Pi_1 \cdot \Pi_3), \Pi_2$ and Π_3 for mechanically-driven smoke spread is shown in Eqs. (6-25) ~ (6-28), in which Eqs. (6-26) ~ (6-28) are derived from $(\Pi_1 \cdot \Pi_3)$ (Eq. 6-14), Π_2 (Eq. 6-12) and Π_3 (Eq. 6-13) respectively. The new modeling method indicates that as long as Eqs. (6-25) ~

(6-28) are satisfied, the dimensionless temperature profile, θ_{sh}, relative *NPL*, φ_{np}, should be the same for the full size experiment and sub-scaled experiment.

Perimeter of the shaft

$$P_m = \frac{H_m}{H_f} P_f \tag{6-25}$$

Bottom opening area:

$$A_{bm} = \frac{H_m^{1.5} C_{df} R_{tf} \rho_{af}}{H_f^{1.5} C_{dm} R_{tm} \rho_{am}} A_{bf} \tag{6-26}$$

Fire temperature:

$$T_{fm} = \frac{(T_{ff} - T_{af}) T_{am}}{T_{af}} + T_{am} \tag{6-27}$$

Mass flow rate:

$$\dot{m}_{bm} = \left(\frac{C_{dm} A_{bm} \rho_{am} H_m^{0.5}}{C_{df} A_{bf} \rho_{af} H_f^{0.5}} \right) \dot{m}_{bf} \tag{6-28}$$

- Natural venting

Similar to the new modeling method of mechanically-driven smoke spread, for naturally-driven smoke spread, $(\Pi_1 \cdot \Pi_3), \Pi_2$ and Π_5 should be kept the same to maintain $\hat{T}_{shx}$, $\hat{v}$ and $\hat{p}$. Therefore Eqs. (6-25), (6-26), (6-27) and (6-29) should be satisfied. Consequently the dimensionless temperature profile, θ_{sh}, relative *NPL*, φ_{np}, and dimensionless mass flow rate, Fr/C_d, should be the same for the full size experiment and sub-scaled experiment.

Top opening area:

$$A_{tm} = \frac{H_m^{1.5} C_{df} R_{tf} \rho_{af}}{H_f^{1.5} C_{dm} R_{tm} \rho_{am}} A_{tf} \tag{6-29}$$

Different from Froude modeling method, the bottom opening area of the new modeling method, A_b, not just considers the size of the shaft represented by the shaft height, H, but also concerns the discharge coefficient of the opening, C_d, thermal resistance between two sides of the shaft wall, R_t, and the ambient air density, ρ_a. Therefore the new modeling method is more flexible to different shaft structure that have different flow resistance inside the structure (different C_d), different materials of shaft (different R_t) and environmental temperature (different ρ_a).

6.4. Experiments

The verification of the new scaling method compared to the Froude modeling method was conducted for a series of experiments in three laboratory shafts. The first shaft is a 1/3 scaled shaft with a total of 12 floors with internal stairs, of which only 6 floors are used in this study (total height = 6.2 m as shown in Fig. 6-2), located at the University of Science and Technology of China (USTC). On each floor, there is one hole on the center of one of the shaft walls to measure the pressure inside the shaft. The cross sectional area of the shaft is 1.5× 1 m^2 with half of the shaft wall made of 12-mm fire-resistant glass and the other half made of 2-mm steel plates. The other two shafts were built at Concordia University, Canada, as sub-scale models of the USTC shaft: 1:1/3-scale for 2.1-m-high Concordia shaft 1 and 1:4-scale for the 1.6-m Concordia shaft 2. Both sub-scaled shafts are without internal stairs. Concordia shaft 1 is made of acrylic panels with the cross-sectional area of 0.5 × 0.3 m^2 and wall thickness of 3 mm. It is divided into 7 floors, each of which is with 0.3 m height with two holes drilled on the side wall at each floor to measure pressures inside the shaft. Concordia shaft 2 is 1.575 m high made of gypsum boards with the cross-section of 0.375× 0.225 m^2 and wall thickness of 9.5 mm.

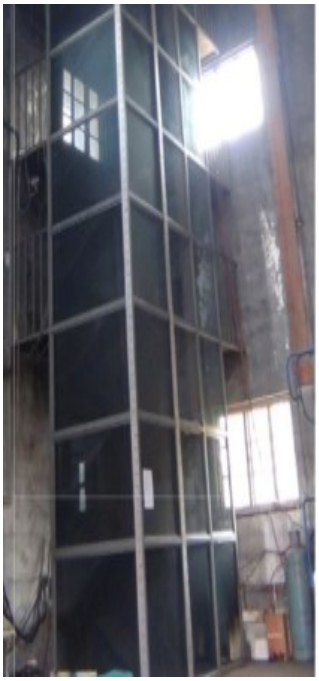

USTC stairwell shaft

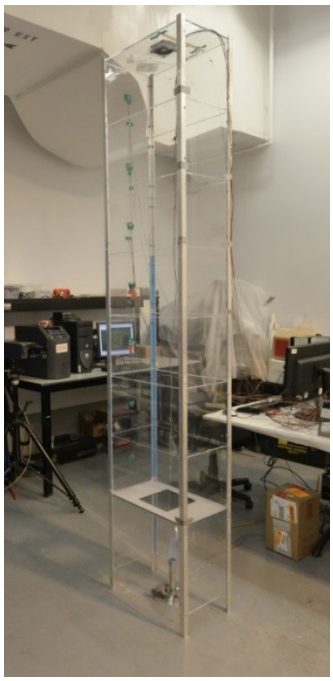

Concordia shaft
(2.1 m height)

Concordia shaft
(1.575 m height)

Figure 6-2 Shafts structures

Thermocouple arrays were installed evenly in the vertical centerline for each shaft. The flow velocities at the openings were measured by hot-wire anemometers. Pressure meter was used to measure pressures at the drilled holes for Concordia shafts, and *NPL* was then estimated accordingly. For USTC shaft, it was hard to measure pressures due to highly turbulent flow from the internal stairs. So the *NPL* was estimated by using incense sticks: smoke exits the shaft above the *NPL* and air enters the shaft below the *NPL* so the approximate *NPL* location can be obtained.

The comparison of the new modeling method against Froude modeling was performed as follows: the designed experiments based on the new method were conducted in the two Concordia shafts, and the experiments based on Froude modeling were only done on Concordia shaft 2.1 height. Table 6-1 summarizes the design parameters for both modeling methods. It shows that the two methods can be quite different, for example, for mechanical venting, the bottom opening of USTC

shaft is 0.42 m^2, which is 0.047 m^2 in Concordia shaft 1 if Froude modeling is used whereas it is 0.0124 m^2 if the new scaling method is used.

Different from the Froude modeling method, for new modeling method, A_b of Concordia shaft 2.1 m height is 0.0124 m^2, only one fourth of that of Froude modeling (0.047 m^2), because the new modeling method concerns the block of the stairwell treads that is presented by C_d by adjusting the bottom opening area. The calculated C_d of USTC shaft is around 0.23 for the bottom opening under mechanical venting, and 0.39 for top and bottom openings under natural venting. C_d of Concordia shaft openings is 0.65. For the natural venting, A_b and A_t of USTC shaft are 0.42 m^2. Using Froude modeling method, A_b and A_t of Concordia shaft 2.1 m height are 0.047 m^2 and 0.0153 m^2 using new modeling method. Three cases are designed, and only Case 2 and Case 3 were conducted on Concordia shaft 1.575 m height because T_f of Case 2 is the minimum fire strength for the burner.

Table 6-1 Experimental design for mechanical venting based on Froude modeling method and new modeling method

	USTC shaft	Concordia shaft (2.1 m)	Concordia shaft (1.575 m)
Mechanical venting	A_b (m^2): 0.42 T_a (K): 303.15 $\dot{m}$ (kg/s):0.24~0.39 E (kW): 31.4	New modeling method: A_b (m^2): 0.0124 T_a (K): 293.15 T_f (K): 345.15 $\dot{m}$ (kg/s): 0.011~0.021 Froude modeling method: A_b (m^2): 0.047 T_a (K): 291.15 E (kW): 2 $\dot{m}$ (kg/s): 0.016~0.025	New modeling method: A_b (m^2): 0.0087 T_a (K): 296.15 T_f (K): 345.15 $\dot{m}$ (kg/s): 0.0068~0.013
Natural venting	A_b (m^2): 0.42 At (m^2): 0.42 T_a (K): 303.75 E (kW): Case 1:14 Case 2:42	New modeling method: A_b (m^2): 0.0153 A_t (m^2): 0.0153 T_a (K): 293.15 T_f (K): Case 1: 326	New modeling method: A_b (m^2): 0.005 A_t (m^2): 0.005 T_a (K): 294.65 T_f (K): Case 2: 351

	Case 3:73	Case 2: 343 Case 3: 372	Case 3: 382
		Froude modeling method A_b (m^2): 0.047 A_t (m^2): 0.047 T_a (K): 303.75 E (kW): Case 1:0.93 Case 2:2.8 Case 3:4.9	

6.5. Results and discussion

For the three different shafts, temperature profiles, θ_{sh}, and relative *NPL*, φ_{np}, are compared for mechanical venting and temperature profiles, θ_{sh}, mass flow rate, $\dot{m}$ and relative *NPL*, φ_{np}, for natural venting. For a quantitative comparison, Normalized Root Mean Square Error (*NRMSE*) (Zhao and Wang 2014) in Eq. (6-30) is used to explain the temperature difference between USTC shaft and Concordia shaft with 2.1 m height. Using the experimental data of the USTC shaft as a baseline. P_1 is the temperature of USTC shaft and P_2 is the temperature of Concordia shaft with 2.1 m height. The less value of *NRMSE* the better performance of scale modeling method is.

$$NRMSE = \frac{1}{P_{1,\max} - P_{1,\min}} \left[\frac{1}{n} \sum_{i=1}^{n} \left(P_{1,i} - P_{2,i} \right)^2 \right]^{\frac{1}{2}} \tag{6-30}$$

6.5.1. Mechanical smoke venting

Temperature profiles of cases with F_r/C_d around 0.38 and 0.42 are compared in Fig. 6-3. Temperature profile is presented by the value of θ_{sh} for the new modeling method and T_{shx}/T_a for Froude modeling method. It can be observed that T_{shx}/T_a of Concordia shaft is much higher than that of USTC shaft by Froude modeling method, because the thermal resistance between two sides of the shaft wall for Concordia shaft is larger than that of USTC shaft but it is neglected in the Froude modeling. Using the new modeling method that considers heat transfer between smoke and

the shaft wall and interior structure resistance, the temperature distribution of Concordia shaft is much closer to USTC shaft. The values of *NRMSE* decrease significantly, from 254 % to 17 % and from 248% to 23% when the new modeling method applied.

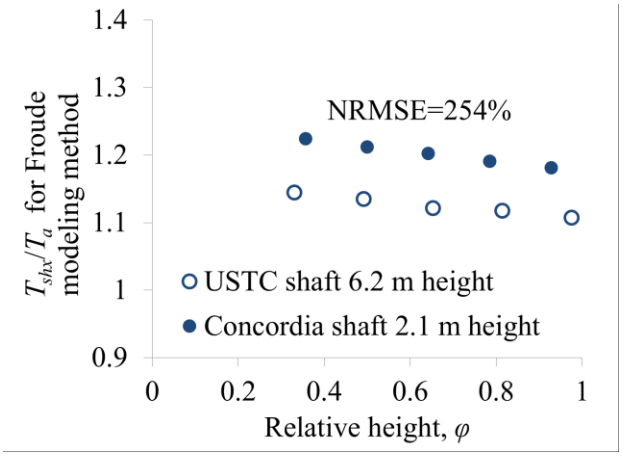

(a) Fr/C_d=0.38, Froude modeling method

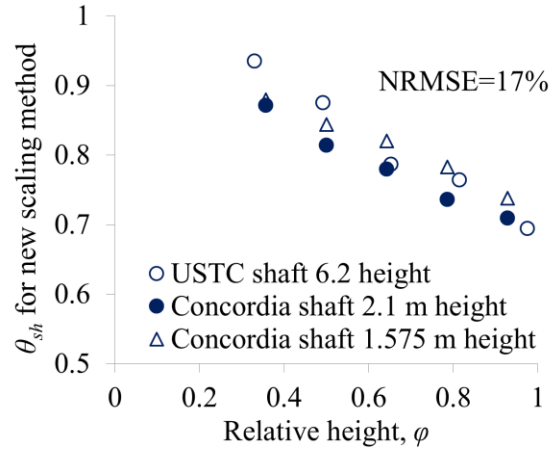

(b) Fr/C_d=0.38, New modeling method

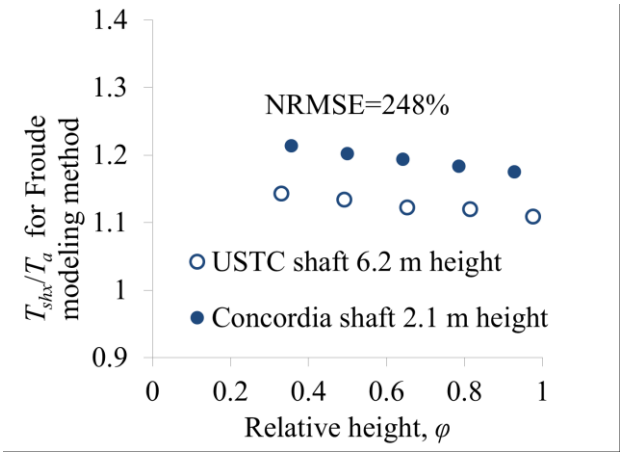

(c) Fr/C_d=0.42, Froude modeling method

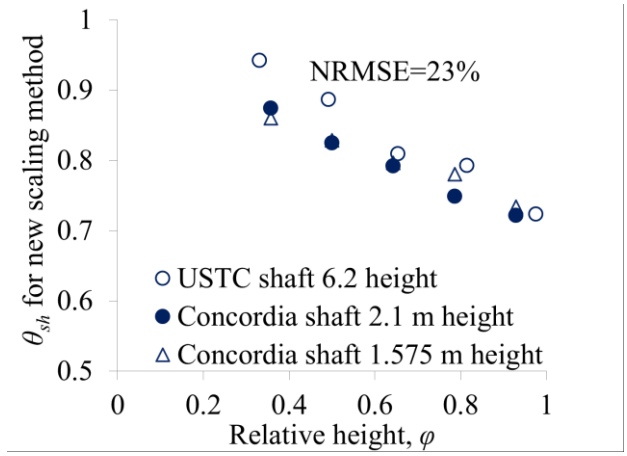

(d) Fr/C_d=0.42, New modeling method

Figure 6-3 Comparison of temperature profiles

Figure 6-4 compares the measured relative *NPL* of the two scaling method, in which the new modeling method performs better than Froude modeling method. Using Froude modeling, for the experiments conducted on USTC shaft, the relative *NPL*, φ_{np}, increases dramatically, from 0.32 to 0.95, when $\dot{m}/H^{5/2}$ increases slightly from 0.003 to 0.004 kg/m$^{5/2}$. However, for the experiments

conducted on Concordia shaft 2.1 m height that use scaling based on Froude modeling, the change of φ_{np} is not so incredibly with the increase of $\dot{m}/H^{5/2}$. φ_{np} varies from 0.02 to 0.7 when $\dot{m}/H^{5/2}$ increases from 0.15 to 0.4 kg/m$^{5/2}$. For experiments conducted on these three shafts using the new modeling method, when F_r/C_d increases from 0.28 to 0.45 for USTC shaft, from 0.26 to 0.47 for Concordia shaft 2.1 m height and from 0.26 to 0.47 for Concordia shaft 1.575 m, the relative *NPL*, φ_{np}, increases from 0.19 to 0.94 for, from 0.26 to 1, from 0.26 to 0.89, which are much closer than results of Froude modeling approach.

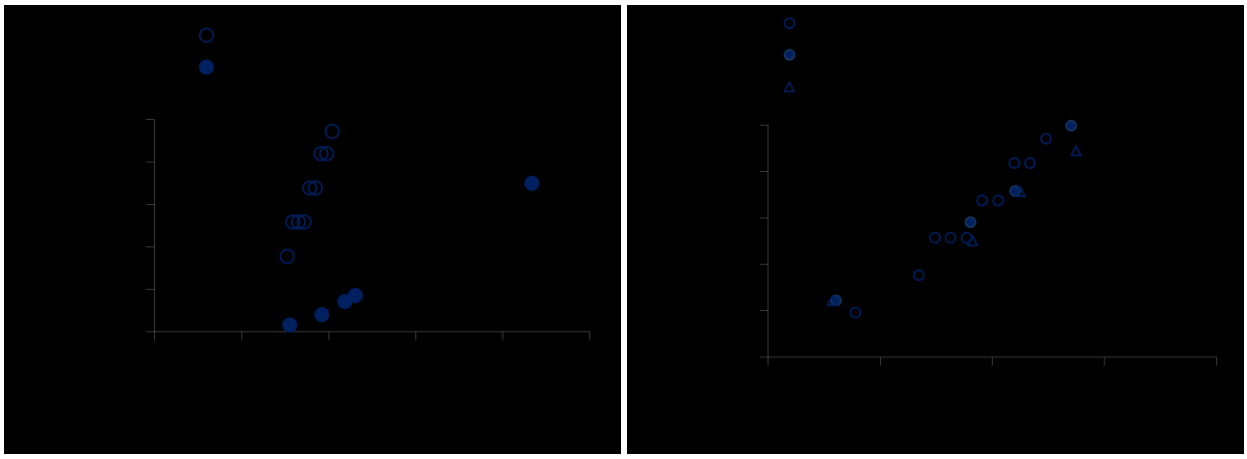

(a) Froude modeling method (b) New modeling method

Figure 6-4 Comparison of neutral plane level

6.5.2. Natural smoke venting

Figure 6-5 shows the temperature profiles of Case 1 ~ Case 3 for the natural venting experiments conducted on the shafts using the two modeling method. The results of the scaling law based on new scaling method are much closer than the results of the scaling law based on Froude modeling. The values of *NRMSE* decrease greatly, from 101% to 9% for case 1, 74% to 7% for case 2, 76% to 21% for case 3 when use new modeling method.

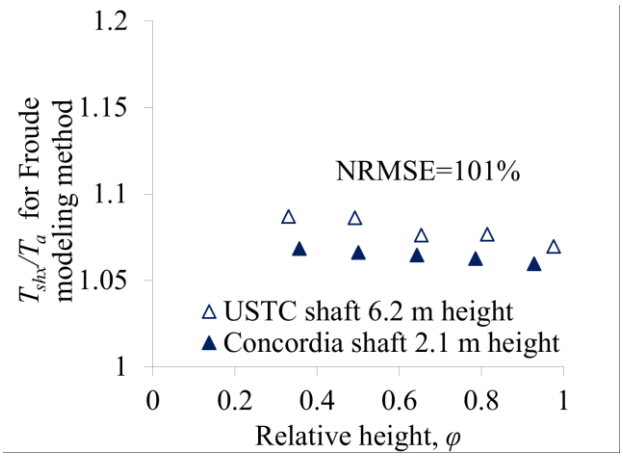

(a) Case 1, Froude modeling method

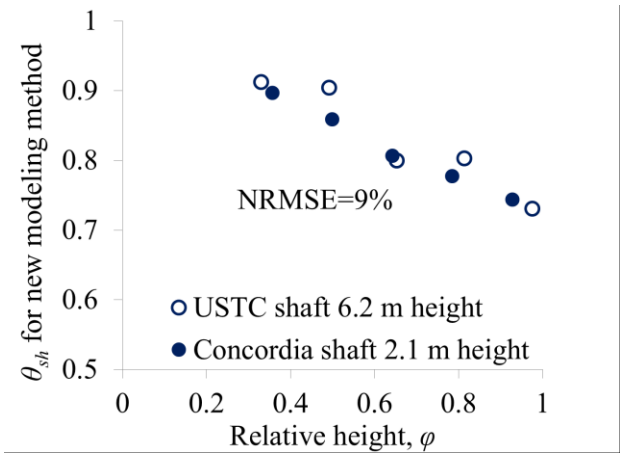

(b) Case 1, New modeling method

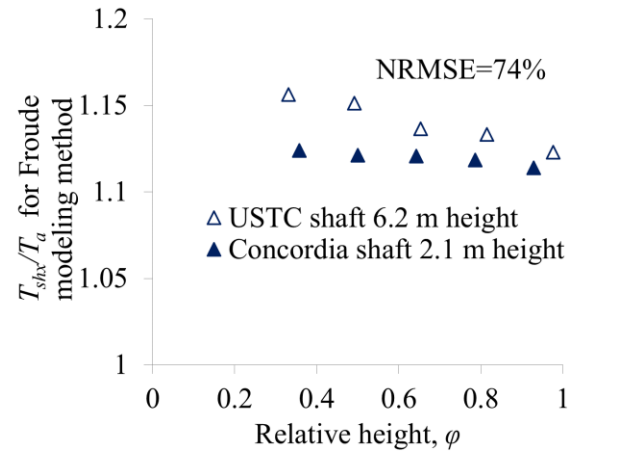

(c) Case 2, Froude modeling method

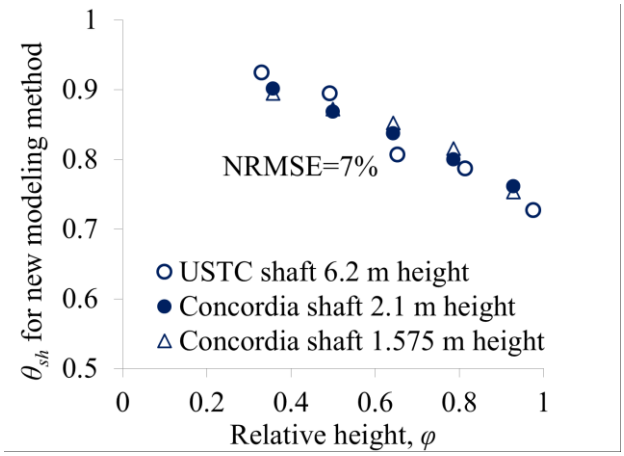

(d) Case 2, New modeling method

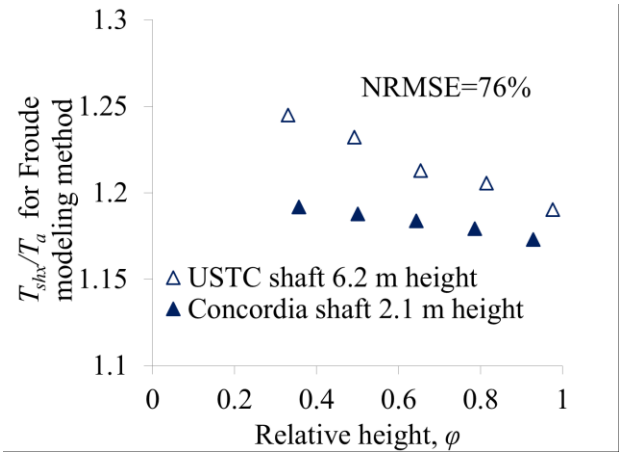

(e) Case 3, Froude modeling method

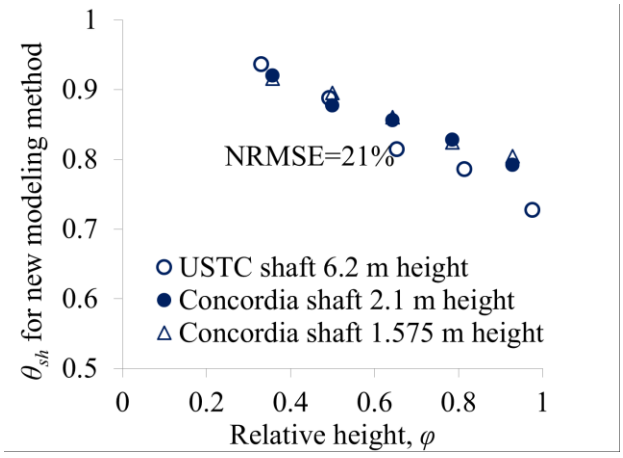

(f) Case 3, New modeling method

Figure 6-5 Temperature profiles

Different from the mechanical venting system, the amount of exhausted smoke for natural venting is not known so it needs to be measured. Therefore beside the temperature and pressure distribution, mass flow rate of the smoke inside the shaft is also compared among the three different size shafts using the two modeling methods for the natural venting conditions.

Figure 6-6 compares the mass flow rate for the natural venting experiments conducted on the shafts using the two scaling law, which is represented by Fr/C_d for scaling law based on new modeling method and $\dot{m}/H^{5/2}$ for scaling law based on Froude modeling. It can be seen that the mass flow rate increases as the fire temperature increases, which is consist with the findings observed by Ji et al.(2013) and Qi et al. (Qi, Wang, and Zmeureanu 2014b). For Froude modeling, $\dot{m}/H^{5/2}$ increases from 0.4 to 0.58 kg/m$^{5/2}$ for USTC shaft when $E/H^{5/2}$ increases from 0.12 to 0.75 kW/H$^{5/2}$. However for the same range of $\dot{m}/H^{5/2}$ for the experiments conducted on Concordia shaft 2.1 m height, $\dot{m}/H^{5/2}$ increases from 0.7 to 1 kg/m$^{5/2}$. The difference is much larger than that of the new modeling method.

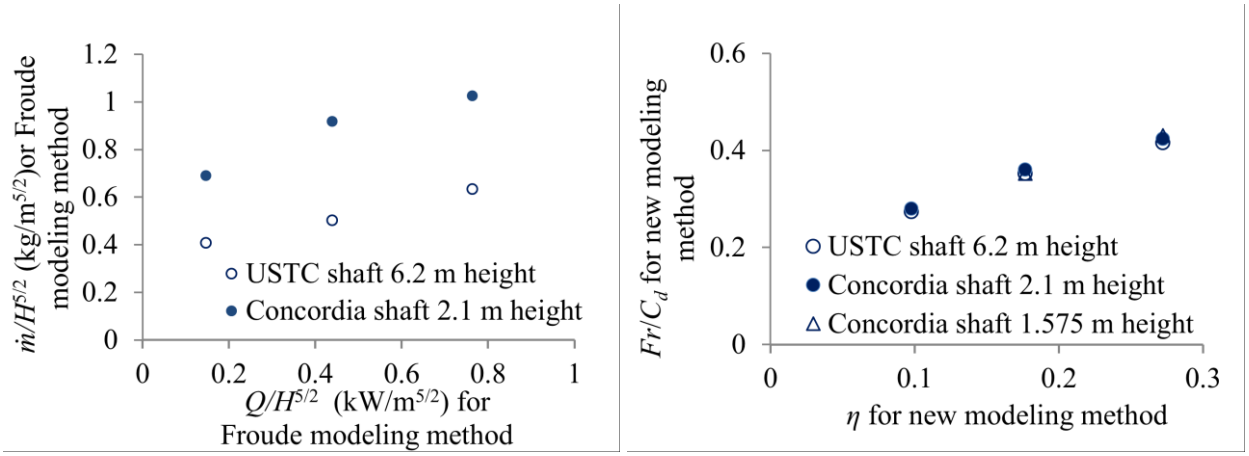

(a) Froude modeling method (b) New modeling method

Figure 6-6 Comparison of mass flow rate for new modeling method

The fire strength has little influence on the relative *NPL*, which is consistent with the study by Li et al. (2014). Table 6-2 compares φ_{np} of Concordia shaft 2.1m height for the two modeling

method .With the increase of fire strength, φ_{np} is around 0.57±0.1 for USTC shaft. When use the new modeling method, φ_{np} is around 0.46±0.05 for the Concordia shaft. It is much better than Froude modeling, for which φ_{np} is around 0.75±0.16.

Table 6-2 Measured relative neutral plane level

		New modeling method	Froude modeling method
USTC shaft	0.57 ± 0.1	/	/
Concordia shaft 2.1m height	/	0.46 ± 0.05	0.75± 0.16

6.6. Conclusion

Smoke tends to spread from lower part of the high-rise buildings to higher part through large vertical spaces, which becomes a major challenge for fire protection. The sub-scaled experiment is an essential practical approach to study smoke movement inside buildings compared with full-size experiments which are costly. However, there lack of modeling method to sub-scale the large vertical spaces that needs to consider heat transfer between smoke and the boundaries. This paper presents a new modeling method to scale smoke movement in large vertical spaces in high-rise buildings during fires, which is derived from differential equations including energy balance and mechanical and energy equations. Heat transfer between smoke and the boundaries and the resistant effect of inside structure, e.g. stairs, on the vertical spreading flow are considered in the new modeling method, which differs from Froude modeling.

To verify the accuracy of this new modeling method, a series of experiments were designed and conducted on three different size shafts for both mechanical venting and natural venting. The results were also compared with Froude modeling methods. This study reached the following major conclusions:

(1) By using the discharge coefficient, C_d, to express the inside structure resistance of the shaft, the shaft with inside structure, like shaft with stairs, could be sub-scaled as the shaft without inside structure, which is simpler to model.

(2) By considering heat transfer between smoke and the boundaries and inside structure resistance, the new modeling method could achieve more accurate results than Froude modeling method.

Chapter 7 Modeling Smoke Movement in High-rise Shafts by a Multizone Airflow and Energy Network Program

The contents of this chapter are published in "Dahai Qi, Liangzhu Wang, Radu Zmeureanu. 2015. Modeling Smoke Movement in Shafts during High-Rise Fires by a Multizone Airflow and Energy Network Program. ASHRAE Transactions 121 (2)". The contents are slightly modified.

Abstract

Multizone airflow network programs are increasingly used to study smoke movement during fires in buildings. Multizone programs often do not solve energy conservation equation so temperatures of rooms/zones need to be specified. The lack of energy model limits the capability of a multizone program for modeling building smoke movement, especially in shafts, where temperature distribution is often unknown. This paper introduces a multizone program with an added energy equation, CONTAM97R, with the focus of its application to simulations of smoke movement, especially in shafts of high-rise buildings. First, CONTAM97R was validated by experimental data from a 1/3 scale building stairwell under fires, and verified by an analytical model of high-rise fires. The program is then used to model a 16-storey building with a fire located at the first floor. To model the building shaft by CONTAM97R, we proposed and compared two zoning methods, Floor Zoning Strategy (FZS) and Adaptive Zoning Strategy (AZS), when the shaft is with and without air infiltrations. It shows that the accuracy of FZS is inversely related to a dimensionless parameter, the temperature attenuation coefficient, α, but can be improved by increasing the number of zones dividing the shaft until the results do not depend on zone numbers. Compared to FZS, AZS obtains results of similar level of accuracy but with fewer zones for the simulations.

7.1. Introduction

A high-rise building is often defined as a building with the height more than 23 m (NFPA 101 2012). As one of the key indicators of modernization, high-rise buildings bring many conveniences for people's lives in populated cities. During the design and construction of a high-rise building, engineers and architects must cope with a variety of security and life safety issues, among which the management of fire smoke movement is one of the most important tasks. Most of the fire-related deaths in buildings are caused by inhalation of smoke. In the United States, fire smoke accounts for approximately 75% of victims in building fires (Beitel, Wakelin, and Beyler 2000). For high-rises, the situation is worsened when fire smoke migrates long distances from the room of fire origin to the rest of a building under stack effect through vertical structures (Shi et al. 2014a; Li et al. 2014), e.g. stair and elevator shafts, light wells, and ventilation ducts, where often little flow resistance is encountered. Therefore a good knowledge of smoke movement, especially in vertical shafts, is extremely important for the design of high-rise fire smoke control systems.

A multizone airflow network program (hereafter multizone program) is often used to study smoke movement during fires in buildings (Black 2009; Klote et al. 2012; Bae, Shin, and Ryou 2014). A whole-building multizone analysis of smoke movement usually only needs a few minutes or even seconds (Wang and Chen 2008). Developed by the US National Institute of Standards and Technology, CONTAM (Walton and Dols 2013) is the multizone program for building fire smoke analysis as suggested by the Handbook of Smoke Control Engineering (Klote et al. 2012). Miller et al. conducted CONTAM simulations to study smoke controls by shaft pressurization in high-rise buildings. CONTAM was employed as a major model for the investigation of the fire smoke movement in the World Trade Center (WTC) on 9/11/2001 (Ferreira and Strege 2005). However, CONTAM does not solve the energy conservation equation so temperature in each zone has to be

specified by users. Therefore, in the studies of Miller et al., a single value of temperature averaged over the entire shaft height was used as the input in CONTAM (Miller and Beasley 2009; Miller 2011). Due to the lack of energy model, inappropriate temperature inputs may lead to simulation errors, especially for the scenarios of buoyancy-driven smoke movement, where smoke temperatures are often unknown beforehand (Ferreira and Strege 2005). Wang, Black, and Zhao (2013) simulated smoke movement in a 40-storey building using CONTAM and compared the results to another multizone-type program added with energy model, COntrol of SMOke (COSMO) (Black 2010). They found that the accuracy of temperature profile in the shaft is the key to the quality of the prediction. Inaccurately specified temperatures will lead to errors in excess of 70%. The addition of the thermal analysis capability to CONTAM thus becomes quite necessary.

There have been some previous efforts to add an energy model to CONTAM (Tang and Glicksman 2005; McDowell et al. 2003; Gu 2011), many of which have not yet resulted in a final product. Among them, CONTAM97R (Axley 2011; Wang, Dols, and Emmerich 2012) is probably the most completed one, which was firstly developed in 1997, and later validated by Axley et al. (2002) for modeling of naturally ventilated buildings. However, there have been scarce studies of modeling building fire smoke movement by CONTAM97R, although CONTAM, the sister program without an energy model, has been increasingly used for building smoke analysis as noted previously. One of the main challenges is how to divide a long shaft in several zones in a multizone program, so-called "zoning strategy": specifically, how many zones should be used and how to distribute the zones in a vertical shaft while each zone is considered to have a uniform temperature under the well-mixed assumption (Wang, Dols, and Emmerich 2012). One of the most common zoning strategies may be to assign one zone for the shaft section of each floor (e.g. a shaft of a 16-story building will be divided into 16 zones) or to further divide each shaft zone into several vertical

sub-zones (hereafter, Floor Zoning Strategy) as what have been done in the previous studies (Miller and Beasley 2009;Wang, Black, and Zhao 2013). However, because each zone is assumed to have a single temperature, how many zones a shaft are divided will directly affect the predicted temperature distribution, and consequently smoke flow rates and pressure profiles. Floor Zoning Strategy (FZS) thus needs to be further evaluated, and if necessary a better zoning strategy should be suggested.

The purpose of this paper is to use CONTAM97R for the simulations of smoke movement in high-rise shafts during fires. First, the energy model in CONTAM97R is briefly introduced. CONTAM97R is then validated by the experimental data from a 1/3 scaled building model under fires, and verified by an analytical model in the literature (Qi, Wang, and Zmeureanu 2014a). We then used CONTAM97R to model the smoke movement in a 16-storey building with a fire located at the first floor when the shaft is with and without air infiltrations. Using the analytical model of the 16-story building as a baseline, we evaluated two zoning strategies to divide the vertical shaft into multiple sub-zones, namely, FZS and an alternative, Adaptive Zoning Strategy (AZS). The conclusions and experiences from this paper can be applied to other studies of using similar multizone network programs for modeling fire smoke movement in high-rise buildings.

7.2. Fundamentals

Energy model in CONTAM97R

The energy model in CONTAM97R can be illustrated by an example of two rooms in Figure 7-1, where zone *i* and zone *j* are connected through path *ij*, surrounded by the ambient zone, zone *a*. For zone *i*, the energy conservation equation for the zone thermal node can be written as:

$$\frac{d\left(C_{pi}T_i m_i\right)}{dt} = \sum_a C_{pa}T_a\dot{m}_{ai} - \sum_j C_{pi}T_i\dot{m}_{ij} + E_i + \sum_k h_{wk}A_{wk}\left(T_{wki} - T_i\right) \quad (7\text{-}1)$$

The convective heat transfer coefficient, h_{wk}, is determined by the temperature difference between the interior wall surface and the indoor air. The conductive heat transfer through the wall *k* from the wall thermal node *ki* to *kj* is considered by the Fourier's Law in Equation 7-2, and solved by a 1-D finite difference method.

$$q = -k\frac{dT}{dy} \quad (7\text{-}2)$$

Equations 7-1 and 7-2 show the equations solved by the CONTAM97R modules of the zone thermal node and the wall thermal node, respectively. During an energy and airflow network analysis, the program solves the mass balance equation of the airflow network (the equation is not provided here but can be found from the CONTAM user guide (Walton and Dols 2013) first to obtain zone pressures and airflows under given initial zone and wall temperatures. Then the zone and the wall thermal node modules are solved sequentially to update the temperature values. Two approaches are provided for the integration of this thermal airflow problem, "Ping-Pong" and "Onion" (Zhai, Johnson, and Krarti 2011). The Onion approach requires the convergence of both thermal and airflow analyses at the same time step whereas the Ping-Pong approach solves each module only once at each time step so it needs shorter time step than the Onion approach. The details of these two approaches can be found in previous studies (Hensen 1999; Sahlin 2003), so they are not included here. All the simulations in this paper used the Ping-Pong approach to obtain final results at steady state.

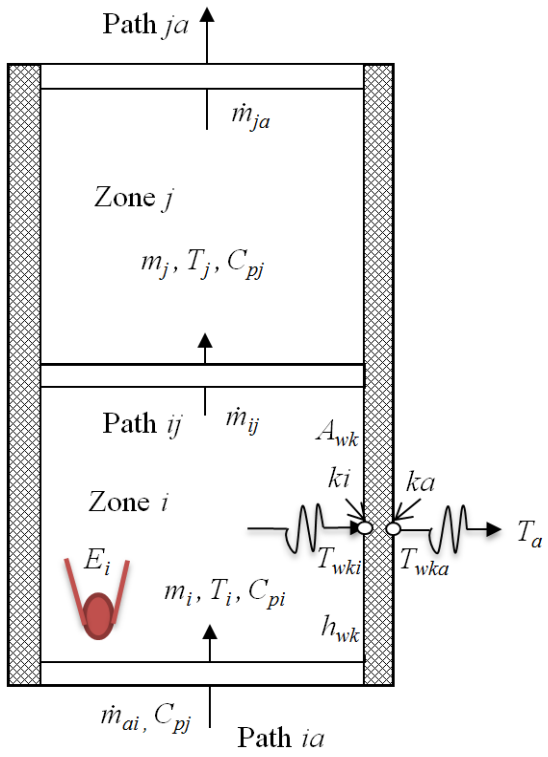

Figure 7-1 Schematic of the energy model in CONTAM97R

Analytical model of high-rise fire smoke movement

The validity of a computer program, such as CONTAM97R, should be better verified by comparing the predicted results to experimental data. High-quality experimental data of full-size high-rise fires are scarce in the literature partly due to the fact that full-scale field measurements are challenging and costly. Therefore, in the later section of this paper, we try to validate CONTAM97R by an experimental study in a reduced-scaled building model and an analytical model of a high-rise building when the data for a full-scale building are needed. This section summarizes the fundamentals of the analytical model (Qi, Wang, and Zmeureanu 2014a). For a building with a fire, e.g. the one located at the first floor as shown in Figure 7-2, the analytical model was developed under the following assumptions:

- smoke movement in shaft is one-dimensional at steady state.
- outdoor air temperature and building temperature at non-fire floors are constant.
- specific heat capacity of the smoke, C_p, is constant.
- smoke is assumed to be incompressible and viscous but thermally expansible satisfying the ideal gas law.
- no smoke leaks through shaft walls.
- heat transfer coefficients (either due to convection or radiation) are constant and do not vary along the height of the shaft.
- temperature of the fire floor is uniform and maintained at the fire smoke temperature.

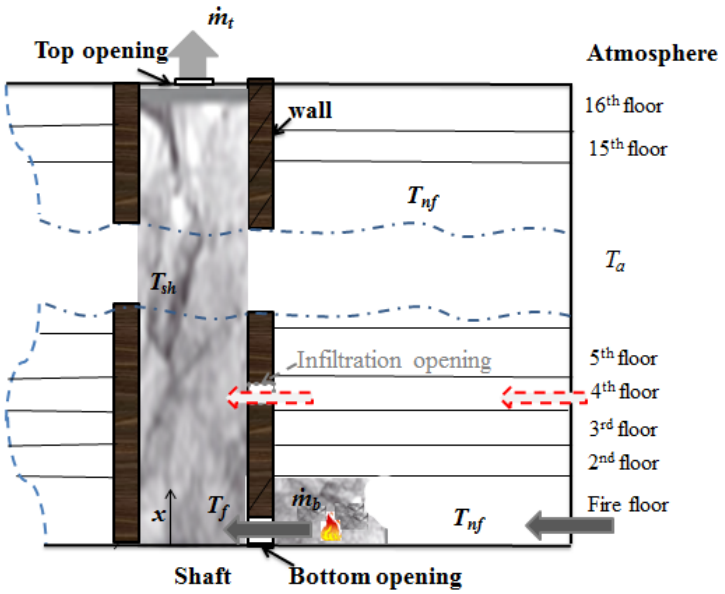

Figure 7-2 Schematic of a building with buoyancy-driven smoke flow in shaft

Equations 7-3 ~ 7-11 show the formulations for smoke temperature profile, pressure profile and smoke mass flow rate, which were derived from coupled mass, heat and mechanical energy

conservation equations (Qi, Wang, and Zmeureanu 2014a).

- Temperatures of smoke

$$T_{shx} = T_{nf} + (T_f - T_{nf}) Exp(-\alpha x / H) \tag{7-3}$$

where

$$\alpha = \frac{PH}{\dot{m} C_P R_t} \tag{7-4}$$

$$R_t = \frac{1}{h_{wi}} + \frac{W}{k} + \frac{1}{h_{wo}} \tag{7-5}$$

- Pressure profile

$$p_{shx} = p_{sh0} - \Delta p_{elx} - \Delta p_{dyx} - \Delta p_{frx} \tag{7-6}$$

where:

$$\Delta p_{elx} = \frac{g p_{a0} H}{R T_{nf}} \left\{ \frac{1}{\alpha} \ln \left[\frac{(T_f - T_{nf}) + T_{nf} Exp\left(\frac{Px}{\dot{m} C_p R_t} \right)}{T_f} \right] \right\} \tag{7-7}$$

$$\Delta p_{dyx} = \frac{\dot{m}^2 R (T_f - T_{nf})}{p_{a0} A_h^{\,2}} \left[Exp(-\alpha x / H) - 1 \right] \tag{7-8}$$

$$\Delta p_{frx} = \frac{f \dot{m}^2 R H T_{nf}}{2 D_h A_h^{\,2} p_{a0}} \left\{ \frac{x}{H} + \frac{1}{\alpha} \frac{T_f - T_{nf}}{T_{nf}} \left[1 - Exp\left(\frac{-Px}{\dot{m} C_p R_t} \right) \right] \right\} \tag{7-9}$$

- Smoke mass flow rate

$$\dot{m}_b = C_d A_b \sqrt{2(p_f - p_{sh0}) p_{a0} / (R T_f)} \tag{7-10}$$

$$\dot{m} = \dot{m}_t = \dot{m}_b = C_d A_t \sqrt{2(p_{shH} - p_{aH}) p_{a0} / (R T_{shH})} \tag{7-11}$$

The above equations show that smoke flow through the shaft is closely coupled with the heat transfer between the smoke and the surroundings. Qi, Wang, and Zmeureanu (2014) developed an iterative procedure to solve the above equations for the risk assessment of the smoke spread from

the fire floor to higher floors. The temperature profiles of smoke and shaft wall are both shown to be exponential functions of the temperature attenuation coefficient, α, defined by Equation 7-4. The accuracy of the analytical model was confirmed by the comparison to numerical simulations and measured data in the literature. The details were not provided here to avoid repetition but can be found in their paper (Qi, Wang, and Zmeureanu 2014a).

7.3. Validation by reduced-scale building model

To validate CONTAM97R in modeling of high-rise shafts during fires, we employed the experimental data from a 1/3 scale stairwell (Ji et al. 2013) in the literature, and the calculated results based on the analytical model in the previous section (Qi, Wang, and Zmeureanu 2014a). The 1/3 scale stairwell model has 12 floors with a floor height of 1 m (3.28 ft) except 1.2 m (3.94 ft) for the ground floor, and with a cross sectional area of 1.5 m (4.92 ft) × 1.0 m (3.28 ft) (L × W). Two sides of the stairwell model are made from 12-mm (0.03937 ft) fire-resistant glass and the other two sides are from 2-mm (0.006562 ft) thick steel plates. The experimental data at steady state were selected here for two square pool sizes of 20 cm (0.66 ft) × 20 cm (0.66 ft) and 30 cm (0.98 ft) × 30 cm (0.98 ft) with the Methanol fire sources located at the height of 0.6 m (1.969 ft). The measured corresponding smoke temperature at the ground level is 310 K (98.3 ^{0}F) and 346 K (163.1 ^{0}F), respectively. The non-fire floor temperature and outdoor temperature were measured to be 279.15 K (42.8 ^{0}F).

Given the above information, a CONTAM97R model of the reduced-scale building model was created with one zone assigned to each floor following the mostly common approach of FZS so a total of 12 zones were created for the shaft. Due to the small thinness of the shaft wall which has good heat conduction with outside atmosphere, in this particular case, the heat loss to the boundary is simplified as a convective process and the conductive heat transfer is ignored (Sun et al. 2011)

in the analytical model and CONTAM97R. Figure 7-3 and Table 7-1 compare the gas temperature rise and mass flow rates among the experiment, CONTAM97R and the analytical model. The temperature predictions of CONTAM97R, analytical model and experimental results are almost identical. CONTAM97R overestimates the smoke mass flow rate with a difference of less than 7% and the analytical model underestimates the flow rate with 7.7% for the 30 cm (0.98 ft) × 30 cm (0.98 ft) fire. Considering the complexities and uncertainties of the experiments, these discrepancies are not quite significant and CONTAM97R predictions are considered acceptable. Meanwhile, the comparison in this section also shows the validity of the analytical model, which will be used as a baseline in the later section when experimental data of full-size buildings are not available.

As mentioned previously, different zoning strategies may affect the predictions of temperatures, smoke mass flow rates and pressure profiles. FZS is shown to be acceptable in this specific experiment but may become inapplicable in other cases, which will be discussed in the following section.

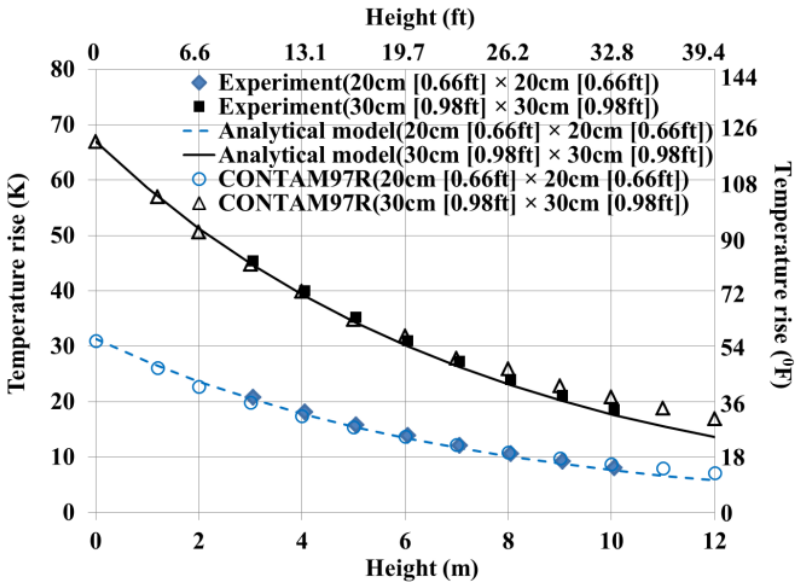

Figure 7-3 Comparison of gas temperature rise

Table 7-1 Comparison of flow rate of experiments (Ji et al. 2013) and analytical model (Qi, Wang, and Zmeureanu 2014a) with CONTAM97R

Pool size	20 cm (0.66 ft) × 20 cm (0.66 ft)			30 cm (0.98 ft) × 30 cm (0.98 ft)		
	Experiment	CONTAM97R	Analytical model	Experiment	CONTAM97R	Analytical model
Mass flow rate	0.291	0.292	0.269	0.402	0.429	0.371
(kg/s [lb/min])	(38.49)	(38.63)	(35.58)	(53.18)	(56.75)	(49.07)
Relative difference	/	0.34%	7.6%	/	6.7%	7.7%

7.4. Simulations of full-size high-rise buildings

7.4.1. Shafts without air infiltration

To explore the capability of CONTAM97R of modeling full-size high-rise fires, this section covers the simulations of a 16-storey building with a floor height of 4 m (13 ft) except the 8-m (26-ft)-high entry hall at the first floor as shown in Figure 7-2. The building has one vertical shaft with a cross section of 5 m (16.4 ft) × 12 m (39.4 ft) (W × L). Both of the bottom and top openings share the same size, 0.1 m^2 (1.08 ft^2) for Case 1, 0.2 m^2 (2.15 ft^2) for Case 2, 0.5 m^2 (5.38 ft^2) for Case 3, and 1.0 m^2 (10.76 ft^2) for Case 4. Thermal conductivity is 1.7 W/ (m·K) (0.406 Btu·ft/(h·ft^2·°F)), and heat transfer coefficient is 10 W/ (m^2·K) (1.76 Btu/(h·ft^2·°F)). We will discuss with a shaft with air infiltration. A fire characterized by a fire room temperature of 975.15 K (1295.6 °F) is located at the first floor, representing one of the worst fire risk scenarios. The corresponding fire heat release rate (HRR) is 5.6 MW (5307.68 Btu/s) in a 20 m (65.6 ft) × 20 m (65.6 ft) floor with a 1.6 m (5.25 ft) × 2 m (6.56 ft) door according to the equations developed by McCaffrey et al.

for relating HRR and the fire room temperature (Karlasson and Quintiere 2002). During the fire, the fire smoke would enter the shaft and spread across all higher floors. The ambient is considered with an outdoor temperature of 253.15 K (-4 °F) under no wind condition. Since the analytical model is for steady state, we run a transient simulation with a time step of 10 minutes till the steady state is reached, which is confirmed when the variation of the predicted temperature in the shaft is less than a threshold value of 1×10^{-4} K (0.56×10^{-4} °F). The simulations were run on a desktop computer with a 2.40-GHz processor and 4GB memory.

Note that since there are no experimental data available for the modeled full-size building, we use the calculated results of the analytical model as the baseline for the comparison. In the following sections, we compare two zoning strategies for the shaft of the modeled building.

Floor Zoning Strategy (FZS)

One of the most common methods of dividing the shaft is probably to assign one zone for each floor or to further divide each floor zone into several sub-zones with equal size (Black 2009; Klote et al. 2012). For this so-called "Floor Zoning Strategy", we first studied the case of one zone assigned for each floor, which results in a total of 16 zones for the modeled shaft. Note that for simplicity without loss of generality, each non-fire floor is assumed to be one open space and modeled as a single zone as what was often done by the previous studies (Wang, Black, and Zhao 2013; Black 2010).

Figure 7-4 compare the predicted smoke temperatures and mass flow rates to the results of the analytical model for all the four cases with different opening sizes. For a given value of α, Figure 7-4(a) shows that the calculated temperatures are all functions of the height in the vertical shaft. The predicted smoke mass flow rates agree better with the analytical model than the temperature

predictions as shown by Figure 7-4(b). The difference is between 0.3% (Case 4) and 6.8% (Case 1). It was also shown that more discrepancies of the predictions (including smoke temperature and flow rate) were observed for larger values of α. Equation 7-4 shows that α is inversely proportional to smoke flow rate so a larger α (e.g. α = 11.56 in Case 1) means fewer smoke entering the shaft and thus higher gradient of smoke temperature at the bottom of the shaft (the bottom three zones spanning 0 ~ 16 m (52 ft) in this case). For such a case, the temperature gradient cannot be well resolved by the FZS with one zone assigned to each floor. Consequently, inaccurate predictions of smoke temperature caused the errors of flow rates. For a smaller α (e.g. α = 0.7 or 1.41 in Figure 7-4(a)), FZS may be enough to resolve a corresponding milder temperature gradient. This explains why the predicted results of CONTAM97R agree well with FZS and the analytical model in Figure 7-3 and Table 7-1. For the scaled experiments in the previous section, the calculated α is around 1.0 for both fire pool sizes, which indicates small temperature gradient as shown in Figure 7-3 so FZS performs well. The simulation time of each case is around 3 minutes, which is 185s, 175s, 180s and 170s for Case 1 ~ Case 4.

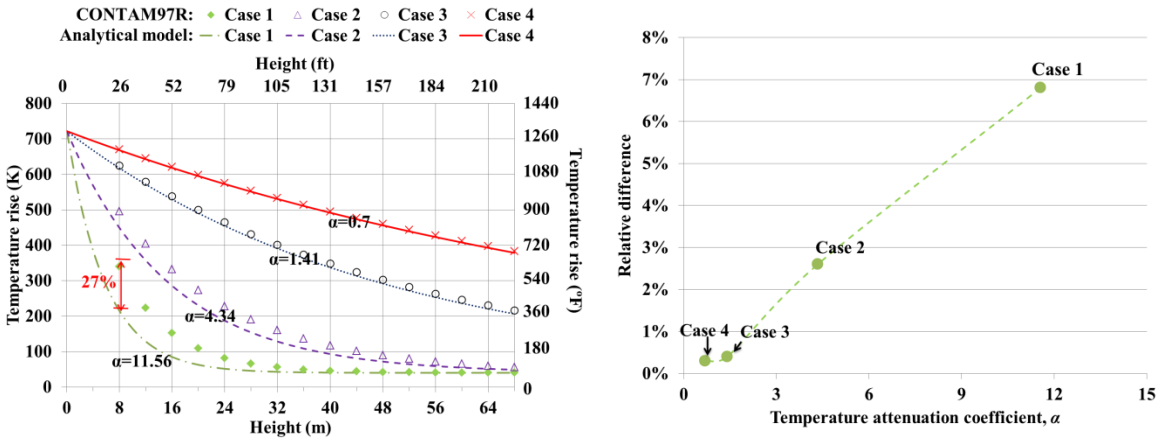

Figure 7-4 Comparison between results of CONTAM97R and analytical model for different cases with FZS (total zones = 16) for (a) temperatures rise of smoke, (b) relative difference of mass flow rate

Considering 16 zones are not sufficient to achieve accurate results for the cases with greater α, we divided each floor into more sub-zones with equal size to increase zone resolution. The following analysis focuses on Case 1, the worst case among the four cases. The zone height is reduced to 2 m (6.56 ft), 1 m (3.28 ft) or 0.5 m (1.64 ft), corresponding to a total zone number of 34, 68, or 136, respectively. The predicted temperature profiles and relative difference of mass flow rates between CONTAM97R and analytical model are plotted in Figure 7-5. As the number of total zones increases, the predicted smoke temperature is closer to the results of analytical model as shown by Figure 7-5(a). However, the results will not improve much when the total zone is more than 68. A similar trend is observed for the prediction of the smoke flow rate in Figure 7-5(b). The error of the predicted smoke flow rate is about 2.7% for the total zone of over 68. In summary, Figure 5 indicates that a long shaft can be correctly modeled by CONTAM97R if the temperature gradient in the shaft can be well resolved, e.g. by using the FZS and dividing the shaft into an enough number of sub-zones. The accuracy of the predictions will not improve further when the number of the sub-zones is over a certain value.

However, the problem now is how many sub-zones a specific shaft should be divided. Trials and errors will probably work but a better zoning strategy would be to relate directly the zoning to the smoke temperature gradient. Figure 7-5(a) shows that the FZS tends to create many unnecessary zones at the top section of the shaft with low temperature gradient ($h > 20$ m (65.6 ft)) whereas not enough zones at the rest of the lower section with high temperature gradient. Therefore it is necessary to improve the FZS by creating sub-zones adaptively based on temperature gradient.

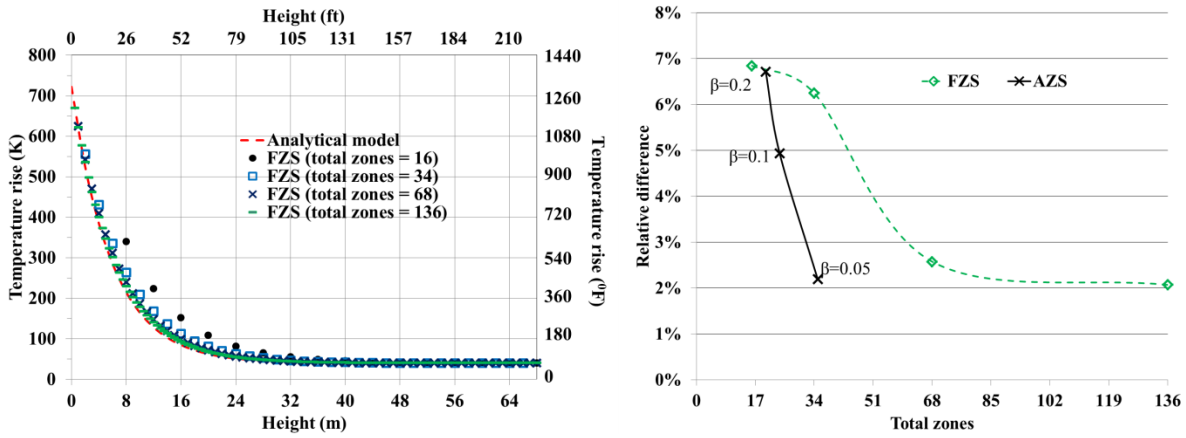

Figure 7-5 Effects of zone numbers on the (a) predicted smoke temperature and (b) relative difference of predicted mass flow rate between CONTAM97R and analytical model for shafts without infiltration in Case 1

Adaptive Zoning Strategy (AZS)

We proposed an Adaptive Zoning Strategy (AZS), which limits temperature difference between two neighboring zones by a temperature constraint, β, defined by Equation (7-14). θ_{shx} is the dimensionless smoke temperature defined by Equation 10 (Qi, Wang, and Zmeureanu 2014a). For a specific temperature constraint, the height of each zone, h_i, can be obtained by Equation 7-12.

$$\beta = \theta_{shx} - \theta_{sh(x+h_i)},\ 0<\beta<1 \tag{7-12}$$

where

$$\theta_{shx} = \frac{T_{shx} - T_{nf}}{T_f - T_{nf}} = Exp\left(\frac{-\alpha x}{H}\right) \tag{7-13}$$

$$h_i = \frac{\ln\left[1 - \beta Exp(x\alpha / H)\right]}{-\alpha} H \tag{7-14}$$

The temperature constraint in the above equations restricts the temperature variation between two neighbor zones. For a section of the shaft with high temperature gradient, a smaller β indicates less temperature variation allowed between zones and thus results in more sub-zones created. For a

smaller temperature gradient, β allows wider spanning of a sub-zone than for the section with higher temperature gradient. As a result, a given β produces more sub-zones in sections with high temperature gradient but fewer for those with low temperature gradient. Moreover, once β is chosen, the zoning method for a specific shaft is thus determined so the simulation results are directly associated with β. For example, smaller β allows for less temperature variation between zones and thus creates more zones and generally higher simulation accuracy. Users can select β according to the acceptable accuracy of their prediction. This AZS feature helps to obtain results with desirable accuracy based on an appropriately selected value of β.

Figure 6 compares different zoning strategies in Case 1. The AZS with $\beta = 0.2$ (corresponding to a temperature gradient of 136 K (245 ^{0}F) for every two zones) creates four zones for the 1st floor (0~8 m (26 ft)) and one zone in the 2nd whereas $\beta = 0.05$ (corresponding to a temperature gradient of 34 K (63 ^{0}F)) results in 15 zones for the 1st and 3 zones in the 2nd. Both cases create fewer zones than the FZS with 136 zones. However, the resultant accuracy is almost the same as the FZS as shown by the predicted smoke temperatures in Figure 7-6: the largest error of temperature is 11% for $\beta = 0.2$ and 4.4% for $\beta = 0.05$ in this case. Figure 7-5(b) also shows that with the decrease of β, the accuracy of the predicted smoke flow rate improves. The AZS can achieve a similar level of accuracy with much fewer zones, i.e. 2.1% for 35 zones with $\beta = 0.05$ compared to the same accuracy by the FZS with 136 zones. Therefore, the AZS is more efficient and flexible than the FZS. Note that in CONTAM97R, each floor of the shaft must contain at least one zone, and each zone cannot cross two floors. Therefore, a minimum of 16 zones is required by the AZS for the shaft modeled.

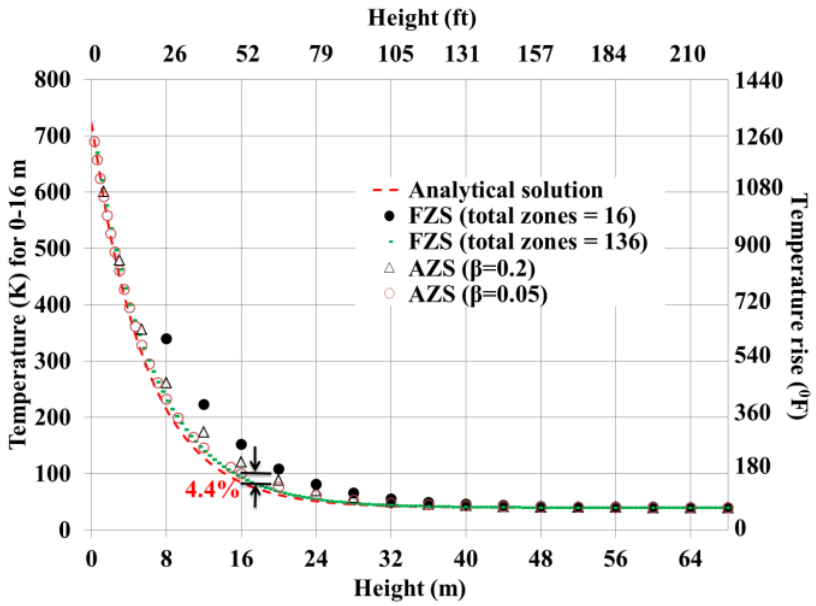

Figure 7-6 Comparison of temperature profiles between analytical model and different zoning strategies in Case 1

7.4.2. Shaft with infiltration

In the previous case study, both FZS and AZS were shown capable of modeling long shafts correctly by CONTAM97R when the shaft is air tight. When a shaft is with infiltrations as what most of actual buildings are, the AZS still applies because a shaft section can be considered air tight between neighboring leakage openings. The following iterative AZS modeling procedure is thus developed for shafts with infiltrations (superscripts show iteration numbers):

(1) Divide a shaft with infiltrations into several air-tight sub-sections by the locations of infiltration openings so that each sub-section has at most one infiltration opening locating at the bottom.

(2) For each sub-section, first start a rough zoning by the FZS with one zone assigned to each floor, then model the building by CONTAM97R to get initial value, $\dot{m}_i^{(0)}$, for each sub-section.

(3) Calculate $\alpha_i^{(0)}$ by Equation (7-15) based on for each sub-section, and apply the AZS for a

selected β to get an updated $\dot{m}_i^{(1)}$ for each sub-section.

(4) For each sub-section, if $|\dot{m}_i^{(1)} - \dot{m}_i^{(0)}| / \dot{m}_i^{(1)}$ is over a convergence threshold, return to the step (3) by updating $\dot{m}_i^{(0)} = \dot{m}_i^{(1)}$ till the desirable accuracy is obtained.

The above procedure is demonstrated by a case study of the same building with an infiltration opening located at the bottom of the fourth floor as shown in Figure 7-2. The opening is with the size of 0.1 m^2 (1.08 ft^2) and modeled by the orifice equation with discharge coefficient of 0.6 and flow exponent of 0.5 (Walton and Dols 2013). All the other settings are kept the same as the previous case of Case 1. As a baseline for comparison, the FZS with the total zone of 153 is applied to obtain the results independent of zone numbers.

Figure 7-7 shows the shaft zoning for the AZS with $\beta = 0.05$ compared to the FZS with 153 zones. There exist two regions with high temperature gradients: one at the 1st floor near the smoke entry location and the other at the 4th floor with air infiltration. The AZS adaptively creates fine zone resolutions at both locations but with only a total of 48 zones in the whole shaft compared to the FZS with 153 zones.

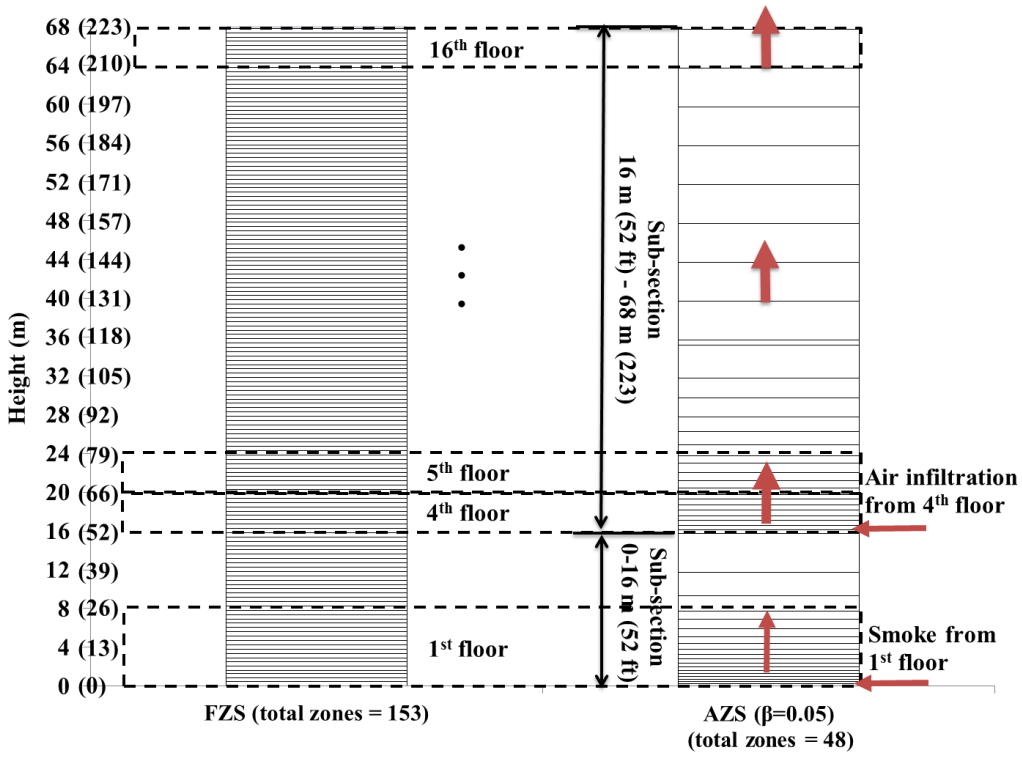

Figure 7-7 Shaft zoning by the FZS with 153 zones and the AZS with β=0.05 for the shaft with an infiltration opening at the 4th floor in the 16-storey building

Table 7-2 Comparison of mass flow rate (kg/s [lb/min]) of the 16-storey building with an infiltration opening at the 4th floor.

	FZS	AZS (β=0.05)	
	(total zone = 153)	First iteration	Second iteration
Sub-section 0 (0)-16 m (52 ft)	0.447	0.441	0.440
	(59.1)	(58.3)	(58.2)
Sub-section 16 (52 ft)-68 m (223 ft)	0.826	0.829	0.829
	(109.3)	(109.7)	(109.7)

Table 7-2 lists the predicted mass flow rate of each zoning method. The ASZ only needs two iterations to reach a convergence threshold of 0.1% for the mass flow rate. The calculated flow rate is pretty close to the baseline value in the FZS. Similarly, the predicted temperature and

pressure profiles by the AZS (β=0.05) with 48 zones are also almost the same with that of the FZS with 153 zones as shown in Figure 7, and the largest temperature difference is only 2.8%. When there is an infiltration at the 4th floor, the smoke temperature decrease sharply near the infiltration opening at 16 m (52.5 ft) because the cold air from the non-fire floor enters the shaft. The smoke temperature decreases about 30 K at the opening and becomes unaffected by the infiltration after 40 m (131.2 ft) when compared to the case without the opening as shown by the curve of "AZS (β=0.05)_without infiltration" in Figure 8(a).

Figure 7-8(b) also reveals the influence of the infiltration opening on the smoke risk in the vertical shaft. Although the opening is quite small (0.1 m^2 (1.08 ft^2)), the addition of the opening reduces the *NPL* significantly from 50 m (164 ft) to 28 m (91.9 ft). Consequently, more floors will be potentially exposed to the smoke. Meanwhile, the pressure difference between the shaft and non-fire floor is generally reduced at the lower section of the shaft but increased at the upper section because of the opening. Since the risk of the smoke is evaluated by both *NPL* and pressure differentials, the final outcome of adding an infiltration opening (e.g., fire fighters pop up a shaft door during a fire) should be carefully evaluated.

It should be also noticed that the current study only covers the case with one infiltration opening. Problem can become more complicated for shafts with many infiltrations. For such cases, the above iterative AZS procedure can be programmed in CONTAM97R so the method here can be automatically applied. These problems are beyond the scope of this paper but can be demonstrated further in later studies.

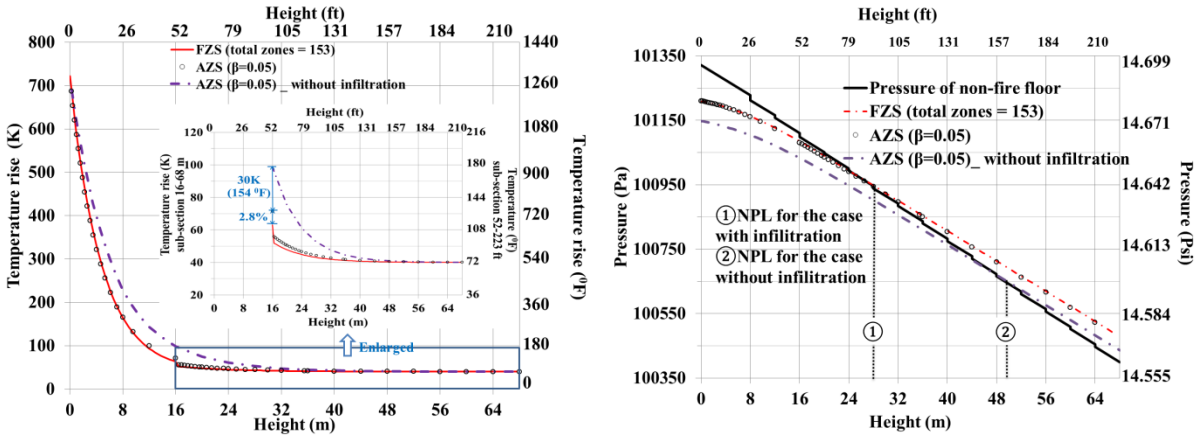

(a) (b)

Figure 7-8 Comparisons of predicted (a) smoke temperatures and (b) smoke pressures for different zoning strategies for the shafts with and without infiltration

7.5. Conclusion

This paper introduces the use of a multizone airflow and energy network model, CONTAM97R, for the modeling of smoke movement in high-rise shafts during fires. CONTAM97R was first validated by the experimental data from a 1/3 sub-scale building model and verified by an analytical model of high-rise fires in the literature. Then the program was used to model the fire smoke movement in a 16-storey full-size building by using two zoning strategies, FZS and AZS, with which the high-rise shaft was divided into multiple sub-zones. The predicted results by FZS and AZS for the shaft without infiltration were compared to the baseline of the high-rise fire analytical model. A new modeling method was also provided and demonstrated for AZS by a case study of the full-size building with an infiltration opening. The study reached the following major conclusions:

- In the study of the smoke dispersion in a high-rise building, the accuracy of FZS is inversely related to the temperature attenuation coefficient, α.
- When a high-rise shaft is divided into enough zones in FZS, the predictions will no longer improve with the increase of zone numbers so zone independent results are obtained.

- Compared to FZS, AZS provides results with similar accuracy as FZS but with fewer zones.
- The case studies reveal that adding an infiltration opening lower than the *NPL* (e.g. pop up a shaft door during a fire), may cause more smoke exposure at the non-fire floors above the fire floor.

It should be noted that although this study is based on CONTAM97R, the proposed zoning strategies and conclusions should also be applicable to other similar multi-zone airflow and energy network models.

Chapter 8 Conclusion and Future Work

8.1. Conclusion

This research established an analytical model of couple heat and mass transfer of fire smoke spread through non-adiabatic vertical shafts of high-rise shafts, which is comprised of energy balance equation, mechanical energy equation, orifice equation and mass balance equation. On the basis of the analytical model, simple calculation method and empirical equation of neutral plane level were proposed. It was found that:

- The temperature attenuation coefficient, α, a non-dimensional parameter associated with the geometrical and thermal properties of the smoke and the shaft, is an important parameter for the solutions of the coupled problem, because the temperature profiles of smoke and shaft wall are both shown to be exponential functions of α.
- The analytical solution provides the important information for the risk assessment of the smoke spread from the fire floor to higher floors, including shaft top temperature, maximum mass flow rate and corresponding fire floor temperature, and location of *NPL*.
- For non-adiabatic shafts, the effects of non-uniform temperature distribution on *NPL* should be considered. The provided case study shows that the uniform temperature assumption leads to over-estimated *NPL*, and the relation between shaft bottom/top temperature and *NPL* predicted based on this assumption is inconsistent to that of the experiments.
- Non-uniform temperature distribution inside of the shaft can be represented by a dimensionless number, T_{shH}/T_a, which is a ratio of shaft top temperature to ambient temperature. This dimensionless number is a function of temperature attenuation coefficient, α, which indicates smoke temperature profile inside the shaft.

- The sensitivity study found that the developed empirical equations, which include the dimensionless number in terms of T_{shH} and T_{sh0}, can predict *NPL* accurately. The existing equation may either underestimate or overestimate the *NPL* locations.

Studies on the dimensionless analytical solutions and similarity were also conducted based on the analytical model, which lead to a better understanding of the physics of smoke movement through vertical shafts as well as developing a new scaling method to sub-scale smoke spreads in high-rise shafts. Experiments on different size and material shafts were designed and carried out, the results of which were used to verify the dimensionless analytical solutions and the new scaling method. The study found that:

- The developed dimensionless model could predict accurate temperature distribution, mass flow rate and neutral plane level. The measured parameters of experiments are close to the predicted results of the dimensionless model.
- By defining the dimensionless number, ω, which equals to ψ times α, the coupled problem of smoke movement inside shaft driven by stack effect can be solved by only two equations, which much simplifies the calculations that cannot be achieved by previous studies.
- For the natural venting, with the increase of fire strength, smoke flow rate through the shaft increases accordingly whereas the temperature gradient does not change significantly, thus leading to minor change of *NPL*.
- The temperature attenuation coefficient, α, is in a form of the Stanton number, *St*, which is the ratio of the heat loss of the smoke over the thermal capacity of the smoke. When the mechanical venting rate (ψ) is increased in a shaft, *St*, becomes smaller, indicating less heat loss from smoke or more smoke thermal capacity, and thus the vertical temperature gradient decreases.

- The adiabatic assumption, which is commonly used in the literature, is found to lead to an overestimation of the mechanical venting rate necessary to keep a high-rise shaft free of smoke. The resultant error depends on the dimensionless number, ω, describing the geometry and thermal properties of the shaft: the adiabatic assumption causes more errors for bigger values of ω.
- By using the discharge coefficient, C_d, to express the inside structure resistance of the shaft, the shaft with inside structure, like shaft with stairs, could be sub-scaled as the shaft without inside structure, which is simpler to model.
- By considering heat transfer between smoke and the boundaries, and the interior structure resistance, the new modeling method could achieve more accurate results than Froude modeling method.

Based on the multizone program with an added energy equation, CONTAM97R, which has the capability of calculating the coupled heat and mass transfer inside the high-rise shafts, a numerical modeling method was developed. The numerical modeling method employs a new zoning strategy called adaptive zoning strategy (AZS), which adapts the temperature gradient inside the shaft. The following conclusions could be achieved:

- In the study of the smoke dispersion in a high-rise building, the accuracy of FZS is inversely related to the temperature attenuation coefficient, α.
- When a high-rise shaft is divided into enough zones in FZS, the predictions will no longer improve with the increase of zone numbers so zone independent results are obtained.
- Compared to FZS, AZS provides results with similar accuracy as FZS but with fewer zones.
- The case studies reveal that adding an infiltration opening lower than the *NPL* (e.g. popping up a shaft door during a fire), may cause more smoke exposure at the non-fire floors above the

fire floor.

8.2. Future work

- Analytical and similarity studies of smoke movement in high-rise shafts under transient state condition

  This thesis is focused on the steady state, the related parameters under which condition are vital for understanding physics of fire smoke movement and the design of the fire smoke protection system. The transient state is also important for the study of fire smoke protection, because during the time of transient state, it is the very important for people to evacuate the high-rise buildings. Therefore, it is also necessary to do the analytical and similarity studies of smoke movement in high-rise shafts under transient state condition.

- Determination of values of constants in the *NPL* empirical equations

  Chapter 5 presents *NPL* empirical equations, which is helpful to understand the underlying physics regarding the *NPL* in high-rise shafts. The constants C_1, N_1 and C_2 of the empirical equations needs to be correlated by more experiments on different size and material shafts, so that the empirical equations could be used to design fire smoke protection shafts.

- Similarity studies of smoke movement in the whole building

  Sub-scaled experiments are important for the research of fire smoke movement in buildings. High-rise shaft is the main space for toxic smoke spreading to higher levels rapidly due to stack effect, and is the subject for the similarity study in this thesis. Previous study has reported the scaling method in a single fire room. It would be meaningful to study the similarity law of smoke movement in the whole building, where the smoke spreads from the fire room to the higher level of the high-rise building through openings between shafts and non-fire floor located at the higher level.

- Integrate the analytical model into the control strategy of high-rise fire protection system

  During the high-rise fires, it is pretty important to indicate where the smoke has spread to and how much smoke flows inside the shafts. Therefore, prediction of neutral plane level and flow rate of smoke for high-rise shafts are useful for the high-rise fire protection system. In this thesis, the analytical model in terms of dimensionless numbers has been developed. Further studies could focus on the integration of the analytical model into the control strategy of high-rise fire protection system to predict and control neutral plane level and flow rate of smoke for shafts.

Reference

Allison C. Carey. 2010. “Scale Modeling of Static Fires in a Complex Geometry for Forensic Fire Applications.” Msc. thesis. University of Maryland, College Park.

ASHRAE. 2009. ASHRAE Handbook–fundamentals. Atlanta, GA: American Society of Heating, Refrigerating and Air Conditioning Engineers.

ASTM D5157-97. 2008. Standard Guide for Statistical Evaluation of Indoor Air Quality Models. West Conshohocken, PA.

Axley, J.W. 2011. Application of Natural Ventilation for U.S. Commercial Buildings: Climate Suitability Design Strategies & Methods Modeling Studies. Reference Number: GCR-01-820. Gaithersburg, MD. http://web.stanford.edu/group/narratives/classes/08-09/CEE215/ReferenceLibrary/Natural Ventilation/Natural Ventilation in US Commercial Buildings.pdf.

Axley, James W, Ph D, Steven J Emmerich, and George N Walton. 2002. “Modeling the Performance of a Naturally Ventilated Commercial Building with a Multizone Coupled Thermal / Airflow Simulation Tool.” ASHRAE Transactions 108 (2): 1260–1275.

Bae, Sungryong, Hyun-Jun Shin, and Hong-Sun Ryou. 2014. “Development of CAU_USCOP, a Network-Based Unsteady Smoke Simulation Program for High-Rise Buildings.” Building Simulation 7 (5): 503–510. doi:10.1007/s12273-014-0172-9.

Beitel, Jesse J., Alison J. Wakelin, and Craig L. Beyler. 2000. Analysis of Smoke Movement in a Building via Elevator Shafts. Beaverton, OR.

Black, W. Z. 2009. “Smoke Movement in Elevator Shafts during a High-Rise Structural Fire.” Fire Safety Journal 44 (2): 168–182. doi:10.1016/j.firesaf.2008.05.004.

Black, W. Z. 2010. “COSMO-Software for Designing Smoke Control Systems in High-Rise

Buildings." Fire Safety Journal 45 (6-8). Elsevier: 337–348. doi:10.1016/j.firesaf.2010.07.001.

CBC news. 2014. "130 Highrise Building Projects in Toronto Lead North America." CBC. http://www.cbc.ca/news/business/130-highrise-building-projects-in-toronto-lead-north-america-1.2504776.

Chan, Y H. 2003. "Biostatistics 104: Correlational Analysis." Singapore Medical Journal 44 (12): 614–619.

Chappell, Bill. 2016. "Fire At Dubai High-Rise Is Blamed On Electrical Issue In Spotlight." NPR. http://www.npr.org/sections/thetwo-way/2016/01/20/463691162/fire-at-dubai-high-rise-tower-is-blamed-on-electrical-issue-in-spotlight.

Chen, Qingyan. 2009. "Ventilation Performance Prediction for Buildings: A Method Overview and Recent Applications." Building and Environment 44 (4). Elsevier Ltd: 848–858. doi:10.1016/j.buildenv.2008.05.025.

Chow, W. K., and Henry H. W. Lo. 2008. "Scale Modeling on Natural Smoke Filling in an Atrium." Heat Transfer Engineering 29 (1): 76–84. doi:10.1080/09647040701677565.

Chow, W. K., and W.M. Siu. 1993. "Visualization of Smoke Movement in Scale Models of Atriums." JJournal of Applied Fire Science 3 (2): 93–111.

Chow, W. K., and J. H. Zhao. 2011. "Scale Modeling Studies on Stack Effect in Tall Vertical Shafts." Journal of Fire Sciences 29 (6): 531–542. doi:10.1177/0734904111410657.

Colaco, Joseph, Girish Dravid, and Vikas Kasilwal. 2012. "The Design and Construction of the Palais Royale , Mumbai." In CTBUH 2012 9th World Congress, edited by Council on Tall Buildings and Urban Habitat, 686–692. Shanghai, China.

Ding, Wenting, Yoshikazu Minegishi, Yuji Hasemi, and Tokiyoshi Yamada. 2004. "Smoke

Control Based on a Solar-Assisted Natural Ventilation System." Building and Environment 39 (7): 775–782. doi:10.1016/j.buildenv.2004.01.002.

Dols, W Stuart, and Brian J Polidoro. 2015. CONTAM User Guide and Program Documentation. Gaithersburg, MD: National Institute of Standards and Technology.

"Dubai Hotel Fire Could Have Been Worse." 2016. European Fire Sprinkler Network. http://eurosprinkler.org/dubai-hotel-fire-could-have-been-worse/.

EN 12101-3 Standard. 2002. Smoke and Heat Control Systems-Part 3: Specification for Powered Smoke and Heat Exhaust Ventilators. Brussels, Belgium.

Ferreira, M.J., and S.M. Strege. 2005. Smoke Management Systems: Federal Building and Fire Safety Investigation of the World Trade Center Disaster, Report, NIST NCSTAR 1-4D. Gaithersburg, MD. http://fire.nist.gov/bfrlpubs/build05/PDF/b05039.pdf.

Gann, Richard G, Vytenis Babrauskas, Richard D Peacock, and John R Hall Jr. 1994. "Fire Conditions for Smoke Toxicity Measurement." Fire and Materials 18 (3): 193–199.

Gu, L. 2011. "Advanced of EnergyPlus and Its Coupling with CHAMPS-Whole Building." In Proceedings of CHAMPS 2011: The 8th International Forum and Workshop on Combined Heat, Air, Moisture and Pollutant Simulations. Nanjing, China.

Guo, Lixia, Lei Guo, Ling Zhong, and Yueming Zhu. 2011. "Thermal Conductivity and Heat Transfer Coefficient of Concrete." Journal of Wuhan University of Technology-Mater. Sci. Ed. 26 (4): 791–796. doi:10.1007/s11595-011-0312-3.

Hadjisophocleous, George, and Q. Jia. 2009. "Comparison of FDS Prediction of Smoke Movement in a 10-Storey Building with Experimental Data." Fire Technology 45 (2): 163–177. doi:10.1007/s10694-008-0075-3.

Hall, J.R. 2011. High-Rise Building Fire. Quincy, MA.

Hall, John R. 2011. Fatal Effects of Fire. NFPA. Quincy, MA.

Harmathy, T. Z. 1998. “Simplified Model of Smoke Dispersion in Buildings by Stack Effect.” Fire Tech 34 (1): 6–17. doi:10.1023/A:1015352714123.

Harmathy, T. Z., and I. Oleszkiewicz. 1987. “Fire Drainage System.” Fire Technology 23 (1): 26–48. doi:10.1007/BF01038364.

Harrison, Roger. 2004. “Smoke Control in Atrium Buildings: A Study of the Thermal Spill Plume.” M.S. thesis. University of Canterbury.

Hensen, J. 1999. “A Comparison of Coupled and Decoupled Solutions for Temperature and Air Flow in a Building.” ASHRAE Transactions 105 (2): 962–969.

Hou, Long Fei, Ming Li, Wu Yuan Cui, and Yu Chen Liu. 2011. “Numerical Simulation and Analysis of on-Building High-Rise Building Fires.” Procedia Engineering 11: 127–134. doi:10.1016/j.proeng.2011.04.637.

Hutcheon, N.B., and G.O.P. Handegord. 1983. Building Science for a Cold Climate. Halethorpe, MD: Construction Technology Centre Atlantic, Incorporated.

International Code Council. 2007. Building Code of New York State. New York State: International Code Council, Inc.

ISO 834. 1975. Fire Resistance Tests. Geneva: Elements of Building Construction. International Organisation for Standardisation.

Ji, J., L. J. Li, W. X. Shi, C. G. Fan, and J. H. Sun. 2013. “Experimental Investigation on the Rising Characteristics of the Fire-Induced Buoyant Plume in Stairwells.” International Journal of Heat and Mass Transfer 64: 193–201. doi:10.1016/j.ijheatmasstransfer.2013.04.030.

Ji, J., M. Li, Z.H. Gao, Y.F. Li, W.X. Shi, and J.H. Sun. 2016. “Experimental Investigation of Combustion Characteristics under Different Ventilation Conditions in a Compartment

Connected to a Stairwell." Applied Thermal Engineering, 1–12. doi:10.1016/j.applthermaleng.2016.01.117.

Ji, Jie, Man Li, Yifan Li, Jiping Zhu, and Jinhua Sun. 2015. "Transport Characteristics of Thermal Plume Driven by Turbulent Mixing in Stairwell." International Journal of Thermal Sciences 89. Elsevier Masson SAS: 264–271. doi:10.1016/j.ijthermalsci.2014.11.009.

Jo, Jae Hun, Jae Han Lim, Seung Yeong Song, Myoung Souk Yeo, and Kwang Woo Kim. 2007. "Characteristics of Pressure Distribution and Solution to the Problems Caused by Stack Effect in High-Rise Residential Buildings." Building and Environment 42 (1): 263–277. doi:10.1016/j.buildenv.2005.07.002.

Karlasson, Bjorn, and James G Quintiere. 2002. Enclosure Fire Dynamics. New York, WA: CRC Press.

Klote, John H. 2011. "Stairwell Smoke Control by Ventilation." ASHRAE Transactions 117 (1): 478–486.

Klote, John H. 1991. A General Routine of Analyzing of Stack Effect. Report, NISTIR 4588. National Institute of Standards and Technology. Gaithersburg, MD.

Klote, John H. 2004. "Analysis of the Life Safety Consequences of Smoke Migration Through Elevator Shafts." Elevator World 52 (11): 81–90.

Klote, John H., James A. Milke, Paul G. Turnbull, Ahmed Kashef, and Michael J. Ferreira. 2012. Handbook of Smoke Control Engineering. Atlanta, GA.: American Society of Heating Refrigerating and Air-Conditioning Engineers.

Lay, Simon. 2014. "Pressurization Systems Do Not Work & Present a Risk to Life Safety." Case Studies in Fire Safety 1 (1). Elsevier Ltd: 13–17. doi:10.1016/j.csfs.2013.12.001.

Li, L. J., J. Ji, C. G. Fan, J. H. Sun, X. Y. Yuan, and W. X. Shi. 2014. "Experimental Investigation

on the Characteristics of Buoyant Plume Movement in a Stairwell with Multiple Openings." Energy and Buildings 68 (Part A): 108–120. doi:10.1016/j.enbuild.2013.09.028.

Lie, T. T., and J. H. McGuire. 1975. "Control of Smoke in High-Rise Buildings." Fire Technology 11 (1): 5–14. doi:10.1007/BF02589996.

Luo, Na, Angui Li, Ran Gao, Zhenguo Tian, Wei Zhang, Sen Mei, Luman Feng, and Pengfei Ma. 2013. "An Experiment and Simulation of Smoke Confinement and Exhaust Efficiency Utilizing a Modified Opposite Double-Jet Air Curtain." Safety Science 55: 17–25. doi:10.1016/j.ssci.2012.12.002.

Marshall, N.R. 1986. "Air Entrainment into Smoke and Hot Gases in Open Shafts." Fire Safety Journal 10 (1): 37–46. doi:10.1016/0379-7112(86)90030-5.

McCaffrey, B. J., J. G. Quintiere, and M. F. Harkleroad. 1981. "Estimating Room Temperatures and the Likelihood of Flashover Using Fire Test Data Correlations." Fire Technology 17 (2): 98–119. doi:10.1007/BF02479583.

McDowell, T.P., S. Emmerich, J.W. Thornton, and G. Walton. 2003. "Integration of Airflow and Energy Simulation Using CONTAM and TRNSYS." ASHRAE Transactions 109 (1): 757–770.

McGrattan, K., R. McDermott, C. Weinschenk, and K. Overholt. 2013. Fire Dynamics Simulator User's Guide. Gaithersburg, MD.

Mercier, G. P., and Y. Jaluria. 1999. "Fire-Induced Flow of Smoke and Hot Gases in Open Vertical Enclosures." Experimental Thermal and Fluid Science 19 (2): 77–84. doi:10.1016/S0894-1777(99)00012-6.

Miller, Richard S, and Don Beasley. 2009. "On Stairwell and Elevator Shaft Pressurization for Smoke Control in Tall Buildings." Building and Environment 44 (6). Elsevier Ltd: 1306–

1317. doi:http://dx.doi.org/10.1016/j.buildenv.2008.09.015.

Miller, Richard S. 2011. “Elevator Shaft Pressurization for Smoke Control in Tall Buildings: The Seattle Approach.” Building and Environment 46 (11). Elsevier Ltd: 2247–2254. doi:10.1016/j.buildenv.2011.05.007.

Munson, Bruce R., Donald F. Young, Theodore H. Okiishi, and Wade W. Huebsch. 2009. Fundamentals of Fluid Mechanics. Sixth edit.

Musser, A., K. McGrattan, and J. Palmer. 2001. Evaluation of a Fast, Simplified Computation Fluid Dynamics Model for Solving Room Airflow Problems. Report, NISTIR 6760. Gaithersburg, MD.

NFPA 101. 2012. Life Safety Code, 2012 Ed. Quincy, MA.

Ng, L, a Musser, Ak Persily, and Sj Emmerich. 2012. “Airflow and Indoor Air Quality Models of DOE Reference Commercial Buildings.” Gaithersburg, MD, National …. http://www.bfrl.nist.gov/IAQanalysis/docs/Tech Note 1734 - CONTAM reference bldgs.pdf.

Ng, Lisa C., Amy Musser, Andrew K. Persily, and Steven J. Emmerich. 2013. “Multizone Airflow Models for Calculating Infiltration Rates in Commercial Reference Buildings.” Energy and Buildings 58: 11–18. doi:10.1016/j.enbuild.2012.11.035.

Peppes, a a, M Santamouris, and D N Asimakopoulos. 2001. “Buoyancy-Driven Flow through a Stairwell.” Building and Environment 36 (2): 167–180.

Peppes, a a, M Santamouris, and D N Asimakopoulos. 2002. “Experimental and Numerical Study of Buoyancy-Driven Stairwell Ow in a Three Storey Building.” Building and Environment 37 (5): 497–506.

Poreh, M, and S Trebukov. 2000. “Wind Effects on Smoke Motion in Buildings” 35 (3): 257–273.

Qi, Dahai, Liangzhu Wang, and Radu Zmeureanu. 2014a. “An Analytical Model of Heat and Mass

Transfer through Non-Adiabatic High-Rise Shafts during Fires." International Journal of Heat and Mass Transfer 72. Elsevier Ltd: 585–594. doi:10.1016/j.ijheatmasstransfer.2014.01.042.

Qi, Dahai, Liangzhu Wang, and Radu Zmeureanu. 2014b. "A Hand Calculation Method of Smoke Movement through High-Rise Building Shaft." In ASHRAE Annual Conference 2014. Seattle, WA.

Qi, Dahai, Liangzhu Wang, and Radu Zmeureanu. 2015. "Modeling Smoke Movement in Shafts during High-Rise Fires by a Multizone Airflow and Energy Network Program." ASHRAE Transactions 121 (2).

Qi, Dahai, Liangzhu Wang, and Radu Zmeureanu. 2016. "The Effects of Non-Uniform Temperature Distribution on Neutral Plane Level in Non-Adiabatic High-Rise Shafts During Fires." Fire Technology. Springer US. doi:10.1007/s10694-015-0554-2.

Quintiere, James G, and Michael E Dillon. 2008. "Scale Model Reconstruction of Fire in an Atrium." In Progress in Scale Modeling, 109–120.

Sahlin, P. 2003. "On the Effects of Decoupling Airflow and Heat Balance in Building Simulation Models." ASHRAE Transactions 109 (2): 1671–1677.

Shi, W. X., J. Ji, J. H. Sun, S. M. Lo, L. J. Li, and X. Y. Yuan. 2014a. "Influence of Staircase Ventilation State on the Airflow and Heat Transfer of the Heated Room on the Middle Floor of High Rise Building." Applied Energy 119: 173–180. doi:10.1016/j.apenergy.2013.12.055.

Shi, W. X., J. Ji, J. H. Sun, S. M. Lo, L. J. Li, and X. Y. Yuan. 2014b. "Influence of Fire Power and Window Position on Smoke Movement Mechanisms and Temperature Distribution in an Emergency Staircase." Energy and Buildings 79: 132–142. doi:10.1016/j.enbuild.2014.02.083.

Siegel, R., and J.R. Howell. 1993. Thermal Radiation Heat Transfer. third ed. Washington, DC: Hemisphere Publishing Corporation.

Steckler, K D, H R Baum, and A X J G Quintiere. 1986. "Multicompartment Enclosures Elements of Salt Water Modeling." Twenty-First Symposium (International)on Combustion/The Combustion Institute, 143–149.

Su, Chung Hwei, Yu Chang Lin, Chi Min Shu, and Ming Chih Hsu. 2011. "Stack Effect of Smoke for an Old-Style Apartment in Taiwan." Building and Environment 46 (12): 2425–2433. doi:10.1016/j.buildenv.2011.04.026.

Sun, X. Q., L. H. Hu, W. K. Chow, Y. Xu, and F. Li. 2011. "A Theoretical Model to Predict Plume Rise in Shaft Generated by Growing Compartment Fire." International Journal of Heat and Mass Transfer 54 (4): 910–920. doi:10.1016/j.ijheatmasstransfer.2010.10.012.

Tamura, G.T. 1994. Smoke Movement & Control in High-Rise Buildings. Quincy, MA.: National Fire Protection Association.

Tang, G. 2005. "Study of Natural Ventilation Design by Integrating the Multizone Model with CFD Simulation." Ph.D. thesis. Massachusetts Institute of Technology,Cambridge, MA.

Tang, G., and Leon R. Glicksman. 2005. "Application of Integrating Multi-Zone Model with CFD Simulation to Natural Ventilation Prediction." Energy and Buildings 37 (10): 1049–1057. doi:10.1016/j.enbuild.2004.12.009.

Walton, George N, and W Stuart Dols. 2013. CONTAM User Guide and Program Documentation. Gaithersburg, MD.: National Institute of Standards and Technology.

Wang, Liangzhu, William Z Black, and Guanchao Zhao. 2013. "Comparison of Simulation Programs for Airflow and Smoke Movement during High-Rise Fires." ASHRAE Transactions 119 (2): 12.

Wang, Liangzhu, and Qingyan Chen. 2008. “Evaluation of Some Assumptions Used in Multizone Airflow Network Models.” Building and Environment 43 (10): 1671–1677. doi:10.1016/j.buildenv.2007.10.010.

Wang, Liangzhu Leon, W Stuart Dols, and Steven J Emmerich. 2012. “Simultaneous Solutions of Coupled Thermal Airflow Problem for Natural Ventilation in Buildings Simultaneous Solutions of Coupled Thermal Airflow Problem for Natural Ventilation in Buildings,” no. April 2013: 37–41. doi:10.1080/10789669.2011.591258.

Wang, Yan, Ehab Zalok, and George Hadjisophocleous. 2011. “An Experimental Study of Smoke Movement in Multi-Storey Buildings.” Fire Technology 47 (4): 1141–1169. doi:10.1007/s10694-009-0132-6.

Wood, Antony, and Salib， Ruba. 2013. Natural Ventilation in High-Rise Office Buildings. Routledge. Chicago, IL: Routledge. https://store.ctbuh.org/PDF_Previews/Reports/2012_CTBUHNaturalVentilationGuide_Preview.pdf.

Xiao, G. Q., J. Y. Tu, and G. H. Yeoh. 2008. “Numerical Simulation of the Migration of Hot Gases in Open Vertical Shaft.” Applied Thermal Engineering 28 (5-6): 478–487. doi:10.1016/j.applthermaleng.2007.05.006.

Yam, Jimmu, Yuguo Li, and Zuohuan Zheng. 2008. “Coupling of Thermal Mass and Natural Ventilation in Buildings.” Energy and Buildings 40 (6): 979–986. doi:10.1016/j.enbuild.2007.08.001.

Yang, Dong, Tao Du, Shini Peng, and Baizhan Li. 2013. “A Model for Analysis of Convection Induced by Stack Effect in a Shaft with Warm Airflow Expelled from Adjacent Space.” Energy and Buildings 62: 107–115. doi:10.1016/j.enbuild.2013.02.045.

Yang, Dong, Bai Zhan Li, Tao Du, and Nan Li. 2012. “Analytical Models for Evaluating Buoyancy-Driven Ventilation due to Stack Effect in a Shaft Considering Heat Transfer from Shaft Interior Boundaries.” Journal of Central South University of Technology (English Edition) 19 (3): 651–656. doi:10.1007/s11771-012-1052-z.

Yii, Ee Hieng. 1998. Exploratory Salt Water Experiments of Balcony Spill Plume Using Laser Induced Flurescent Technique. Fire Engineering Research Report 98/7. Christchurch. file:///C:/Users/dahai/Downloads/FireEngResearchReport98-7.pdf.

Zhai, Zhiqiang, Mary Hall Johnson, and Moncef Krarti. 2011. “Assessment of Natural and Hybrid Ventilation Models in Whole-Building Energy Simulations.” Energy and Buildings 43 (9). Elsevier B.V.: 2251–2261. doi:10.1016/j.enbuild.2011.06.026.

Zhang, J. Y., W. Z. Lu, R. Huo, and R. Feng. 2008. “A New Model for Determining Neutral-Plane Position in Shaft Space of a Building under Fire Situation.” Building and Environment 43 (6): 1101–1108. doi:10.1016/j.buildenv.2007.02.004.

Zhao, G., and L. Wang. 2014. “Using Helium Smoke as a Surrogate of Fire Smoke for the Study of Atrium Smoke Filling.” Journal of Fire Sciences 32 (5): 431–447. doi:10.1177/0734904114529403.

Zhong, Maohua, Weicheng Fan, T. M. Liu, P. H. Zhang, X. Wei, and G. X. Liao. 2004. “China: Some Key Technologies and the Future Developments of Fire Safety Science.” Safety Science 42 (7): 627–637. doi:10.1016/j.ssci.2003.10.003.